Critical Evaluation and Optimization of a Hypocycloid Wiseman Engine

by

Thomas Conner

A Thesis Presented in Partial Fulfillment
of the Requirements for the Degree
Master of Technology

Approved November 2011 by the
Graduate Supervisory Committee:

Sangram Redkar, Chair
Trian Georgeou
Bradley Rogers

ARIZONA STATE UNIVERSITY

December 2011

ABSTRACT

In nearly all commercially successful internal combustion engine applications, the slider crank mechanism is used to convert the reciprocating motion of the piston into rotary motion. The hypocycloid mechanism, wherein the crankshaft is replaced with a novel gearing arrangement, is a viable alternative to the slider crank mechanism. The geared hypocycloid mechanism allows for linear motion of the connecting rod and provides a method for perfect balance with any number of cylinders including single cylinder applications.

A variety of hypocycloid engine designs and research efforts have been undertaken and produced successful running prototypes. Wiseman Technologies, Inc provided one of these prototypes to this research effort. This two-cycle 30cc half crank hypocycloid engine has shown promise in several performance categories including balance and efficiency. To further investigate its potential a more thorough and scientific analysis was necessary and completed in this research effort.

The major objective of the research effort was to critically evaluate and optimize the Wiseman prototype for maximum performance in balance, efficiency, and power output. A nearly identical slider crank engine was used extensively to establish baseline performance data and make comparisons. Specialized equipment and methods were designed and built to collect experimental data on both engines. Simulation and mathematical models validated by experimental data collection were used to better quantify performance improvements. Modifications to the Wiseman prototype engine improved balance by 20 to 50% (depending on direction) and increased peak power output by 24%.

DEDICATION

To my mother, father and his father whose answers to my questions always led to more questions.

ACKNOWLEDGMENTS

I would like to acknowledge and thank the following for their tremendous support and guidance in completing this thesis:

Dr. Sangram Redkar for going well above and beyond what is asked of a committee chair.

Brian Eidson, John Payne, Al Tercero, and everyone at MTD Southwest Inc. for supplying engines, answers, ideas, knowledge and invaluable lab time for engine testing.

The ASU Edson Entrepreneurship program for partially funding this project.

The Wiseman Group including Keith Voigts, Mark Smith, and Jerry Blankinchip for sponsoring the most enjoyable project I've ever been a part of and providing never ending support and the origin of this thesis: The Wiseman prototype engine.

John Howell for endless hours developing the Land and Sea dynamometer on which most of the engine testing took place.

Kyle Ester for engine part fabrication and dynamometer design and fabrication.

Brittney, for too many reasons to list.

TABLE OF CONTENTS

Page

LIST OF TABLES VII

LIST OF FIGURES VIII

INTRODUCTION 1

BACKGROUND 4

Hypocycloid Concept 4

Geared Hypocycloid Mechanism 5

Geared Hypocycloid Engine 7

GHE Research and History 9

SCOPE OF WORK 18

Objective 1: Analyze and Balance the Wiseman Engine 20

Objective 2: Peak Power and Efficiency Analysis 22

30cc Wiseman Engine Background 27

ENGINE BALANCE 34

Perfect Balance Approach 34

Motion Simulation Vibration Study 37

Balanced Design 44

Pinion Shaft Balance 45

Carrier Shaft Balance 55

Piston/Rod Fabrication 63

Empirical Vibration Analysis 70

Empirical Vibration Results 75

ENGINE PERFORMANCE 80

Engine Test Fixture Design 80

Page

Motored Power Loss Test....84
Output Torque vs. Crankshaft Angle....88
Baseline Performance Evaluation....104
MTD dynamometer and BSFC....104
Land and Sea Dynamometer and Peak Power....108
Primary Compression Ratio (PCR)....110
Lotus Engine Simulation (LES)....112
Connecting Rod Seal....119
Wiseman Power and Efficiency Conclusions....124
SUMMARY AND FUTURE WORK....126
Future Work....128
APPENDIX A: LES MODEL INPUT PARAMETERS....134

LIST OF TABLES

Table Page

1. – Engine Specifications 19

2. – Accelerometer Calibration Values 74

3. – Primary Compression Ratio of Wiseman and Stock Engine 111

LIST OF FIGURES

Figure Page

1. – Singe Cylinder Slider Crank Engine 1
2. – Hypocycloid Concept 4
3. – Geared Hypocycloid Concept in 45º Increments of Rotation 6
4. – Single Cylinder Hypocycloid Engine Schematic 8
5. – Model Hypocycloid Steam Engine 9
6. – Sketch from Wiseman US Patent # 6,510,831 (Wiseman, 2001) 10
7. – Theoretical Results from Ishida and Matsuda 11
8. – Experimental Vibration Results of a Two-Cycle Engine..... 13
9. – Vibration Amplitude vs. Crank Angle at a Fixed 1800 rpm 14
10. – Section View of 125cc Two-Stroke GHE from (Andriano, 1998)..... 17
11. – Wiseman (left) and Stock Engine (right)..... 19
12. – Half-Crank Engine Design 21
13. – Wiseman and Stock Engine (Wiseman Technologies, Inc.) 24
14. – WTI Fuel Efficiency Test Run..... 24
15. – Wiseman 30cc Prototype Section View..... 27
16. – Wiseman Driveline..... 29
17. – Isometric Assembly View, Right Rear 29
18. – Back View, Engine at TDC..... 30
19. – Back View, Engine at 90º ATDC 31
20. – Back View, Engine at BDC 32
21. – Back View, Engine at 270º ATDC 33
22. – Balance Approach Adapted from (Ifield) 34
23. – Ifield's Concept Translated to the 30cc Wiseman Engine at TDC 36

Figure Page

24. – Stock Engine, Section View of Dynamic Model 38

25. –Stock Engine, Transparent Isometric View..... 38

26. – Stock Engine Simulation Window 39

27. – Wiseman Engine Simulation Window..... 40

28. – Coordinate System for Simulation Outputs 41

29. – Baseline Shaking Force vs. Crank Angle in Y at 3000 rpm 42

30. – Baseline Shaking Force vs. Crank Angle in X at 3000 rpm 42

31. – Baseline Shaking Moment vs. Crank Angle at 3000 rpm..... 44

32. – Original Piston, Rod, and Bearing..... 45

33. – Provided Wiseman Piston and Rod Assembly 46

34. – Piston, Rod, and Bearing Dynamic Equivalence 47

35. – CM Relative to Pinion Shaft Centerline 47

36. – Piston and Connecting Rod Assembly..... 50

37. – Pinion Shaft with 43.2-gram Bob Weight..... 51

38. – Material Removal Required on Pinion Shaft..... 52

39. – After Pinion Balance (APB) Shaking Force vs. Crank Angle in Y 53

40. – After Pinion Balance (APB) Shaking Force vs. Crank Angle in X 54

41. – After Pinion Balance (APB) Shaking Moment vs. Crank Angle..... 55

42. – Carrier Shaft CM..... 56

43. – Carrier Shaft with Tungsten Slugs Installed 57

44. – ACB Wiseman Shaking Moment vs. Crank Angle 58

45. – ACB Wiseman Shaking Force in X vs. Crank Angle..... 59

46. – Balanced Wiseman Shaking Force in Y vs. Crank Angle 59

47. – Shaking Moment and 3D Balance..... 60

Figure Page

48. – Shaking Moment Counterweights for 3D balance 61

49. – Shaking Moment vs. Crankshaft Angle with 3D Balance..... 62

50. – Connecting Rod CAM OP01 64

51. – Connecting Rod CAM Program OP02..... 65

52. – OP03, Mill Sides Flat 66

53. – OP03, Contour Mill Center Hole to Ø0.5600 inches 66

54. – Machined Connecting Rod..... 67

55. – Piston OP02 68

56. – OP03 Finish Toolpath 69

57. – Machined Piston and Connecting Rod 70

58. – Wiseman Engine Mounted in Vibration Test Fixture..... 73

59. – Wiseman Baseline Vibration Tests 76

60. – Vibration in X vs. RPM 77

61. – Vibration in Y vs. RPM 78

62. – Omega Strain Gauge Load Cell and Meter 81

63. – Engine Test Fixture and Reaction Torque Concept..... 82

64. – Load Cell Measuring Engine Reaction Torque..... 83

65. – Motored Friction Power Loss & Torque vs. RPM..... 86

66. – Power loss vs. RPM Extrapolated to 7000 RPM 87

67. – Gas Torque vs. Crank Angle @ 1.0 bar Pressure on Piston 90

68. – Degree wheel Attached to Flywheel..... 92

69. – Pressure Torque Test Fixture Plumbing Schematic 92

70. – Wiseman Gas Torque vs. Crank Angle at 1.0 bar 93

71. – Stock Gas Torque vs. Crank Angle at 1.0 bar 93

Figure Page

72. – Wiseman and Stock Gas Torque vs. Crank Angle 95

73. – Scaled Gas Pressure vs. Expansion Stroke Crank Angle Curve 96

74. – Gas Torque vs. Crank Angle for Scaled Pressure 97

75. – Gas Torque vs. Crank Angle for Wiseman stroke = 1.27 in 99

76. – Wiseman (Hypocycloid) Piston Position Diagram 101

77. – Expansion Stroke Crank Angle vs. Volume above Piston 103

78. – Average Lamda During Peak Power Runs 106

79. – Average Horsepower During Peak Power Runs 106

80. – BSFC Wiseman and MTD 31cc 108

81. – Wiseman Engine Mounted to Land and Sea Dynamometer 109

82. – Baseline Peak Power Dynamometer Runs 110

83. – LES Engine Simulation Model 113

84. – Power Curve at PCR=1.14 115

85. – Power Curve at PCR=1.42 116

86. – Case Stuffer Drawing 118

87. – Connecting Rod Seal installed in Wiseman Engine 120

88. – Power Curve for PCR = 2.17 121

89. – Connecting Rod Seal Run with original baseline runs 123

Chapter 1

INTRODUCTION

The slider crank internal combustion engine (ICE) is a dominating force in the modern industrialized world with annual production exceeding 100 million units worldwide (Wiseman Engine Group, 2010). The ICE is the primary driving force behind generators, automobiles, aircraft, locomotives, motorcycles and numerous other pieces of equipment vital to everyday life in developed parts of the world. In all of these applications and almost all successful commercial applications, the well-known slider crank mechanism (see Figure 1) is used to convert the reciprocating motion of the piston into rotary motion of the output shaft.

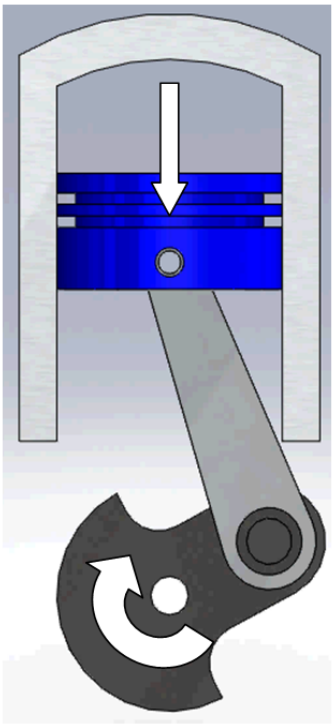

Figure 1 – Singe Cylinder Slider Crank Engine

There has been tremendous advancement of the ICE over the past 100 years but the fundamental slider crank or crankshaft based mechanism has remained essentially unchanged. There are two important of shortcomings of the slider crank mechanism:

1. The inclination of the connecting rod produces a force on the piston perpendicular to the axis of the cylinder causing piston side load. This Piston side load causes friction between the piston and the cylinder wall resulting in reduced efficiency and additional heat, which must be dissipated by the cooling system.
2. The reciprocating motion of the piston combined with the complex motion of the connecting rod is difficult to balance and virtually impossible in simple single cylinder applications. The motion of the piston is also non-sinusoidal causing a second order vibration at twice engine speed, which further complicates engine balance.

A tremendous amount of research and development has involved overcoming these two major shortcomings and modern engines have come a long way in doing so. However, the solutions tend to come in the form of increased engine cost and complexity. Radical alternatives to the slider crankshaft mechanism are numerous but few have had any commercial success. The Wankel or rotary engine is arguably one of the few exceptions reaching high volume production in Mazda automobiles and small aircraft applications. Another alternative mechanism especially related to item's 1 and 2 above is the Geared Hypocycloid Engine or GHE. In a GHE the standard crankshaft is replaced with a geared mechanism that provides some unique advantages over a conventional slider crank crankshaft. A variety of moderately successful prototypes have been

constructed using the hypocycloid concept (Andriano, 1998) (Beachley & Lenz, 1988) (Ishida & Matsuda, 1975). A 30cc two-cycle GHE was provided for this research effort by Wiseman Technologies Inc. (WTI). The primary focus of this research effort was to critically evaluate and optimize this prototype engine, hereafter referred to as the Wiseman engine. The major objectives required to accomplish this focus were:

1. Critically analyze the Wiseman engine prototype using software simulations and empirical testing.
2. Use the results to explore possible areas of improvement in balance, efficiency, and peak power.
3. Modify the Wiseman prototype where possible to improve in these areas.
4. Assess levels of improvement through simulations and empirical testing.
5. Compare performance before and after modifications to a similar slider crank engine.

Chapter 2

BACKGROUND

Hypocycloid Concept

The GHE is made possible by taking advantage of the hypocycloid concept. A hypocycloid can be described as a “curve produced by fixed point P on the circumference of a small circle of radius b rolling around the inside of a larger circle of radius a > b.” (Wolfram MathWorld, 2010) (See Figure 2).

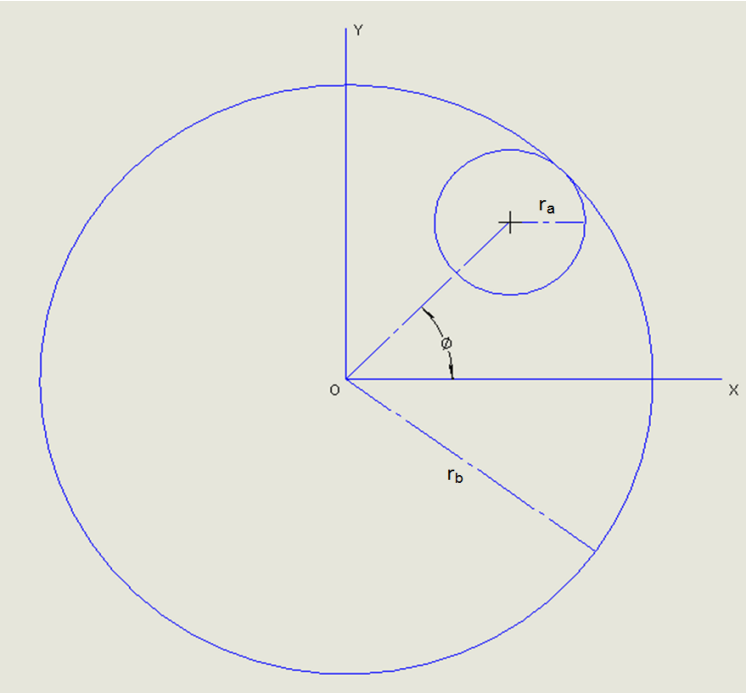

Figure 2 – Hypocycloid Concept

A unique hypocycloid curve can be generated for a given diameter ratio of “a” to “b”. The equations for a hypocycloid that define the path of point P are Equation 1 and Equation 2 from (Hsu, 2008).

$$x = (r_a - r_b)\cos\emptyset + r_b \cos\left(\frac{r_a - r_b}{r_b}\emptyset\right) \qquad \text{Equation 1}$$

$$\boldsymbol{y = (r_a - r_b)\cos\emptyset + r_b \cos\left(\frac{r_a - r_b}{r_b}\emptyset\right)}$$ Equation 2

where:

r_a is the radius of the smaller circle.

r_b is the radius of the larger circle.

$\emptyset$ is the angle from the x axis to the line that intersects the center of circle a and circle b.

Of special interest to an ICE is the case where the diameter of circle “b” is exactly half that of circle “a”. The 2:1 circle ratio has an interesting result; any point located on the perimeter of circle “a” draws a perfectly straight line as circle “a” rolls around the inside of circle “b”.

Geared Hypocycloid Mechanism

If the two circles in Figure 2 are replaced with gears the concept becomes practical for use in a mechanism. Shown in Figure 3 is a 2:1 pitch diameter hypocycloid gear pair. The smaller pinion gear is analogous to circle “a” in Figure 2 and the larger internal ring gear is analogous to circle “b”. Figure 3 illustrates one full revolution of the geared mechanism in 45º increments of rotation starting and ending at 0º.

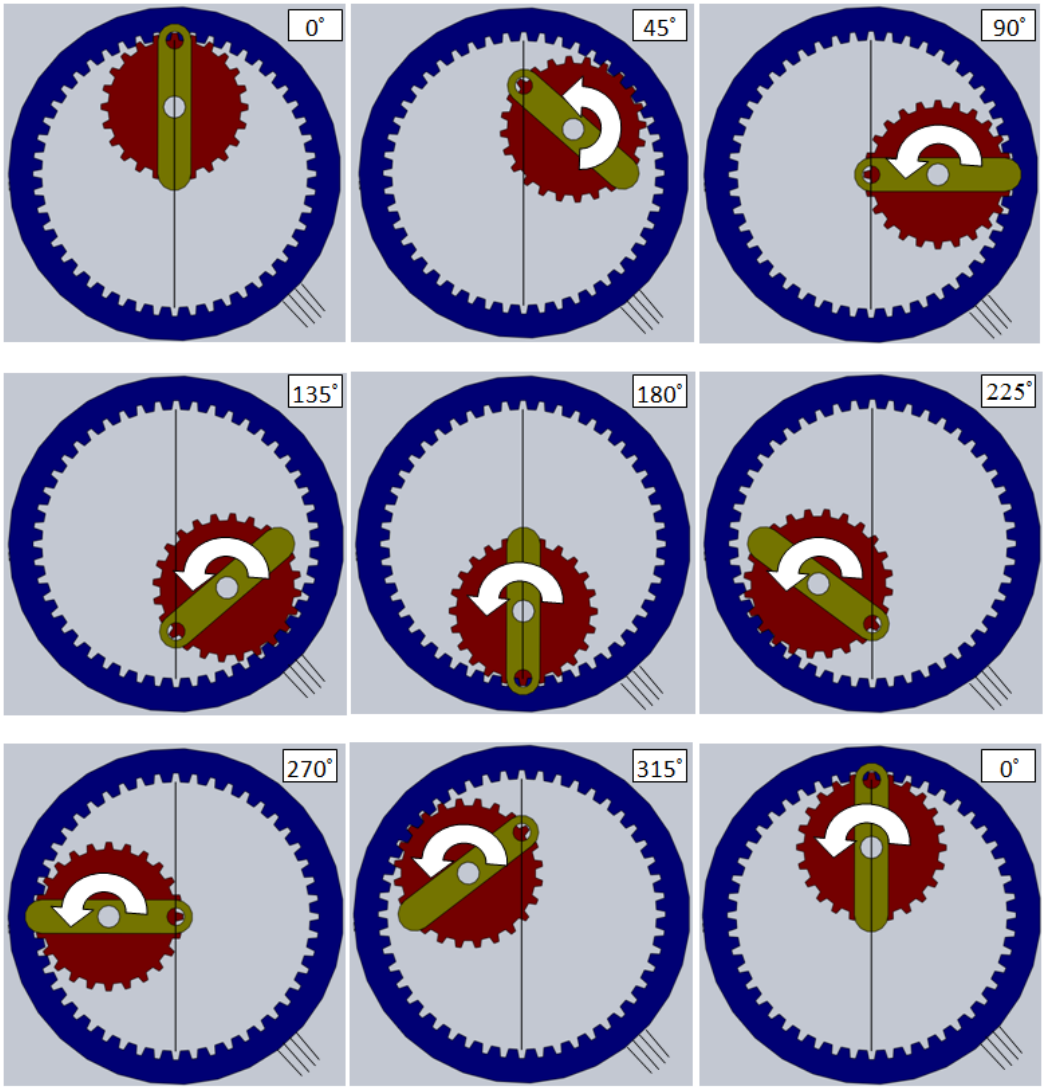

Figure 3 – Geared Hypocycloid Concept in 45º Increments of Rotation

Starting at the upper left corner of Figure 3 and moving to the right, the smaller pinion gear (red) rotates counterclockwise about its own axis. Note that the mechanism will also work in the clockwise direction. As the smaller pinion gear rotates about its own center it also rotates about the center of the fixed internal ring gear (blue). As the pinion gear rolls around the ring gear, a specific point of interest located on the pitch diameter of the pinion gear, remains coincident with the vertical black line shown.

Geared Hypocycloid Engine

The 2:1 gear ratio is of special interest for an ICE because any point located on the pitch circle of the pinion gear will travel in a perfectly straight line and with sinusoidal motion. Sinusoidal motion is important when the mechanism undergoes balancing. The particular point chosen in Figure 3 draws the perfectly vertical straight line shown in black. Any other point chosen on the pitch circle of the smaller pinion gear will also draw a straight line but at a different angle than vertical. There is also a point on the pitch circle of the pinion gear that draws a perfectly horizontal line. For an ICE to take advantage of this mechanism some additional components are required:

1. To achieve useful output rotary motion an additional link is required to support the pinion gear and transfer its rotary motion to an output shaft. This can be accomplished in a number of ways. One method is shown in Figure 4. The additional link is called the rotating output shaft or L2. This method is simple, however not very practical in highly stressed mechanisms.
2. The bottom of the connecting rod must attach to point D1 in Figure 4. The point D1 on the end of the pinion arm is coincident to the point P that traces the same vertical straight line shown in Figure 3.

It should be noted that Figure 4 is a simplified 2D schematic of the GHE and does not represent a practical design of an actual engine. It is useful however in understanding how the mechanism can be applied to a piston ICE.

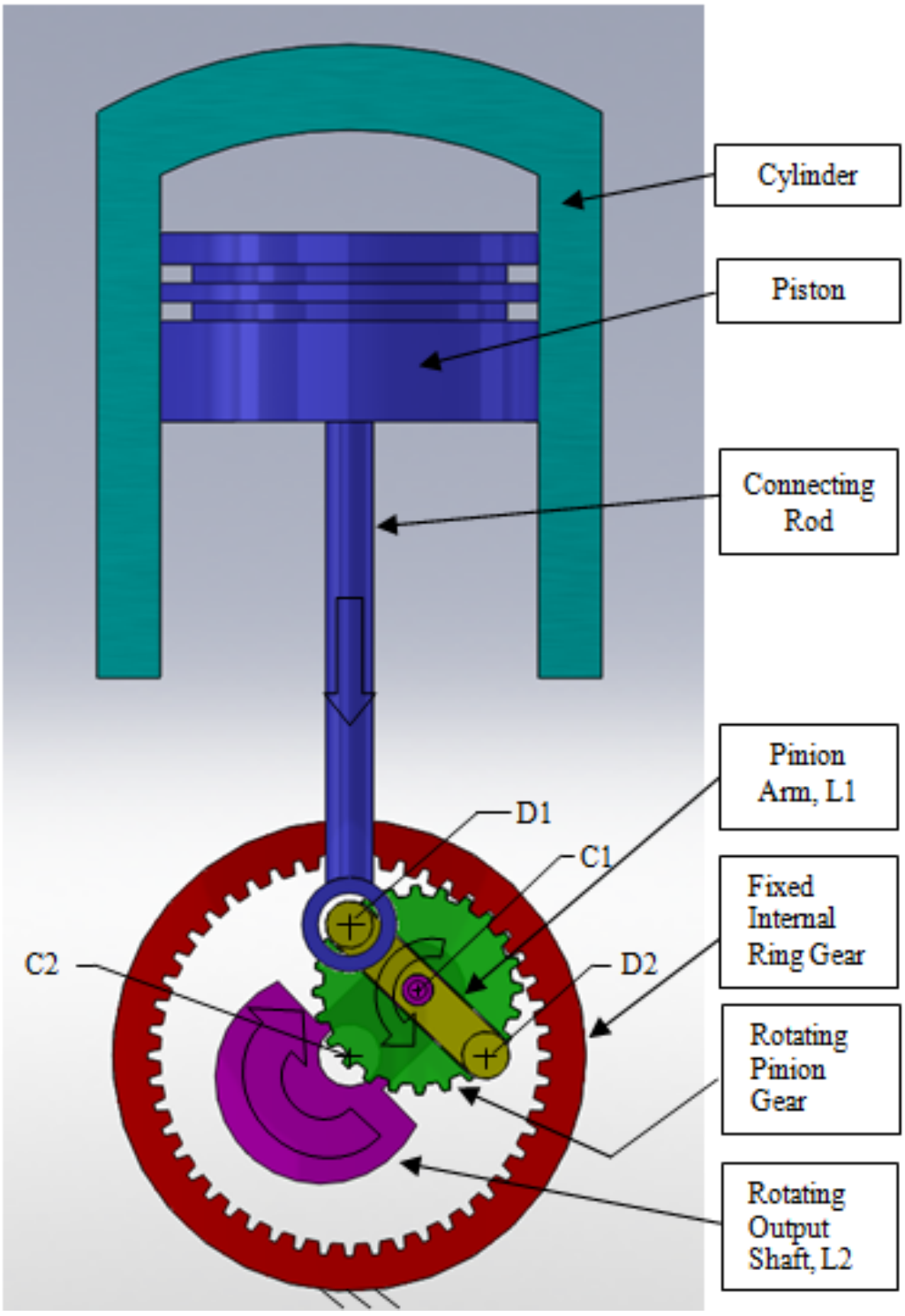

Figure 4 – Single Cylinder Hypocycloid Engine Schematic

GHE Research and History

The GHE has received some research attention from a number of different groups and universities around the world. A number of patents have also been filed dating back to 1802 when Matthew Murray applied the hypocycloid concept to a steam engine (Karhula, 2008). A replica model of Murray's hypocycloid steam engine is shown in Figure 5 and is actually quite similar to the design shown in Figure 4 (Polly Model Engineering Limited, 2010).

Figure 5 – Model Hypocycloid Steam Engine

One of the more recent patents and a major focus of this research effort was the Wiseman Mechanism patent filed in 2001 by Mr. Randal Wiseman (Wiseman, 2001).

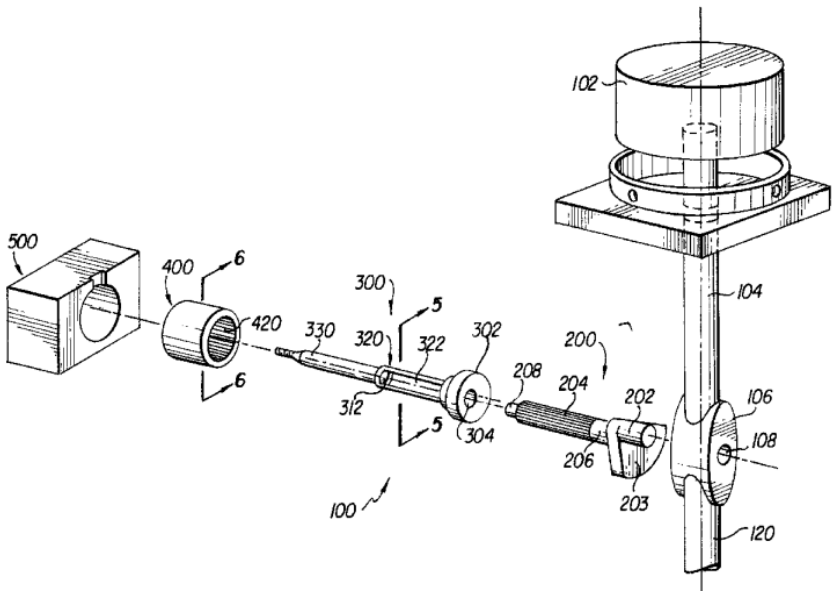

Figure 6 – Sketch from Wiseman US Patent # 6,510,831 (Wiseman, 2001)

An additional link is required to support the pinion gear shaft and there are a number of different approaches. One unique approach is covered in Mr. Wiseman's patent and is illustrated in Figure 6. Item 100, called the carrier shaft, is responsible for supporting the pinion gear shaft (Item 200). It also provides a cavity (item 322) for the pinion gear teeth (item 204) to mesh with the fixed internal ring gear (item 6). This patent is utilized in the Wiseman prototype provided for this research effort.

Other patents and research efforts have also produced running prototypes and some mathematical predictions that indicate the GHE is a viable alternative to the slider crank engine. However, this is where development currently stalls for the modern GHE. At the time of writing there is no known GHE design that has successfully transitioned into production on any recent high volume commercial application.

GHE research that is of particular interest to this work began in the mid 1970's with Mr. Kenjiro Ishida and his colleagues. Ishida published an excellent paper that focused on the inertial shaking forces and moments of a GHE compared to a conventional slider crank engine (Ishida & Matsuda, 1975). Using kinematic vector equations Ishida calculated the unbalanced inertia forces and moments of production single cylinder slider crank engine with a 40mm stroke and 40mm bore. Ishida then finds the inertial shaking forces and moments for a GHE of the same bore and stroke. His theoretical results show that a hypocycloid engine can be perfectly balanced and both the inertial forces and moments are zero. Ishida plots the inertial forces and moments for the slider crank engine and hypocycloid engine together for comparison in Figure 7. The slider crank is plotted using multiple balancing techniques including half and over crank balance. (Ishida & Matsuda, 1975).

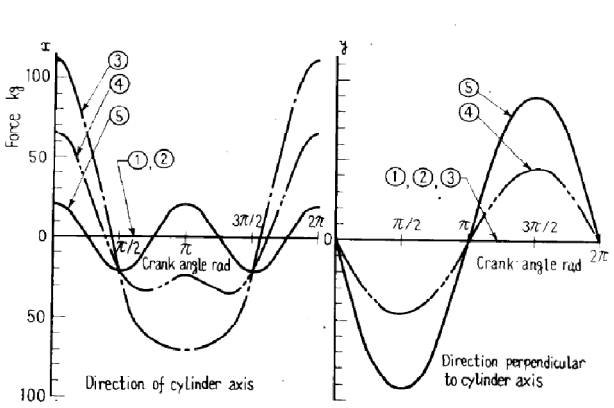

Fig.5 Unbalanced inertia force
(Rotational speed of crank 6000 rpm)

1 Perfect balance 2 Static balance
3 Rotation balance 4 Half balance
5 Over balance

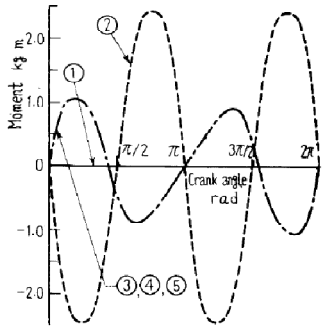

Fig.6 Unbalanced inertia moment
(Rotational speed of crank 6000 rpm)

1 Perfect balance
2 Static balance
3 Rotation balance
4 Half balance
5 Over balance

Figure 7 – Theoretical Results from Ishida and Matsuda

Figure 7 shows the unbalanced forces for a conventional single cylinder engine can be reduced in the direction of the cylinder axis (Figure 7, line 5) by

over-balancing the crankshaft. However, this comes at the cost of dramatically increasing the vibration perpendicular to the cylinder axis (Figure 7, line 5). The more commonly used half balance (Figure 7, line 4) can accomplish the same beneficial result in the perpendicular axis but suffers in the direction of the cylinder axis vibration. In a conventional single cylinder engine “there is no way to completely eliminate the reciprocating unbalance with a single, rotating counterweight,” (Norton, 2005). In a balanced GHE however this problem is solved because the unbalanced inertia forces are zero (Figure 7, line 1) in both the vertical and horizontal directions when balanced properly. In single cylinder applications the ability to theoretically perfectly balance a GHE is arguably the largest advantage over a conventional slider crank engine.

Ishida extended his work into prototype engines to verify the theoretical results and validate his predictions are correct. Using another two stroke engine as a platform he tests multiple balance approaches and finds the perfectly balanced GHE performed very well compared to all other common slider crank balancing techniques. See Figure 8 (Ishida & Matsuda, 1975).

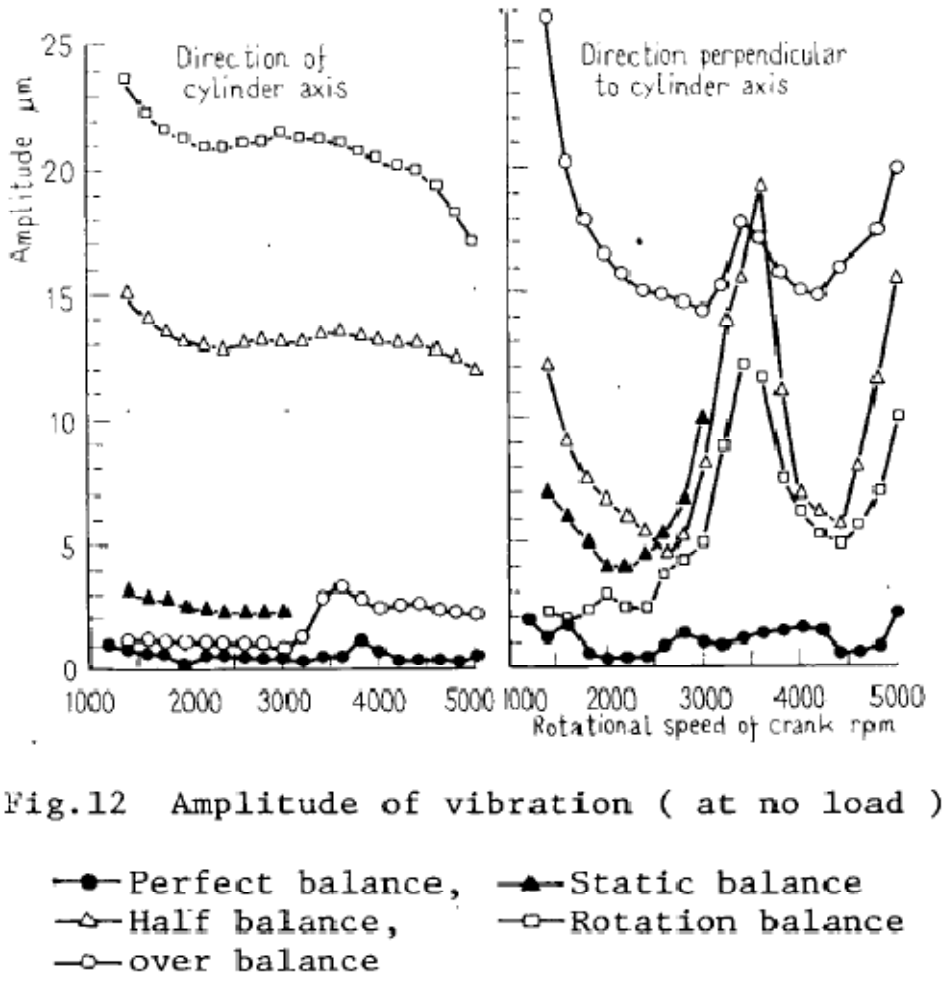

Figure 8 – Experimental Vibration Results of a Two-Cycle Engine

The perfect balance line is the GHE prototype engine built by Ishida and his team. The vibration level is far lower especially in the direction perpendicular to the cylinder axis. The over balance design almost matches the vibration performance of the GHE in the direction of the cylinder axis but not in the direction perpendicular to the cylinder axis. It can also be seen here that natural frequency excitement at just over 3000 rpm is a major issue except in the GHE. The overall vibration level is much lower for the GHE and this is a strong competitive advantage in chainsaws and other handheld power tools.

Ishida also looked at vibration amplitude vs. crank angle at a fixed, motored 1800 rpm for the same group of engines (See Figure 9).

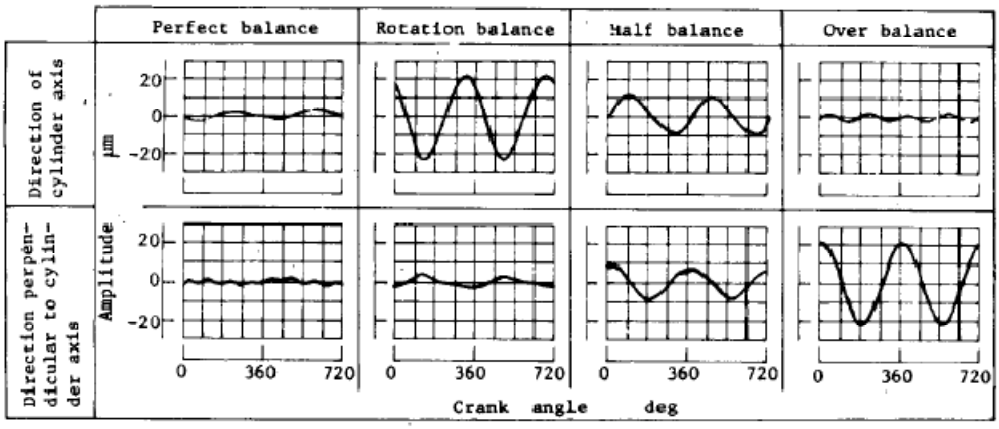

Fig.13. Wave form of vibration amplitude
(At no load, rotational speed of crank 1800 rpm)

Figure 9 – Vibration Amplitude vs. Crank Angle at a Fixed 1800 rpm

Figure 9 (Ishida & Matsuda, 1975) provides further evidence of the superior vibration performance of the GHE. In all other balance approaches there is always a tradeoff between the direction of vibration and magnitude. If vibration in all directions must be kept to a minimum the half balance design is arguably second best to the GHE. One tradeoff to achieving perfect balance in a GHE is that it requires significantly more mass in counterweights assuming equivalent piston and rod mass. For this reason it would be a challenge to build a perfectly balanced GHE equal in size and mass to a half balance slider crank engine (all else being equal). However, if low vibration is a dominating design consideration and size/mass less so, then a GHE could be an attractive alternative.

Ishida also studied the power and efficiency of a 63 cc hypocycloid chainsaw engine compared with its slider crank equivalent. In dynamometer testing he found the following (Ishida & Yamada, Research on a Two-Stroke Cycle Single

Cylinder Vibrationless Reciprocating Engine Chain Saw Utilizing an Internal Gear System, 1986):

- Hypocycloid peak power was 2.0 kW (2.7 hp) at 6400 rpm with a brake specific fuel consumption (BSFC) of 751.5 g/hp•hr.
- Conventional slider crank power was 2.5 kW (2.25 hp) at 7000 rpm with a BSFC of 295 g/hp•hr.

Ishida concludes the reduced performance of the hypocycloid version is due to larger crankcase volume resulting in a lower primary compression ratio (PCR).

Expanding on the work by Ishida, Norman H. Beachley and Martha A. Lenz published “A Critical Evaluation of the Geared Hypocycloid Mechanism for Internal Combustion Engine Application” (Beachley & Lenz, 1988). This paper provides a clear explanation of the method used to attain perfect balance using two sets of counterweights. Others discovered the method but Beachley and Lenz clearly summarize the balance technique. In a slightly different form, the described dual counterweight balancing method was used in this work to balance the Wiseman prototype provided by WTI.

Another excellent contribution to the study of GHE’s comes from authors David M. Ruch, Frank J. Fronczak, and again Norman H. Beachley (Ruch, Fronczak, & Beachley, 1991). Their paper “Design of a Modified Hypocycloid Engine” provides a list of proposed benefits, design equations, and introduces another version of the basic GHE called the modified hypocycloid engine. The authors find that the modified hypocycloid engine, which has a third gear, reduces overall individual gear tooth loads. The authors reiterate that the basic GHE is a sinusoidal engine that allows for perfect balance.

Mr. Ruch and his team also explain that there is a significant reduction in piston assembly friction because the GHE piston should not require skirts. In a conventional slider crank engine piston skirts are necessary to manage side loads. Side load is produced when the connecting rod articulates causing a component of the gas force to push the piston perpendicular to its intended path and into the cylinder wall. Using typical friction loss data from other studies, Mr. Ruch estimates a 1.97% reduction in mechanical losses is possible by eliminating piston side load piston and reducing skirt area. A 1.97% reduction in overall mechanical losses results in an equivalent improvement of overall mechanical efficiency.

In 1998 researchers from Italy, M. Badami and M. Andriano, published work on the design and testing of a full crank 125cc two-stroke hypocycloid engine (Andriano, 1998). Their design takes advantage of the linear path of the connecting rod and incorporates a seal around the connecting rod to isolate the crankcase from the top end. The engine ran well enough for low and medium load tests on a dynamometer. Power levels reached almost 5 kW (6.8 hp) at 6000 rpm and were still climbing. Unfortunately the bottom end suffered from thermal issues at high speeds. The thermal issue prevented thorough testing at full load and high output. A cutaway view of the engine is shown in Figure 10.

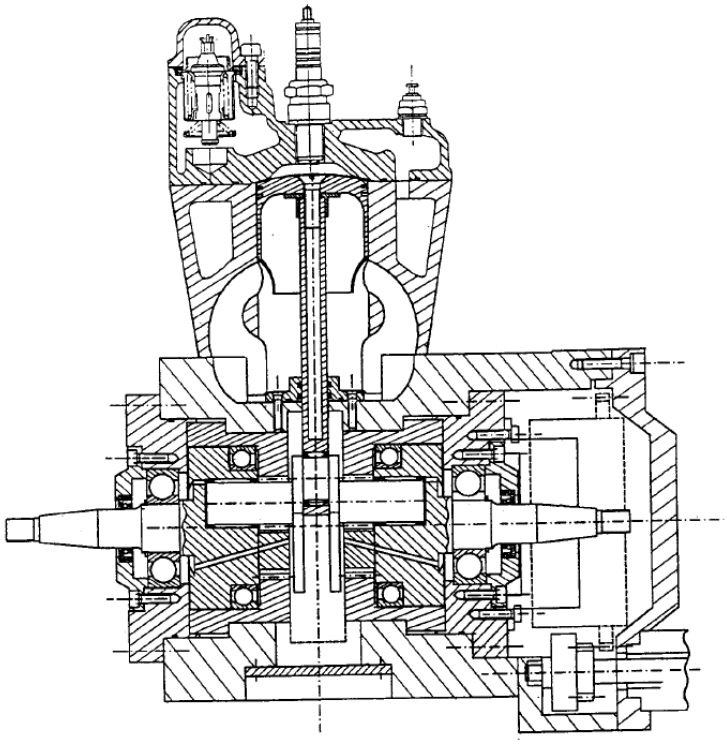

Figure 10 – Section View of 125cc Two-Stroke GHE from (Andriano, 1998)

One of the most recent compressive studies of GHE's, authored by Jukka Karhula in 2008, provides extensive insight into the comparison of slider crank and hypocycloid engines of equal dimensions (stroke, bore, etc…) (Karhula, 2008). Making some typical assumptions for slider crank engines (range given depends on stroke length) Karhula used mathematical models to predict the following for hypocycloid engines:

- Maximum piston velocity is 3 to 8% lower in the hypocycloid engine
- Maximum piston acceleration is 20 to 30% lower in the hypocycloid engine
- The maximum gas torque is 13 to 22% smaller in the hypocycloid engine.
- The mean gas torque is 8 to 15% smaller in the hypocycloid engine.

Chapter 3

SCOPE OF WORK

Wiseman Technologies Inc. (WTI) completed extensive design, development, and some testing of the Wiseman prototype engine prior to handing it over for this research effort. The objective in this effort was to further evaluate and develop the Wiseman engine according to industry standard methods. The Wiseman prototype engine was designed around a production 30cc Homelite brand string trimmer engine. An unmodified 30cc Homelite engine was also provided by WTI and used in this research effort to establish benchmark performance data to evaluate the Wiseman engine against. The unmodified 30cc Homelite string trimmer engine is hereafter referred to as the “stock” engine. It should be noted that the Wiseman prototype retains many of the same engine components and dimensions as the stock production engine. A side-by-side photo of the two engines is shown in Figure 11 and a summary of their design specifications is detailed in Table 1.

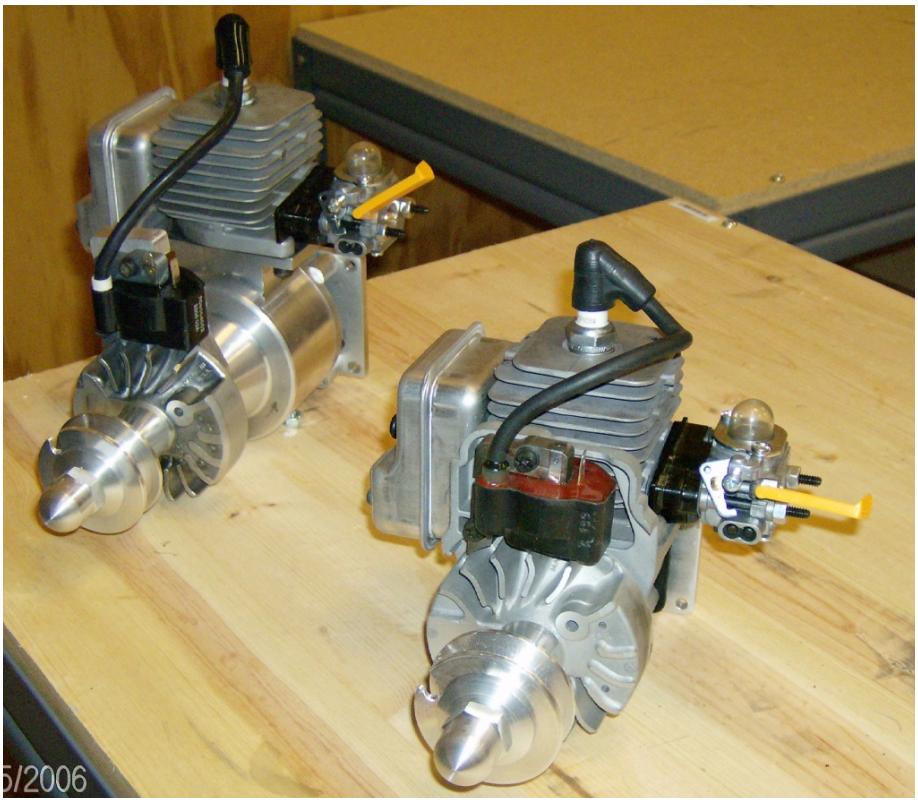

Figure 11 – Wiseman (left) and Stock Engine (right)

Note that the stock and Wiseman engines used for testing share the same carburetor, ignition system, flywheel/magneto, exhaust/muffler, and cylinder.

Engine	Stroke	Bore Ø	Displacement
Wiseman Prototype	1.125 in (28.6 mm)	1.435 in (36.5 mm)	1.819 in^3 (29.81 cc)
Stock Homelite	1.114 in (28.3 mm)	1.435 in (36.5 mm)	1.802 in^3 (29.53 cc)

Table 1 – Engine Specifications

The majority of the prior research and development by WTI on these two engines focused on fuel efficiency in low speeds at less than wide open throttle operation. The results of some of the testing and development completed by WTI are discussed further in Objective 2 below. Balancing, efficiency and peak performance at typical operating speeds had not been thoroughly researched and was therefore a major focus of this research effort.

Objective 1: Analyze and Balance the Wiseman Engine

In single cylinder applications one of the most desirable advantages of the GHE over a slider crank design is the ability to obtain perfect balance. The first major task was to explore, understand, and optimize the overall balance of the Wiseman prototype to ensure this advantage was realized. To compare the balance characteristics of the Wiseman prototype a thorough analysis of the stock engine was necessary and carried out. To accomplish these tasks the following steps were executed on both engines in the order listed:

1. A dynamically accurate solid assembly model was generated in Solidworks CAD software.
2. Models were imported into Solidworks motion simulation to predict shaking forces and directions at a specific engine speed.
3. Simulation outputs were compared.
4. The physical engines were mounted and motored to measure actual vibration using accelerometers.
5. Feasible design modifications were developed to improve balance of the Wiseman prototype.
6. Components were manufactured or modified to obtain improved balance of the Wiseman prototype.

7. Another motored vibration analysis was carried out on the Wiseman engine after the balancing modifications to validate improvements.

Similar work has been published on GHE engines by other researchers on the balance of full crank hypocycloid engines. However, the Wiseman prototype is fundamentally different from other GHE prototypes analyzed by other research efforts. The stock and Wiseman engines are half-crank designs, meaning the crankshaft is supported by bearings on one side only (Figure 12) and there is only one crankshaft counterweight. The counterweight is offset from the piston cylinder centerline. The offset causes an imbalanced shaking moment that required a unique three dimensional balancing effort of the Wiseman engine.

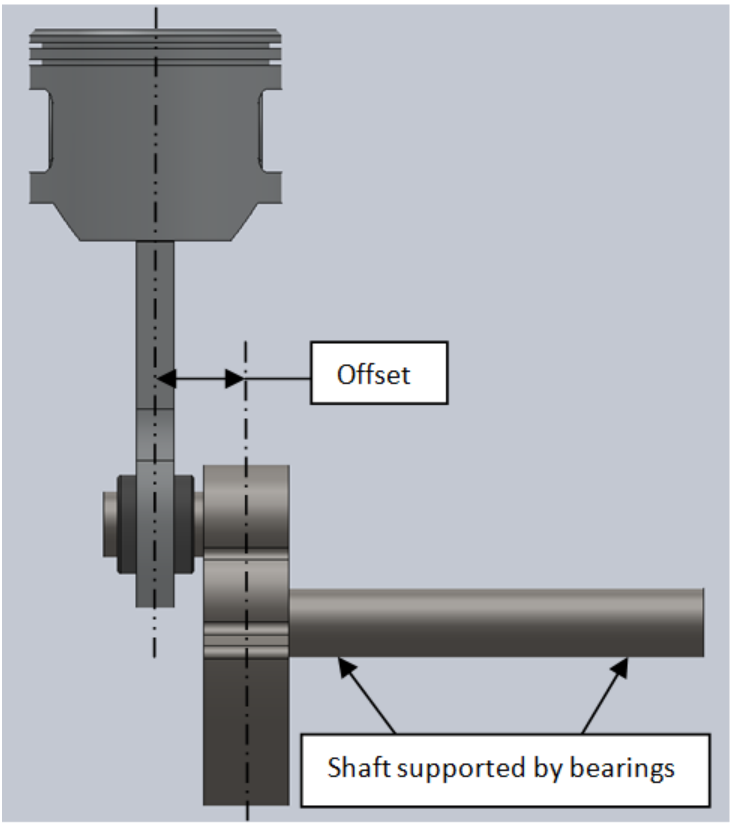

Figure 12 – Half-Crank Engine Design

A half-crank engine design is generally used in low cost and lightweight engines. The shaking moment is generally allowable and small in a slider crank design because the centerline of the piston is a small distance from the crankshaft counterweight centerline. However, the Wiseman engine design requires a larger offset resulting in a larger shaking moment. The degree to which it is larger was investigated and additional balancing techniques were explored to reduce the Wiseman engine shaking moment.

Objective 2: Peak Power and Efficiency Analysis

The Wiseman engine was provided by WTI in good running condition and had undergone some testing by WTI prior to the start of this research effort. This prior testing was done at speeds (about 4000 rpm) well below the typical peak power speed of this style of engine (about 7000 rpm). WTI's testing method showed the Wiseman engine could achieve roughly double the fuel efficiency of the stock engine at these low speeds. An understanding of the method and results of prior testing by WTI was important for deciding what type of testing was to be carried out in this research effort. The methods and results obtained by WTI are included here for historical background purposes and summarized by WTI below:

"Due to the simplicity of the engine and ease of modification, a standard 30cc Homelite 2 cycle engine was modified with the Wiseman mechanism and compared to a stock engine. The engines are identical in all respects, with the exception of the Wiseman mechanism. For this test, the <u>same</u> carburetor, spark plug, and exhaust system (not identical ones) were used on each engine. The engines were both brand new and were each broken in for 2 hrs at 4,000 RPM, with regular gas and manufacturer's recommended 30:1 2-cycle oil. After break

in the fuel was changed to Shell High Test, and AMS synthetic oil was used at 100/1. For this test the engines were run on the same day with temperature and barometric pressure almost identical. Engine RPM's were set for the test at 4,050 and verified by tachometer. The load was identical for each engine (the same 20" X6 wooden propeller). Once each engine reached stable RPM, cylinder head temp was measured by thermocouple, and fuel weight was noted. A series of 6-minute runs was conducted on each engine to measure and compare fuel consumption.

***(Aside**: Because the engine with the Wiseman mechanism installed ran so much cooler than the stock motor, the cylinder head with standard cooling fins had to be shrouded with aluminum sheet to get the temperature up to roughly equal that of the stock motor.)*

The average 6-minute fuel consumption for the stock motor running with an average cylinder head temperature of 310˚F was 27.67 grams.

The average 6-minute fuel consumption for the motor with the Wiseman mechanism installed, running with an average cylinder head temperature of 320˚F, was 14.00 grams.

The improved fuel efficiency realized with the Wiseman mechanism in this comparison test is 50.5%!

This Wiseman engine, while producing the same power output will run virtually twice as long as the identical stock engine on the same amount of fuel! This same comparison testing has been independently verified and documented on two other occasions." (Wiseman Technologies, Inc.)

A photo of the two test engines used by WTI and in this research effort is shown in Figure 13. A photo of one of the fuel efficiency test sessions carried out by WTI is shown in Figure 14.

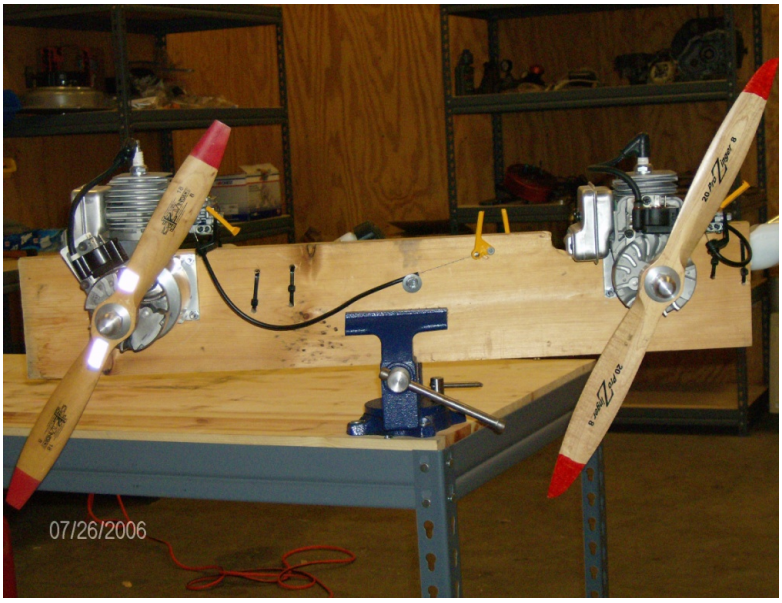

Figure 13 – Wiseman and Stock Engine (Wiseman Technologies, Inc.)

Figure 14 – WTI Fuel Efficiency Test Run

These tests proved to be very valuable in helping to validate the potential efficiency gains possible with a Wiseman engine. The following items should be noted however with respect to these prior tests by WTI:

- The tests were performed at only 4050 rpm but the stock engine, and most engines of this type, are designed to idle near 3000 rpm and produce peak output near 7000 rpm. The reported efficiency advantage of the Wiseman could improve or worsen when the engines are run closer to their true design speed at wide open throttle.
- Like many two-cycle engines, the crankcase is a working chamber that inducts the fuel-air charge and then pumps it into the combustion chamber through transfer ports. The volume of the crankcase determines the crankcase or primary compression ratio (PCR) which affects the performance and efficiency of the engine. The crankcases of these two engines are not the same in volume and therefore have different PCR's.

Because of these issues it is difficult to attribute the improvement in fuel efficiency to the Wiseman mechanism alone. It is also difficult to define which design features or settings of the Wiseman resulted in an efficiency gain and by how much. The single and low speed testing is also not ideal if peak power is important to the end user of these engines.

Further tests were proposed and carried out in this research effort in an attempt to better compare the performance of the Wiseman engine to the stock engine. The goal was to control and minimize variables between the two engines. The desired output of the proposed tests for Objective 2 included

- Brake Specific Fuel Consumption (BSFC) measured at maximum output
- Power versus rpm curves
- Motoring friction
- Output torque vs. crankshaft angle for given cylinder pressure.

To achieve the outcomes above, unique test equipment was developed and utilized. High rpm and full load testing was carried out to better understand performance closer to the original design speed. For efficiency testing, a state of the art engine test lab and dynamometer was made available by MTD Southwest Inc. in Chandler, Arizona. For peak power testing a modified off the shelf dynamometer was developed and used extensively to test and tune both engines for maximum performance. A variable speed electric blower was used to provide cooling air so engine temperature could be controlled independently of engine rpm, load and engine type.

A custom motoring test fixture was designed and constructed to evaluate and compare motored losses of the stock and Wiseman engine. The custom designed engine test fixture allowed measurement of the following:

- Motoring losses
- Static output torque while supplying a know pressure on the piston

A more detailed description of the test equipment designed and constructed is included in Chapter 5.

30cc Wiseman Engine Background

A nearly complete section view of the dynamic CAD model for the Wiseman prototype is shown in Figure 15.

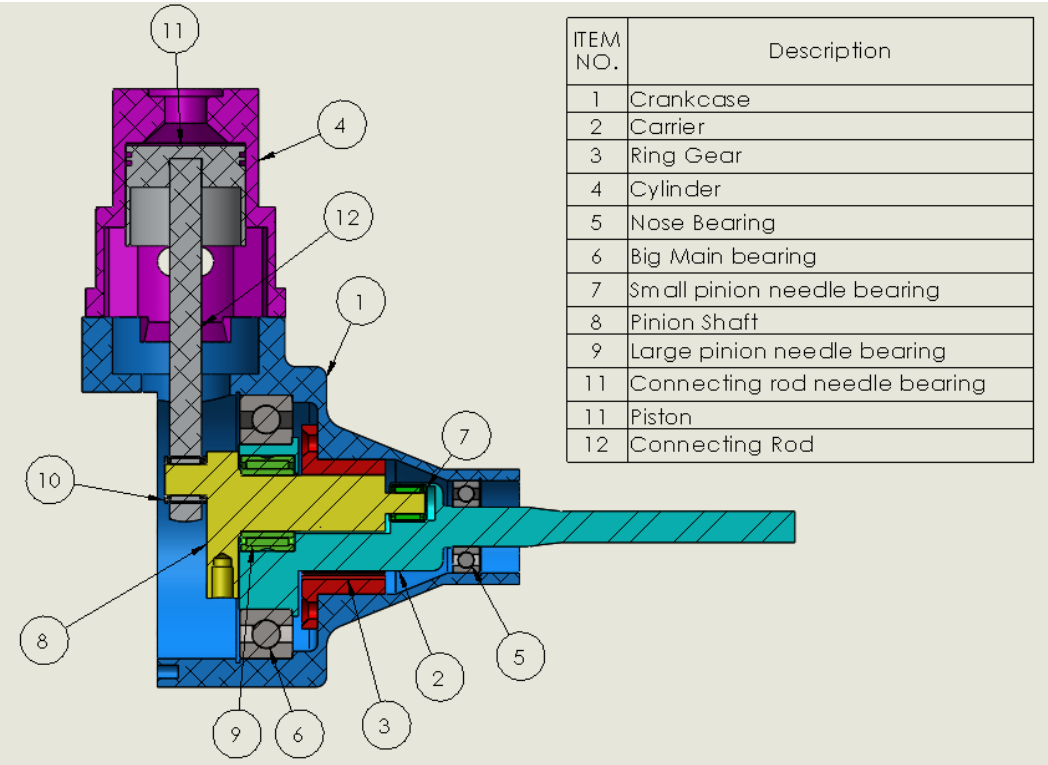

ITEM NO.	Description
1	Crankcase
2	Carrier
3	Ring Gear
4	Cylinder
5	Nose Bearing
6	Big Main bearing
7	Small pinion needle bearing
8	Pinion Shaft
9	Large pinion needle bearing
11	Connecting rod needle bearing
11	Piston
12	Connecting Rod

Figure 15 – Wiseman 30cc Prototype Section View

The engine back plate, spark plug, front shaft seal, rings, and cylinder cooling fins are not shown in Figure 15. Item 5 and Item 6 are the main support bearings for the carrier shaft and held laterally in place by internal cir-clips in the crankcase (also not shown). The crankcase (Item 1) was machined from 6061-T6 billet aluminum and is the main support structure for the engine. Item 4 is the cylinder shown without cooling fins and is the same cylinder used by the stock engine. Item 11 is the piston (machined from 6061-T6) and threads onto Item 12, the connecting rod (also 6061-T6), using undercut threads for a friction fit. Item 10 is the connecting rod bearing which is secured with a mild press fit and

Loctite into the base of the connecting rod. The carrier shaft is the main output shaft of this engine and is 1045 steel. Item 8 is the pinion shaft (also 1045 steel) and provides multiple, vital functions in the operation of the Wiseman engine. It comprises the external gear teeth, a counterweight, and the bearing surfaces for the connecting rod and carrier shaft. Item 3 is the ring gear, and includes the internal teeth the pinion shaft teeth mesh with. The pitch diameter of the pinion shaft gear and the ring gear are a 2:1 ratio in order to achieve linear motion. The pinion shaft pitch diameter is 14.2875 mm (0.5625 in) and the ring gear pitch diameter is 28.575 mm (1.125 in) resulting in a stroke of 28.575 mm (1.125 in). The meshing gear teeth are not obvious in Figure 15 but can be easily seen in Figure 16. Figure 17 is an isometric view of the Wiseman engine. Figure 18, Figure 19, Figure 20, and Figure 21 represent snapshots of the engine moving through one full rotation at 90º increments. Note that the connecting rod remains vertical and the pinion shaft is both rotating and oscillating vertically. It is also worth noting here that the pinion shaft rotates in the opposite direction of the carrier shaft at the same speed. If follows then that the pinion shaft bearings must be designed to manage the load at a speed equal to twice the output shaft speed.

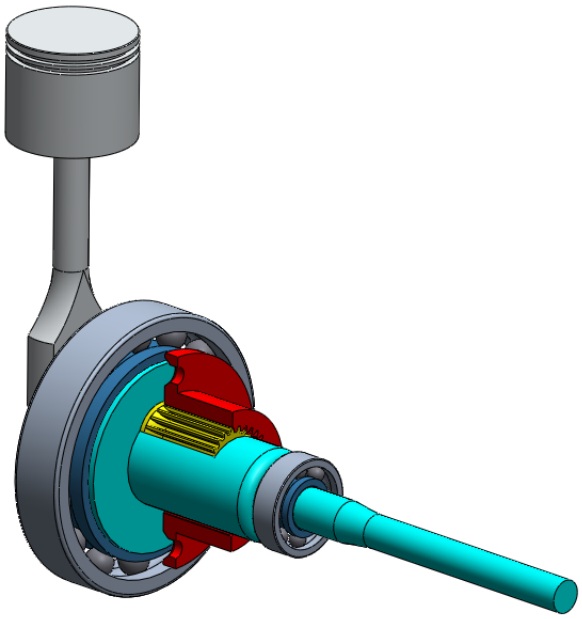

Figure 16 – Wiseman Driveline

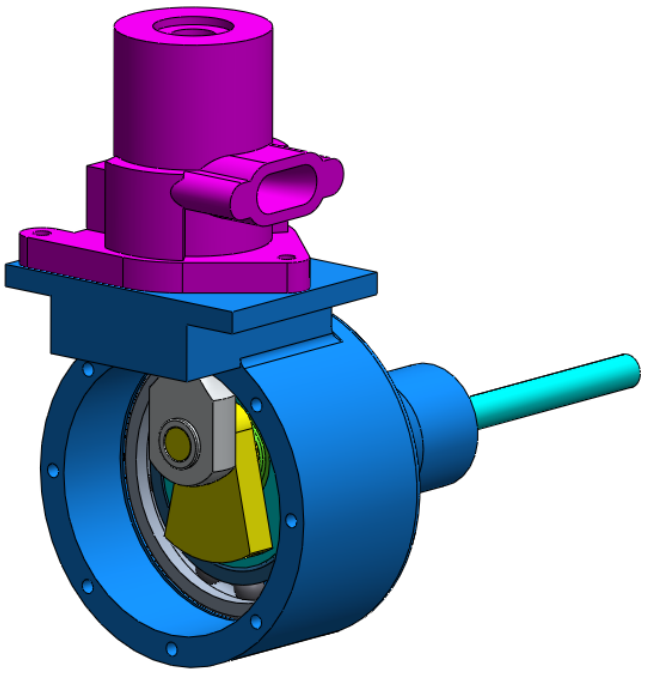

Figure 17 – Isometric Assembly View, Right Rear

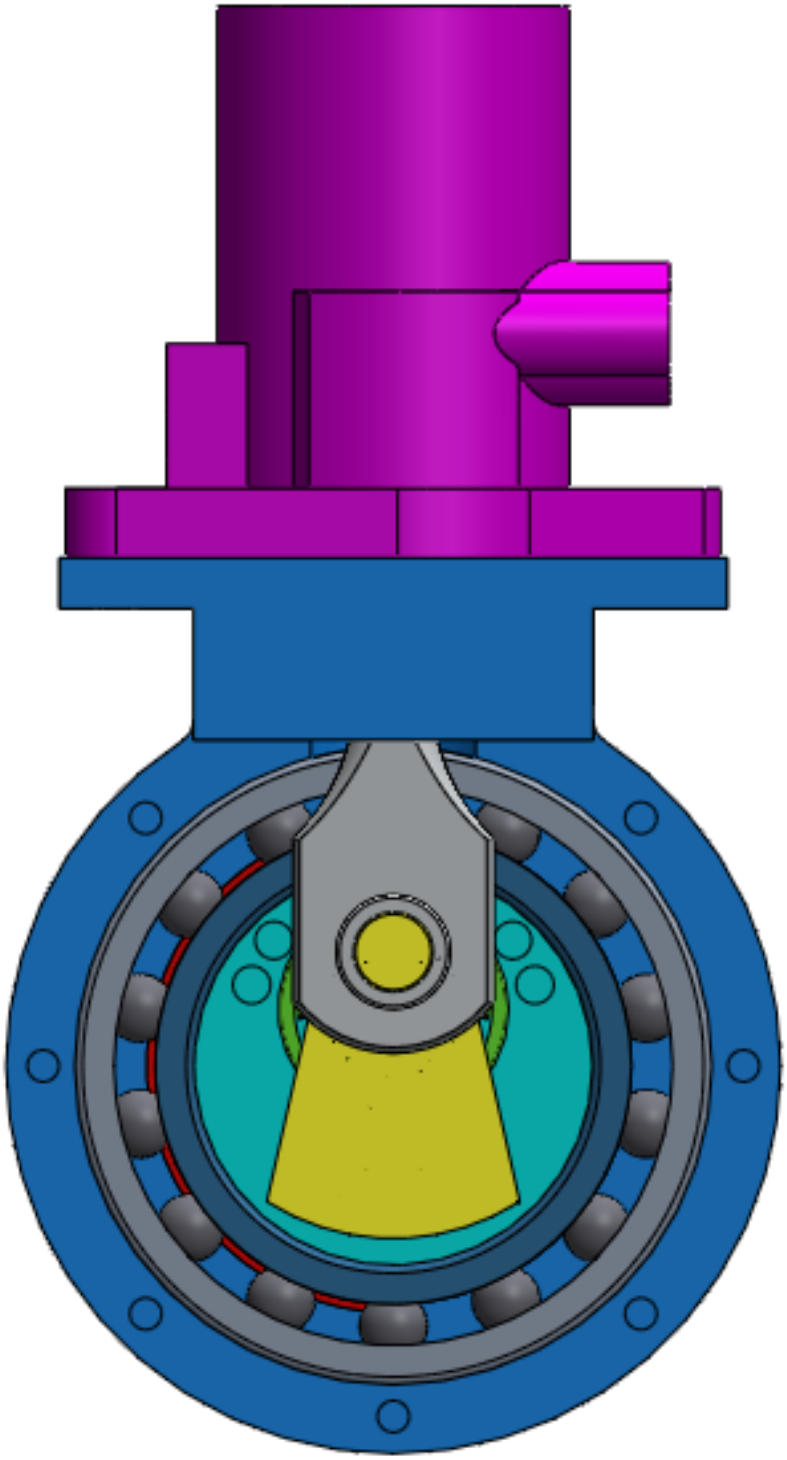

Figure 18 – Back View, Engine at TDC

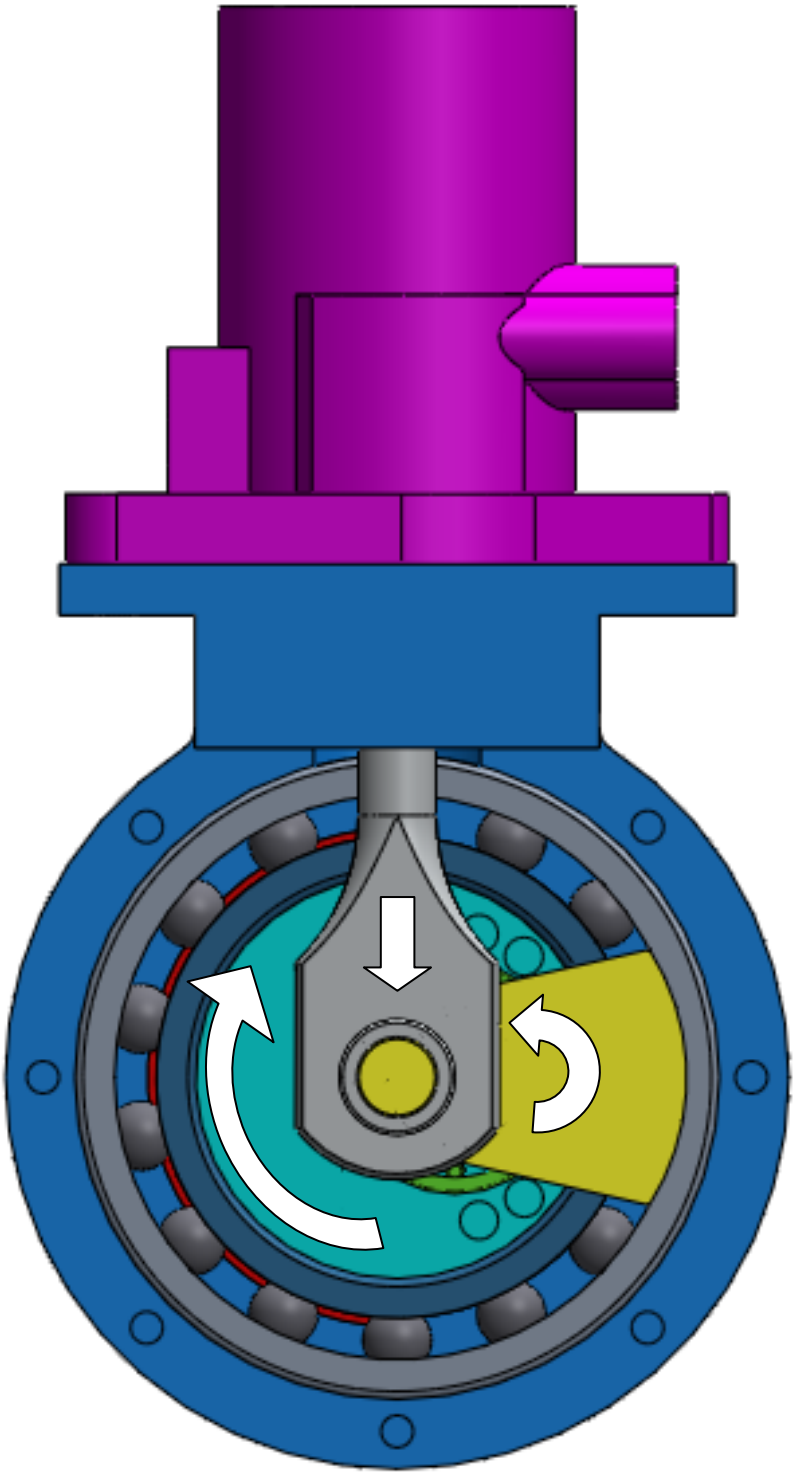

Figure 19 – Back View, Engine at 90º ATDC

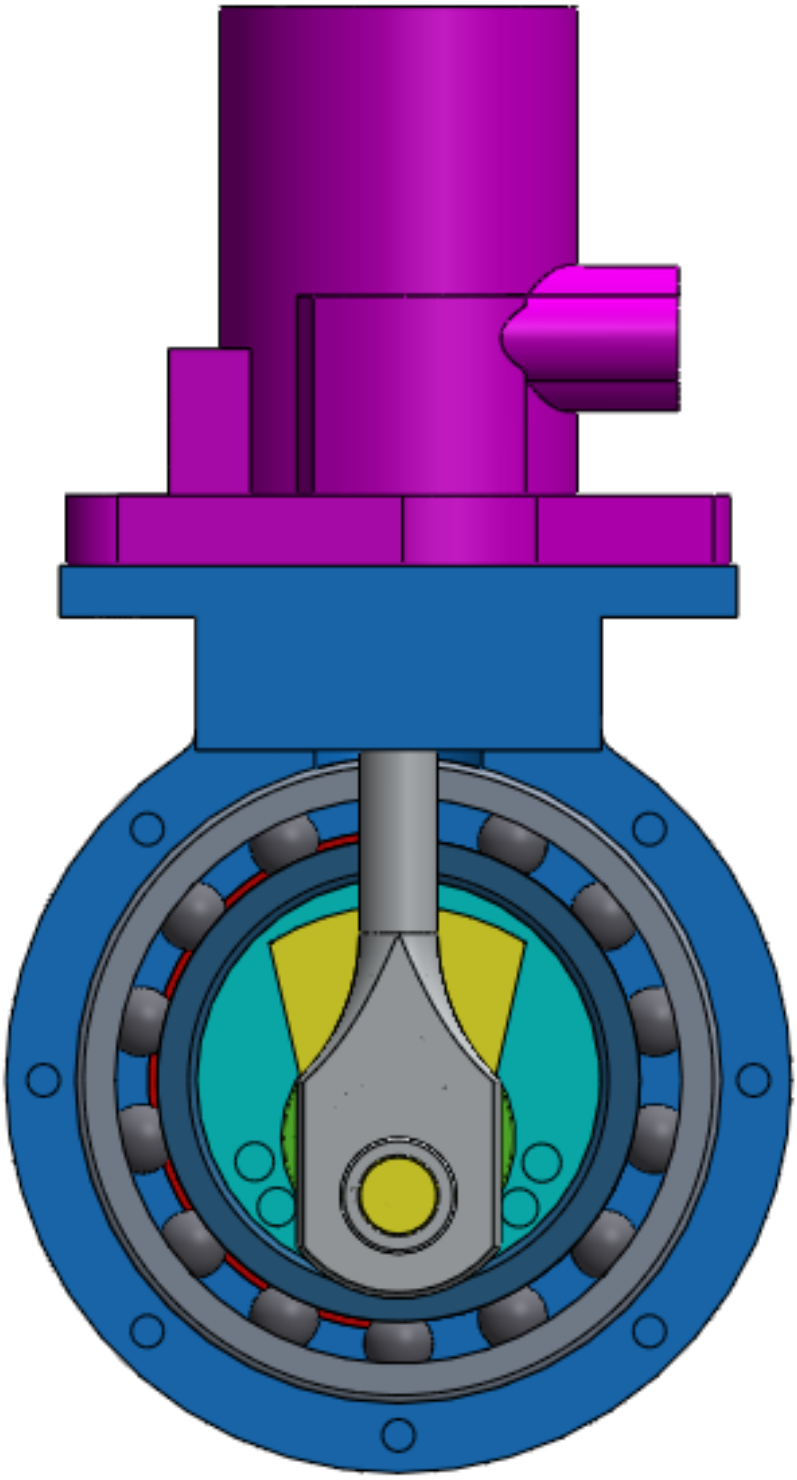

Figure 20 – Back View, Engine at BDC

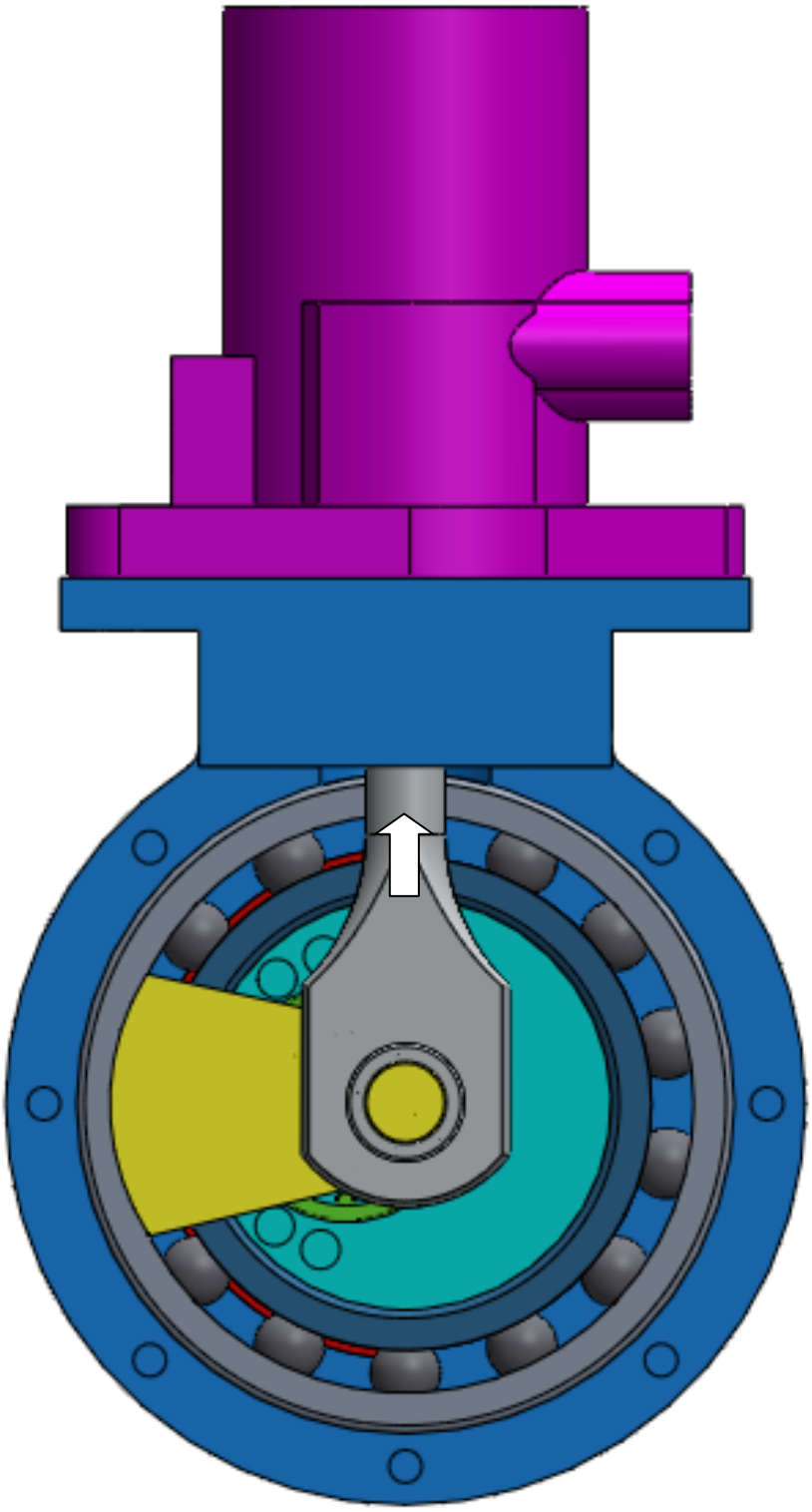

Figure 21 – Back View, Engine at 270º ATDC

Chapter 4

ENGINE BALANCE

Perfect Balance Approach

The balancing method for a hypocycloid engine is unique and requires a different approach than that of a slider crank engine. The basic method used to statically balance a single cylinder hypocycloid engine in a single plane can be seen graphically in Figure 22 adapted from (Ifield).

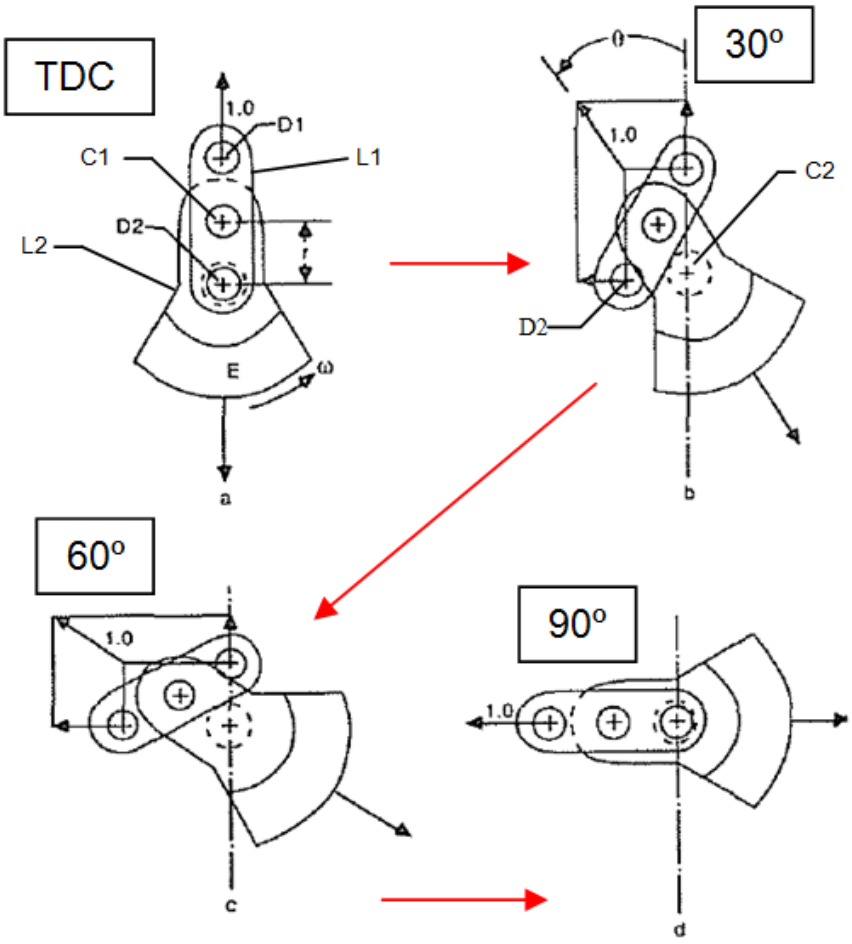

Figure 22 – Balance Approach Adapted from (Ifield)

The four diagrams represented in Figure 22 are in 30-degree increments of output shaft rotation starting in the upper left where the piston is at top dead

center (TDC). The total output rotation shown is only the first 90º but it is possible to extend this concept for a full rotation. The link L2 is analogous to the crankshaft of a conventional engine and is responsible for the output rotary motion. The link L1 is attached to and rotates the pinion gear in the opposite direction of L2 at the same rpm. As noted earlier, the relative speed of the two shafts is double that of engine rpm. The total stroke of this hypocycloid mechanism from TDC to Bottom Dead Center (BDC) is four times the distance r.

According to (Beachley & Lenz, 1988), (Ifield), and (Ishida & Matsuda, 1975), when attempting perfect balance in the plane shown in Figure 22 it is dynamically equivalent to assume that the mass of the piston and connecting rod assembly is concentrated at D1. Therefore, the mass distribution of the piston and connecting rod do not require consideration except as an equal point mass located at D1. The first step in balancing this mechanism is to focus on the total mass located at point D1, which includes the piston and connecting rod mass. This dynamic equivalent concentrated mass is rotating about point C1 and therefore generates an inertial force that is highest at TDC. Note that even as D1 is rotating about C1 it remains on the vertical centerline at all times. In order to balance the mass at D1 a second mass at D2 is sized and located such that the center of mass (CM) of D1 and D2 is located at C1. This CM location at C1 allows the combined masses of D1 and D2 to be assumed dynamically equivalent when concentrated at C1. The inertial forces generated by D1 and D2 when vector summed together act in line with points C1 and C2 at all times. This inertial force can then be balanced by placing a counterweight E with its CM located 180º and equidistance (r) from C1. The inertial force vectors will then cancel and perfect balance is achieved in the plane shown.

This concept is applicable to the Wiseman 30cc prototype. Link L2 and L1 in are equivalent to the carrier shaft and pinion shaft, respectively, in the Wiseman Engine. The points D1, D2, C2 and C1 from Ifield's drawing have been translated to the Wiseman Engine in Figure 23.

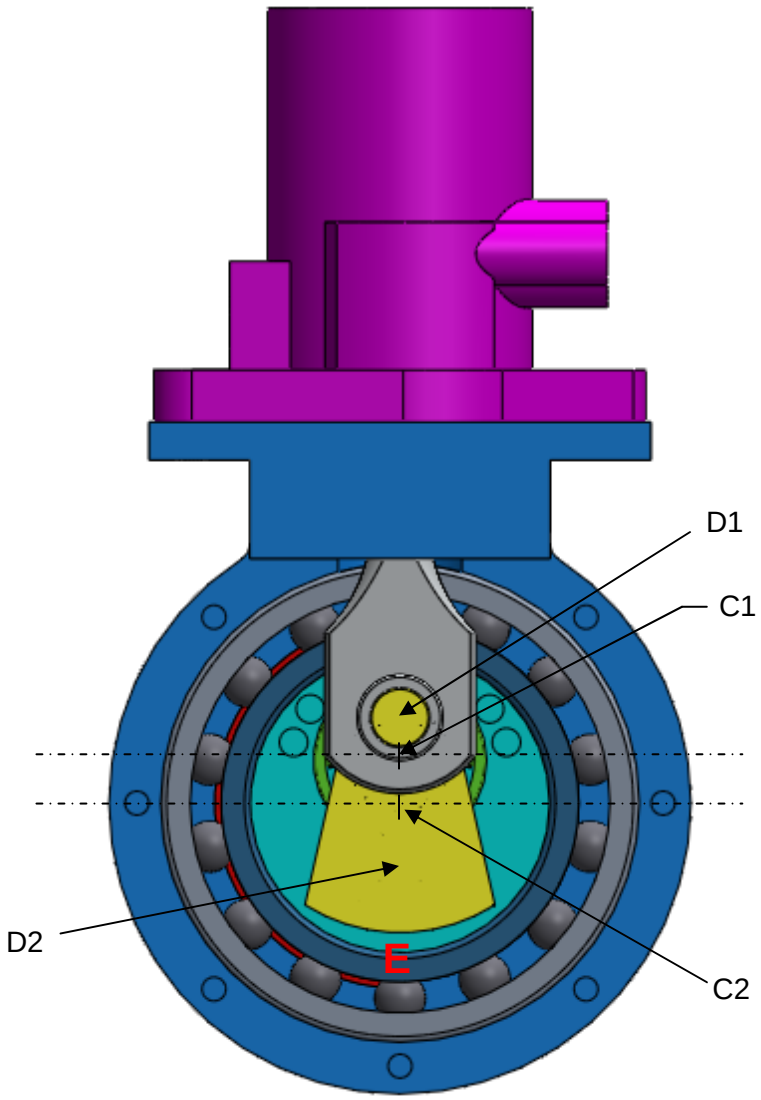

Figure 23 – Ifield's Concept Translated to the 30cc Wiseman Engine at TDC

Motion Simulation Vibration Study

The goal for the motion simulation vibration study was to evaluate how much improvement could be gained and what was ultimately possible by applying the hypocycloid balance technique to the Wiseman prototype. However, because the Wiseman Engine is a half crank design it was expected behave differently than hypocycloid engines of past research efforts.

The analysis began with modeling and simulating the Wiseman prototype in order to establish a balance baseline and compare it with the stock engine. WTI was not aware of this balancing technique when designing the Wiseman engine so it was unlikely perfect balance was already integrated into the original design.

Each individual part was first modeled in Solidworks to the same dimensions of the actual parts inside the Wiseman 30cc engine. Density properties were assigned based on part material which allowed total mass and CM locations to be determined easily from the CAD models. The predicted CAD model mass of each component was then verified by weighing the physical components. The assembly model was built in Solidworks using the individual components constrained in a way that reproduced the motion of the actual engines. The constraints and components used were assumed perfectly rigid and gear backlash was not considered.

The dynamically accurate CAD model for the 30cc Wiseman Engine is shown in many of the previous figures. The dynamically accurate model for the stock engine was also created using the same method described for the Wiseman engine. A section and transparent view of the completed model is shown in Figure 24 and Figure 25, respectively.

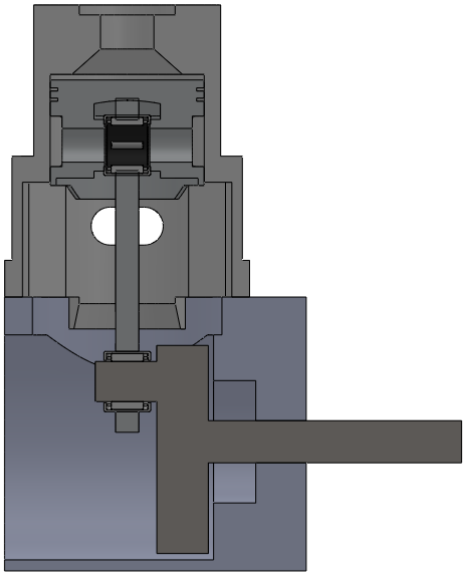

Figure 24 – Stock Engine, Section View of Dynamic Model

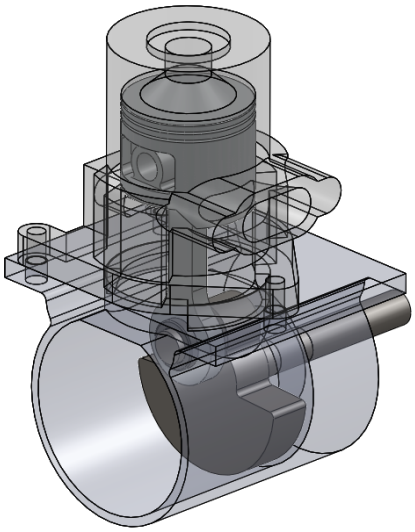

Figure 25 –Stock Engine, Transparent Isometric View

A counter-clock wise simulation motor was applied to the output shaft of each engine to rotate it at 3000 rpm. This motion simulation analysis assumed all components were perfectly rigid, crankshaft speed was constant, and inertia

forces generated by combustion were not considered. Two full revolutions of the output shaft at 3000 rpm was the total simulation duration. A rate of 5,000 frames per second was chosen. Since all components were assumed rigid the default GSTIFF integrator type was used. Screen shots of the stock engine and Wiseman simulation windows are shown in Figure 26 and Figure 27, respectively.

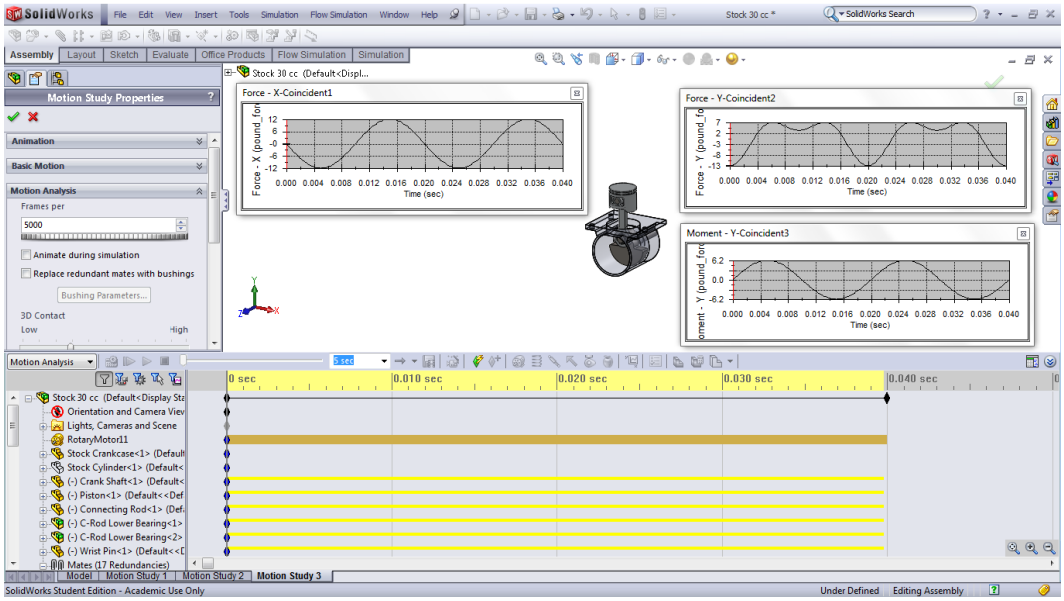

Figure 26 – Stock Engine Simulation Window

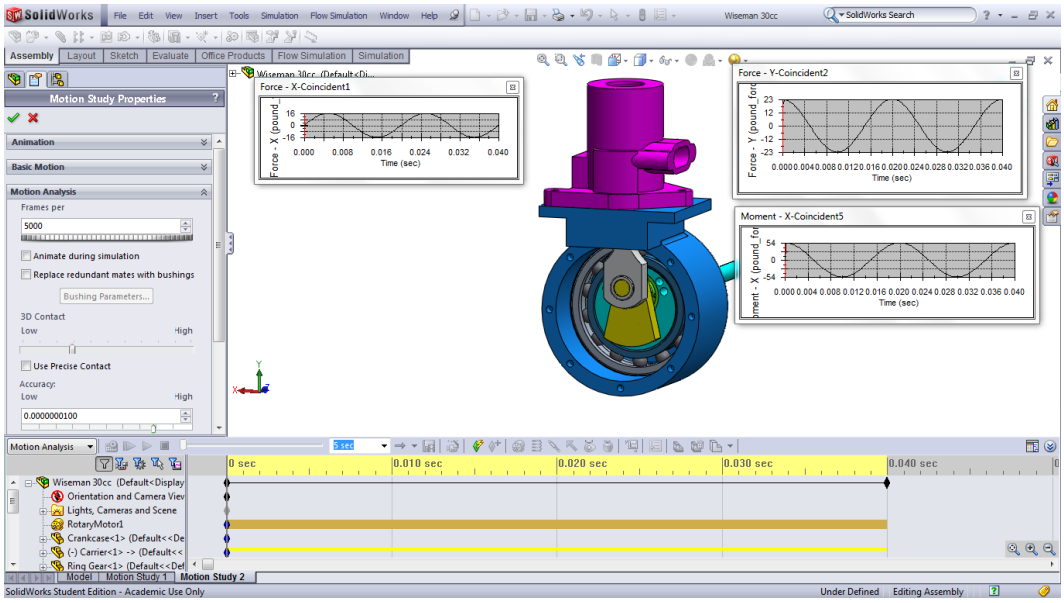

Figure 27 – Wiseman Engine Simulation Window

The desired output of these engine simulations was chosen based on the previous research by Ishida (Ishida & Matsuda, 1975). These outputs included the following versus output shaft angle:

- Y: The shaking force in the cylinder axis direction
- X: The shaking force in the direction perpendicular to the cylinder axis
- M: The shaking moment

Refer to Figure 28 for a visual representation of the coordinate system used.

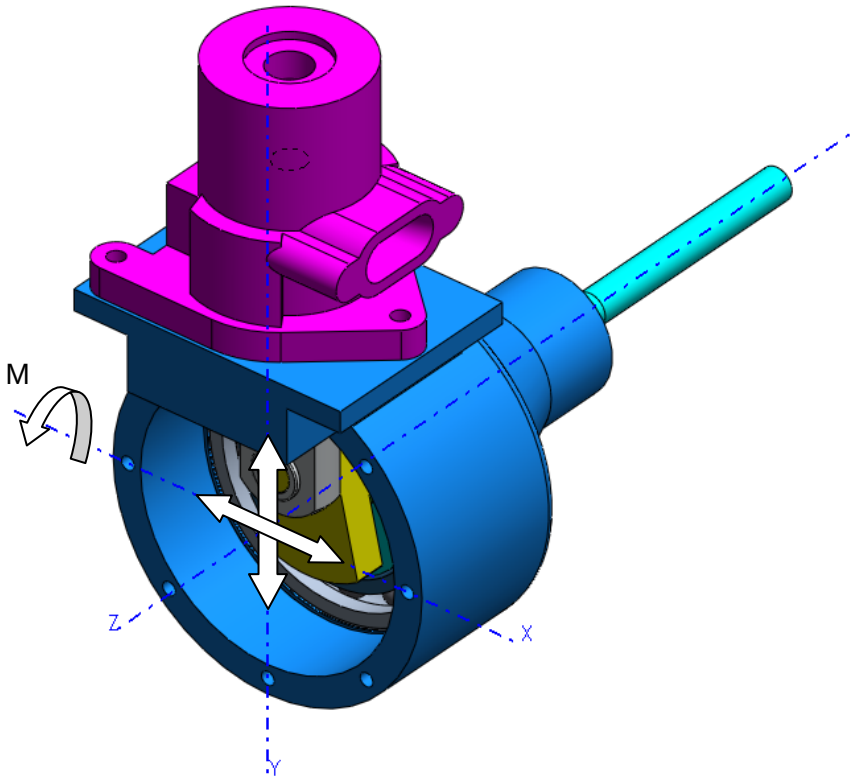

Figure 28 – Coordinate System for Simulation Outputs

The baseline simulation results for the shaking force in the X and Y directions are shown in Figure 29 and Figure 30, respectively.

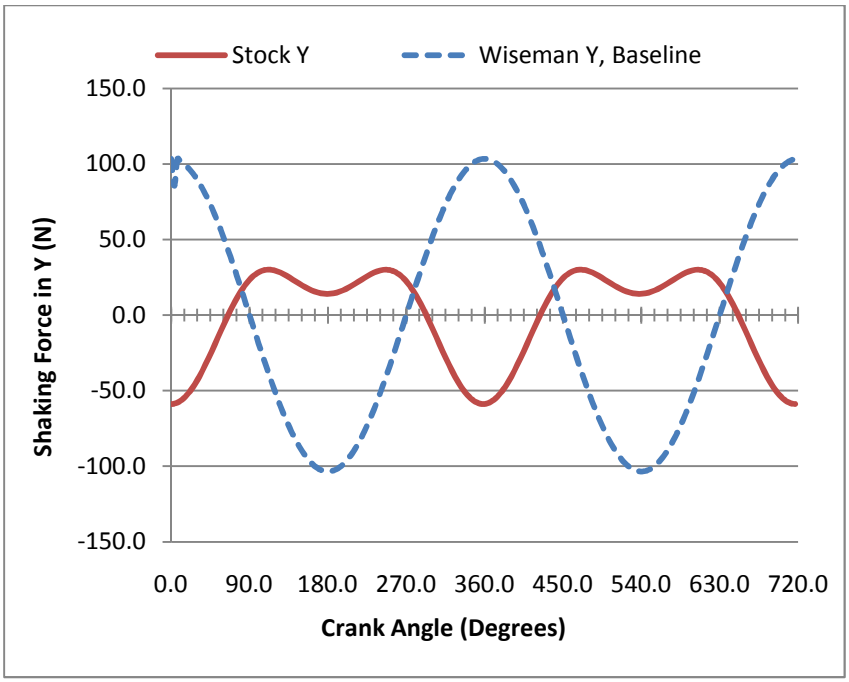

Figure 29 – Baseline Shaking Force vs. Crank Angle in Y at 3000 rpm

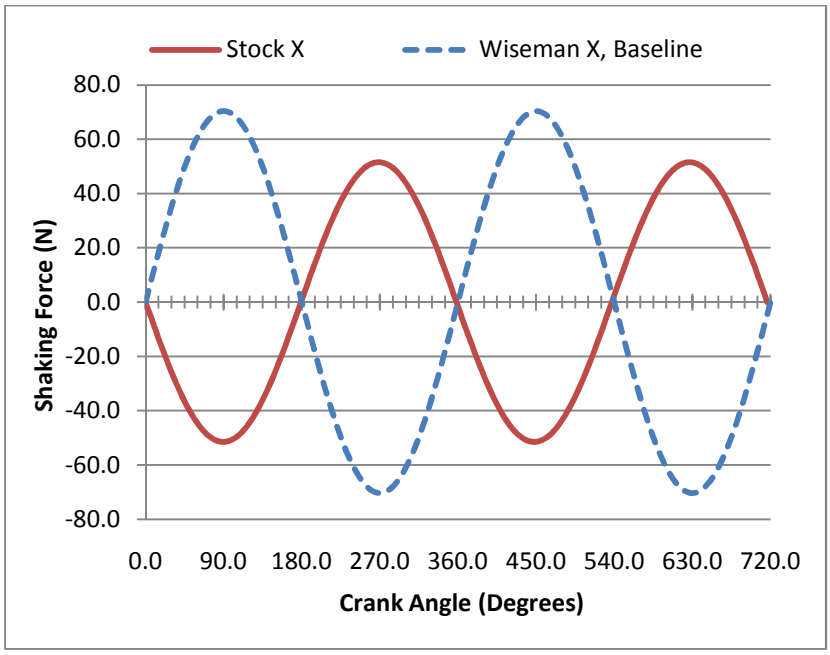

Figure 30 – Baseline Shaking Force vs. Crank Angle in X at 3000 rpm

The baseline peak shaking force of the Wiseman engine in Y was 103.5 N while the stock peak in Y was only -58.9 N. The high positive shaking force in Y

indicated a significant reciprocating imbalance in the Wiseman engine. The piston was too heavy and or the pinion shaft counterweight was too small. The peak shaking force of the Wiseman engine in X was 70.4 N while the stock peak in X was 51.6 N. The baseline results showed the Wiseman engine was not very well balanced compared to the stock engine.

These plots provide additional information about the balance of both engines. The stock engine appears to be half a balanced design. The crankshaft counterweight is sized to minimize vibration in all directions as opposed to a purely rotational balance. In a purely rotational balanced engine the shaking force is typically zero in X but very high in Y. The nearly equivalent peak value in X and Y is strong evidence of a half balance approach for the stock engine. Also apparent in the stock engine is the non-sinusoidal motion of the piston which shows up as a “dip” in the shaking force in the Y-axis direction. This dip is evidence of the second order harmonic that is difficult to balance even in multi-cylinder slider crank engines. Note that in the Wiseman engine this dip does not appear which validates the true sinusoidal motion of the piston.

Looking three dimensionally at the balance of each engine required that the simulation output include a shaking moment. The baseline predicted shaking moment, which should not be directly compared to X and Y, is shown in Figure 31.

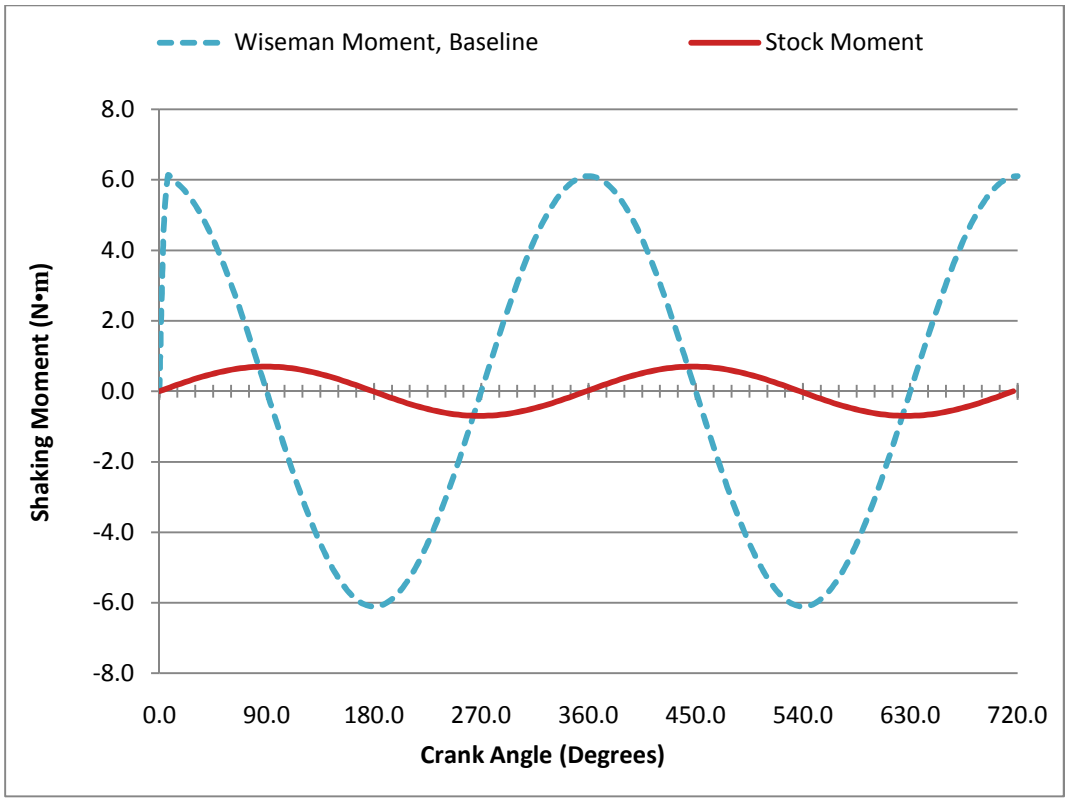

Figure 31 – Baseline Shaking Moment vs. Crank Angle at 3000 rpm

The peak shaking moment for the Wiseman engine was 6.1 N•m while the peak for the stock was 0.7 N•m. The baseline Wiseman engine shaking moment was 8.7 times higher than the stock engine initially. The higher shaking moment was due to both the imbalance in X and Y and the larger offset to piston/cylinder centerline.

Balanced Design

As expected the results of the prior analysis indicated a significant imbalance and it was worthwhile to explore modifying the Wiseman engine to obtain improved balance. The following feasibility study attempted to improve the balance of the Wiseman engine while keeping in mind the ease of modification and fabrication of components. The objective was to achieve the largest balance

improvement possible in motion simulation software first and then implement the changes on the actual engine.

Pinion Shaft Balance

According to the CAD model the total reciprocating mass, which included the piston, rod, bearing, and rings, as received from WTI was 84 grams (See Figure 32, rings not shown). The actual assembly on a digital scale also weighed in at 84 grams. Further details and dimensions of the provided Wiseman piston and rod can be seen in Figure 33.

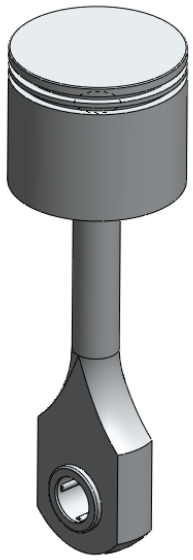

Figure 32 – Original Piston, Rod, and Bearing

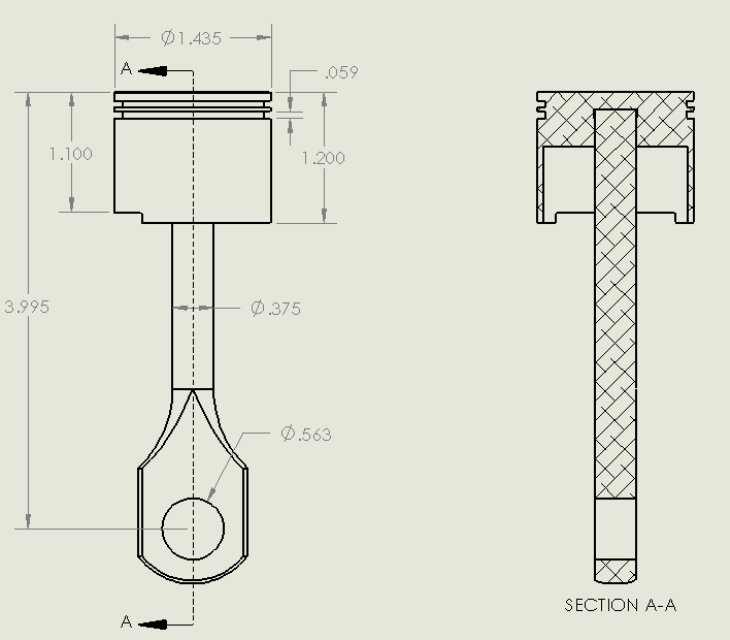

Figure 33 – Provided Wiseman Piston and Rod Assembly

Because the Wiseman piston motion is linear, dynamic equivalence is maintained when the total reciprocating mass is replaced by a bob weight mass of 84 grams located as shown in Figure 34, right. An 84-gram bob weight was created in CAD software and used to initially simplify the balance effort. The two models in Figure 34 were assumed dynamically equivalent meaning each will behave exactly the same in a dynamic balance analysis. This assumption was validated in simulation by replacing the bob weight with the piston, rod, and bearing. Identical results were obtained for the shaking moment and shaking forces in X and Y with the bob weight or the piston rod assembly.

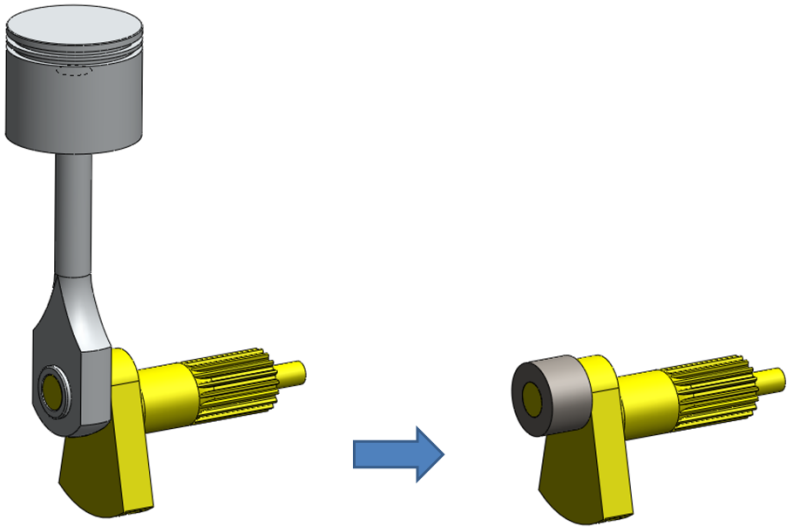

Figure 34 – Piston, Rod, and Bearing Dynamic Equivalence

The use of the bob weight made it possible to check the level of imbalance by simply finding the CM for the pinion shaft and bob weight assembly. To balance the pinion shaft the CM must be coincident with the pinion shaft centerline. The CAD model showed the CM was .689 mm (0.027 inches) above centerline (Figure 35).

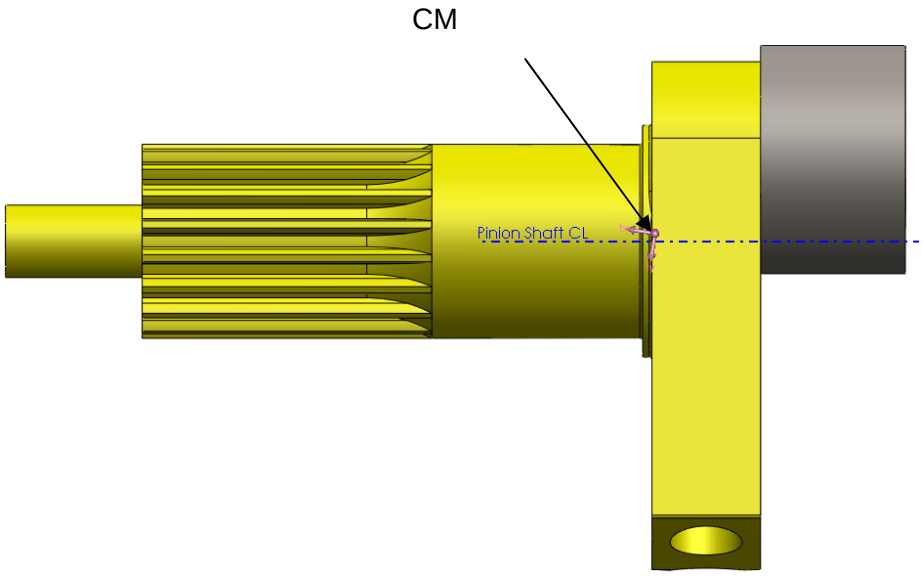

Figure 35 – CM Relative to Pinion Shaft Centerline

One approach to solve this imbalance would be to simply add mass to the pinion shaft counterweight to move the CM down by .689 mm (.027 in). An alternative approach is to lighten the piston and or rod. Either approach would result in perfect 2D balance of the piston, rod, and bearing with the pinion shaft.

The latter approach has the advantage of reducing overall engine weight and ultimate size required for counterweights. The significance is illustrated by the following example. Assume the total reciprocating mass (piston and rod assembly) is 100 grams. Also assume point masses and that the radial distance from the counterweight CM to centerline is equal and fixed. In other words the only method for adjusting balance is adding/removing weight but not relocation of existing mass relative to centerline. Referring to Figure 22, a 100-gram piston and rod assembly would require a counterweight mass at D2 of 100 grams. The carrier counterweight mass required at E is then 100 + 100 = 200 grams. The total of all point masses for a 100-gram piston and rod is 400 grams. Now assume the piston and rod mass can be reduced to only 50 grams. The point mass required at D2 is now only 50 grams and the point mass at E is 100 grams. The total of all point masses is now only 200 grams. In this example, reducing piston and connecting rod mass by 50 grams results in a 200 gram savings in total engine weight.

The piston and rod provided with the Wiseman prototype are simple and effective but overdesigned. A major advantage of the Wiseman engine is the lack of piston side load. Null side load allows for significant reduction in weight involving the skirts and was a design advantage worth pursuing. In fact, the skirt's only purpose in the Wiseman engine is to valve the intake and exhaust ports. The skirts were designed for minimal loads and overall weight. The

original Wiseman piston is also heavy on the underside where the connecting rod threads into the piston. The connecting rod itself is also overdesigned and a new design could undergo weight-reducing measures. For all these reasons, a complete redesign and fabrication of a new piston and connecting rod was decidedly the best approach to improve balance and reduce overall engine weight. The lightweight piston and rod design was completed in CAD first, tested in motion simulation, and then CNC-machined from billet pieces of material.

It was proposed to machine the piston and connecting rod as a single piece in a preliminary design effort. This would have offered some weight savings and provide for easier assembly in high volume applications, but ultimately the added effort/cost did not justify these advantages.

Therefore, a two piece design was the chosen solution. The new connecting rod design maintained the same outside diameter as the original connecting rod but reduced weight was achieved by utilizing a tubular construction. The lack of bending loads in the connecting rod makes a tubular design an attractive way to save weight. The tubular connecting rod attaches to the lightweight piston with a cap screw. Using a cap screw allowed for further weight savings in the piston crown and made it easier to maintain the correct relationship between the piston skirts and the rod.

The critical dimensions, including ring width/location, piston diameter, and skirt length were all taken directly from the stock 30cc piston. The distance from the piston crown to the center of the connecting rod bearing bore was taken from the provided Wiseman piston and connecting rod assembly. All dimensions were maintained with an accuracy of +/- .008 mm (.003 in).

The resulting design with all critical dimensions can be seen in Figure 36. Note that in the section view the connecting rod is hollow and a significant amount of material was designed out from under the piston. The skirts, bearing very light loads, no longer wrap around the entire circumference of the cylinder. In addition to lower weight the reduced skirts have less contact area and friction.

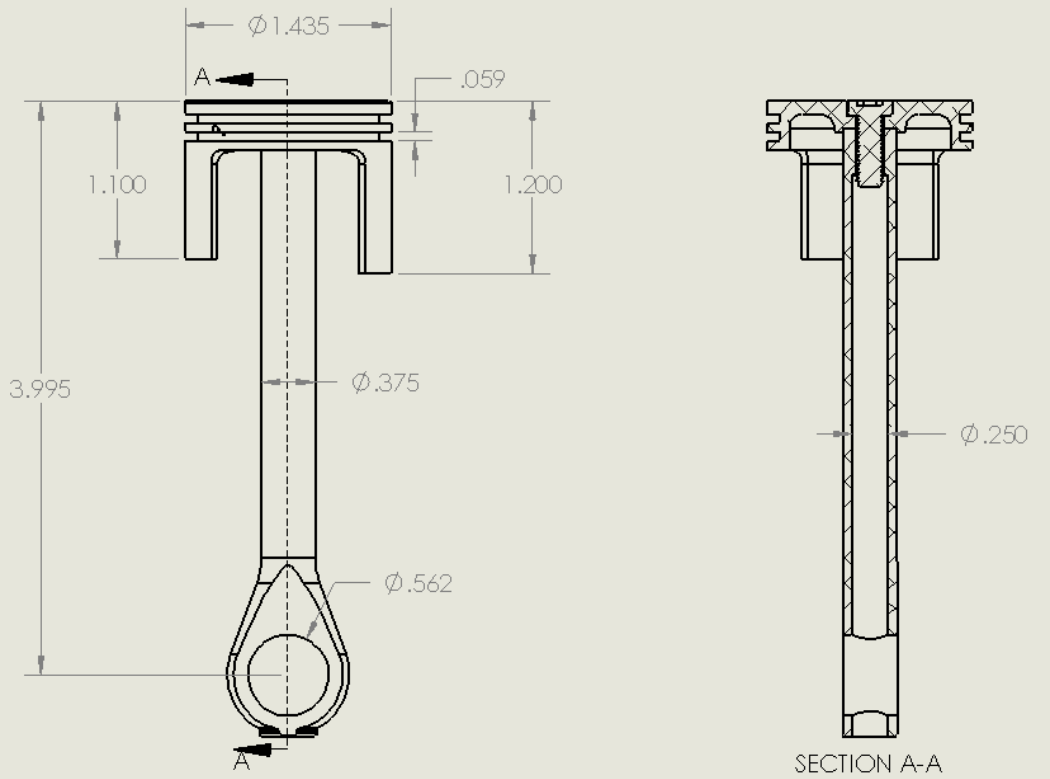

Figure 36 – Piston and Connecting Rod Assembly

The completed piston and rod design was ready for rebalance in motion simulation software. This was easily done by adjusting the mass of the bob weight to equal the new mass of the lightweight piston, connecting rod, and bearing, which is 43.2 grams. 43.2 grams is the total reciprocating mass and includes the rings as well. The pinion shaft with a 43.2-gram bob weight can be seen Figure 37.

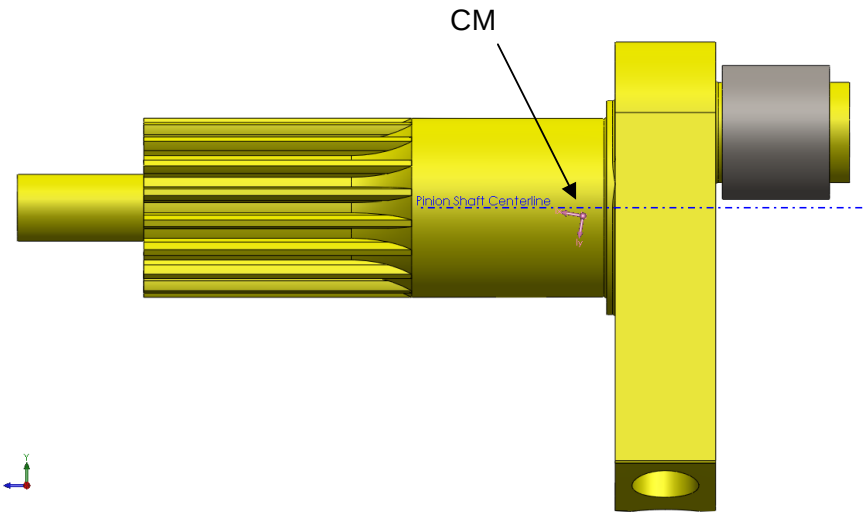

Figure 37 – Pinion Shaft with 43.2-gram Bob Weight

The CM was now .4720 mm (.0185 in) below the required location on the pinion shaft centerline. Reducing the mass and or radius of the pinion shaft counterweight was required to move the CM up to centerline. The easiest way to modify the actual pinion shaft was to remove material from the bottom of the counterweight. The required material removal to properly locate the CM on centerline is shown in Figure 38.

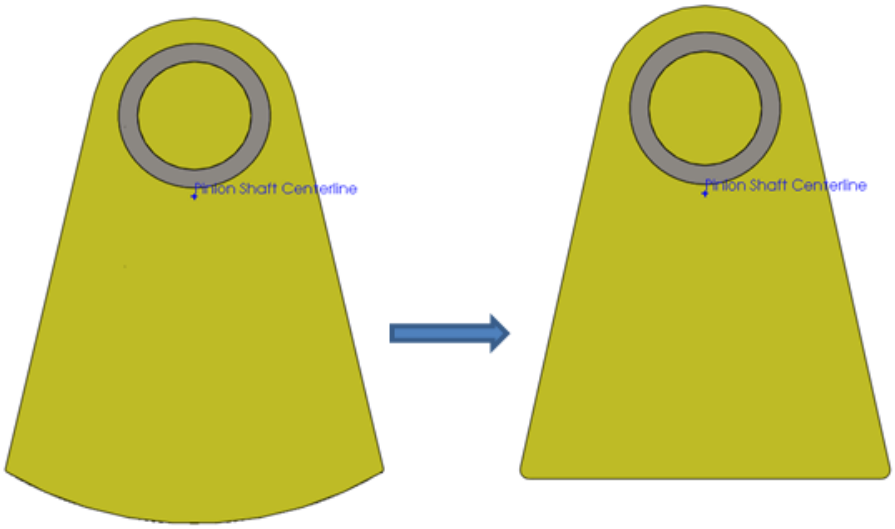

Figure 38 – Material Removal Required on Pinion Shaft

With the pinion shaft CM on centerline, the bob weight was replaced with the lightweight piston and connecting rod assembly model in simulation. The balance simulation was repeated using the new piston/rod design along with the modified pinion shaft to evaluate the changes after pinion balance (APB). The results of the simulation APB at 3000 rpm are shown in Figure 39, Figure 40, and Figure 41 along with the original baseline curves.

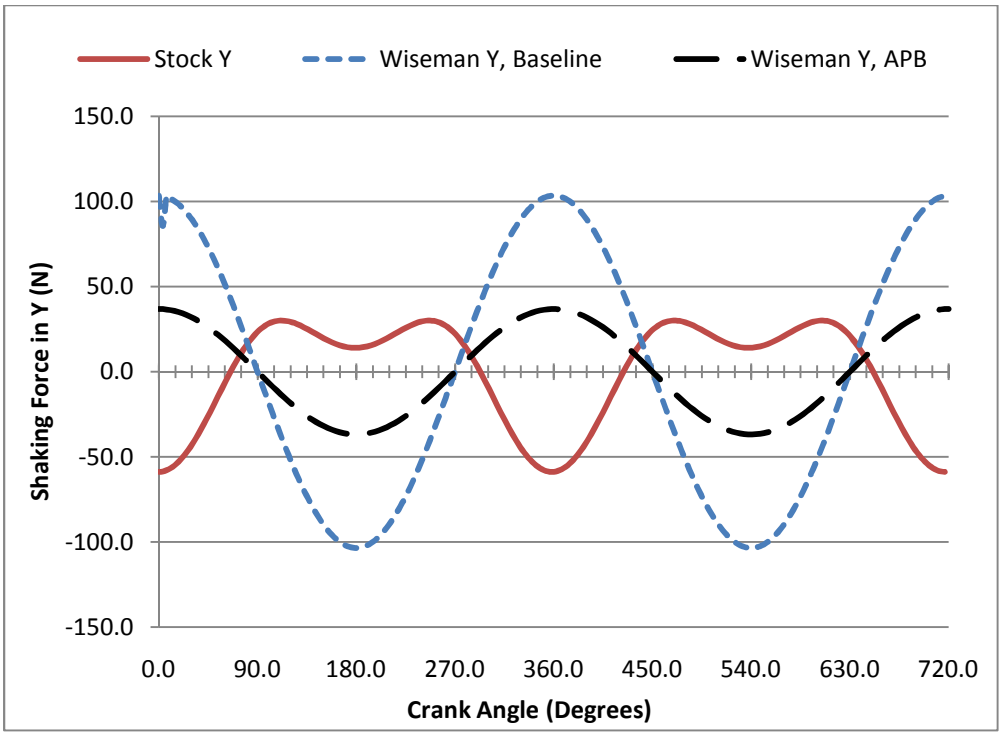

Figure 39 – After Pinion Balance (APB) Shaking Force vs. Crank Angle in Y

The largest improvement in peak shaking force was in Y which was reduced from 103.5 to 36.8 N after pinion balance. The reduced peak value in Y was also now less than the stock peak value. The remaining Y imbalance can be attributed to the carrier shaft and is addressed in the section to follow.

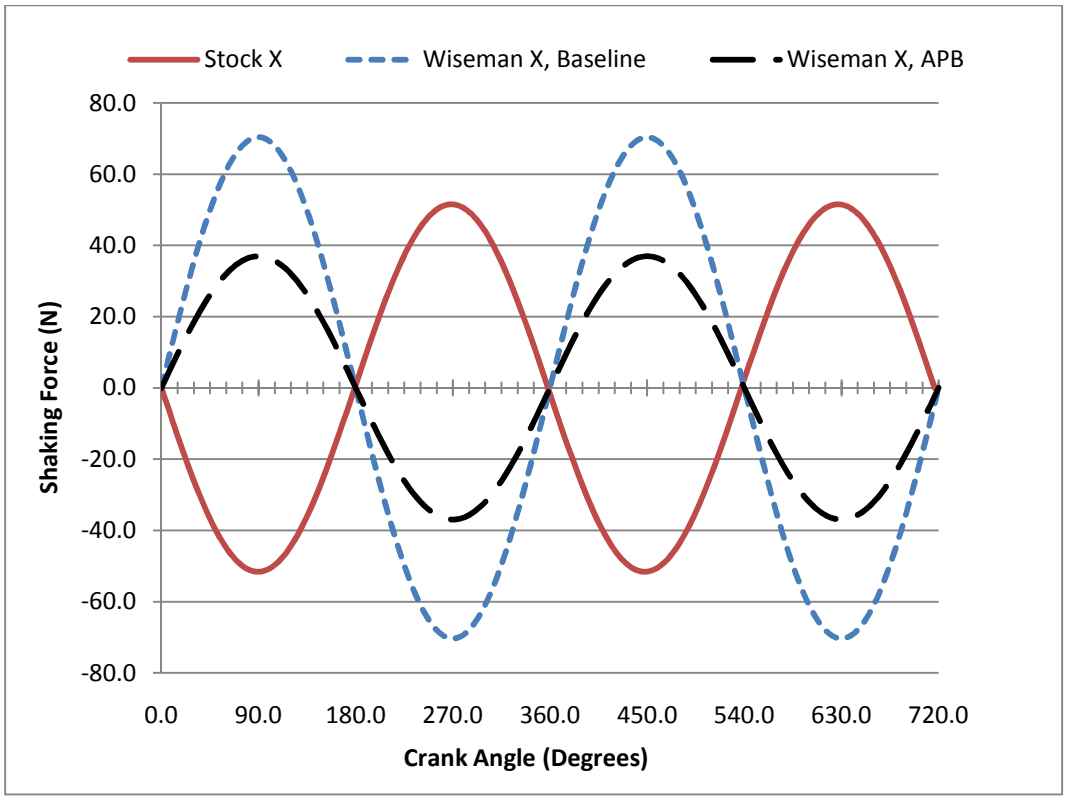

Figure 40 – After Pinion Balance (APB) Shaking Force vs. Crank Angle in X

The peak shaking force in X was reduced from 70.4 to 36.9 N APB. The remaining imbalance in X can also be attributed to the carrier shaft imbalance and is addressed in the following section. The peak shaking force in X for the Wiseman engine was now less than the stock engine.

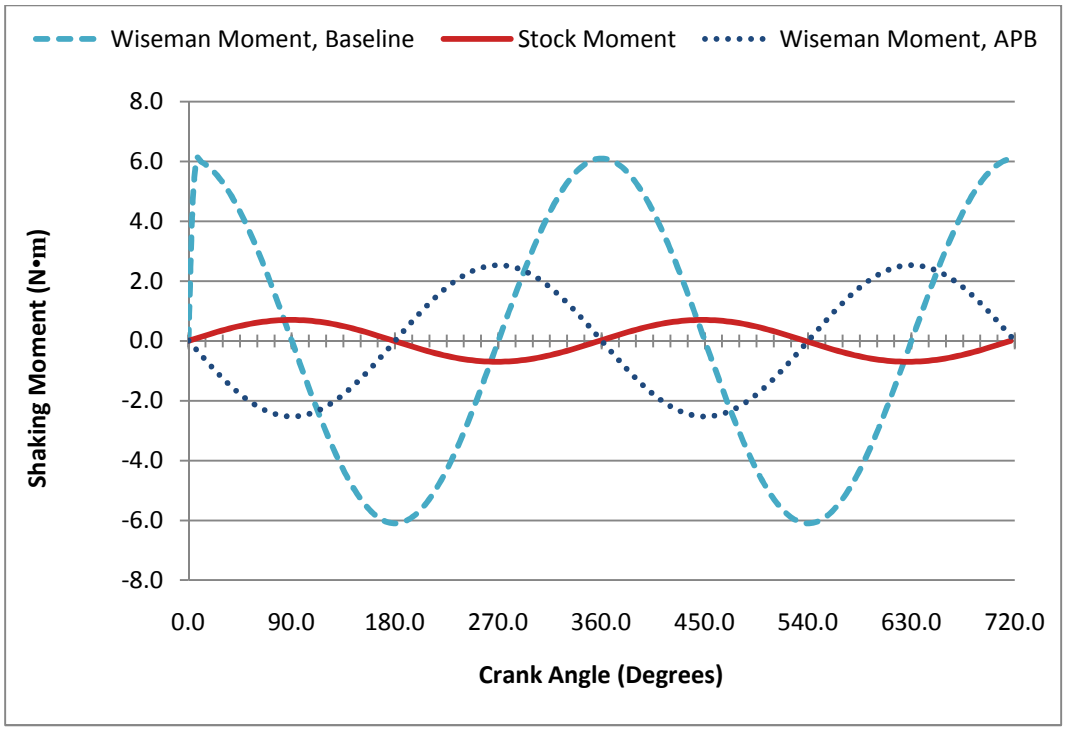

Figure 41 – After Pinion Balance (APB) Shaking Moment vs. Crank Angle

The peak shaking moment was reduced from 6.1 N•m to 2.5 N•m APB. However, the peak shaking moment in the Wiseman Engine was still larger than the stock engine. The large offset from the piston centerline to the carrier shaft counterweight centerline is partially to blame. Improving the balance of the carrier shaft will further reduce the shaking moment.

Carrier Shaft Balance

Theoretically the peak shaking force in the X and Y axis should reduce to zero if the carrier shaft can be balanced to the APB pinion shaft and piston/rod. The method used to balance the carrier shaft is very similar to balancing the pinion shaft. The piston/rod assembly was again replaced with the same bob weight. The pinion shaft bearings and their masses were also included because they are not symmetrical about the carrier shaft centerline. Accurate CAD

models of the bearings were used and actual masses were assigned to ensure simulation accuracy. Once all rotating components were assembled in software, the CM location was .6248 mm (0.0246 in) above the carrier shaft centerline (See Figure 42).

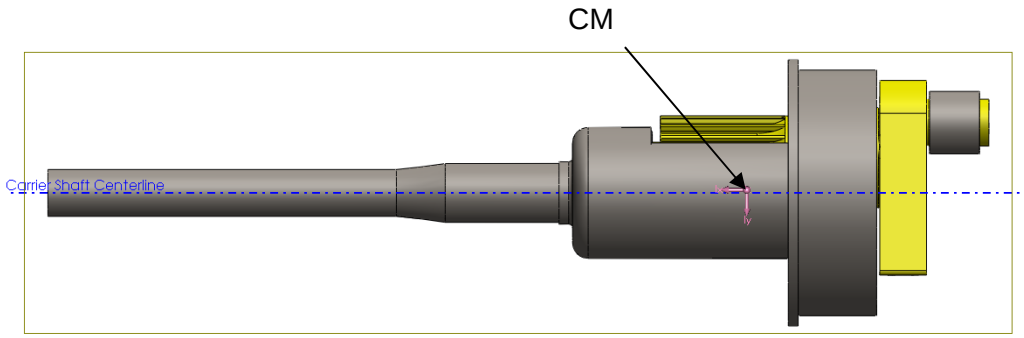

Figure 42 – Carrier Shaft CM

Ideally, mass should be removed from the carrier shaft above centerline to move the CM down and reduce overall engine weight. However, two lightening holes already drilled made it impossible to remove enough additional mass. The only alternative was adding mass below centerline. In future prototypes the carrier could be designed with correct balance in mind and total weight would be less. For this research effort however mass was added below centerline by boring two holes in the carrier face and pressing in heavy metal slugs. The heavy metal material of choice was 90% tungsten alloyed with 6% nickel and 4% copper. This alloy is a durable metal that is machineable while possessing a high density of 17.0 g/cc^3 (compared to 7.85 g/cc^3 for 1045 steel). The use of this material is common for crankshaft balancing and was a simple and effective way to balance this assembly. To move the CM for the entire rotating assembly coincident to the carrier shaft centerline required 2 slugs at Ø12.7 mm (.500 in) x

10.668 mm (.420 in) long be installed at 30 degrees either side of the carrier shaft vertical center. The radial distance to the center of the slugs is 17.526 mm (.690 in) (See Figure 43). Although it was also possible to use a single long slug the benefit would be reduced because more mass is required further away from the piston centerline. The balance in X and Y would not change with a single slug but the shaking moment would be higher. Two shorter slugs was therefore a better solution.

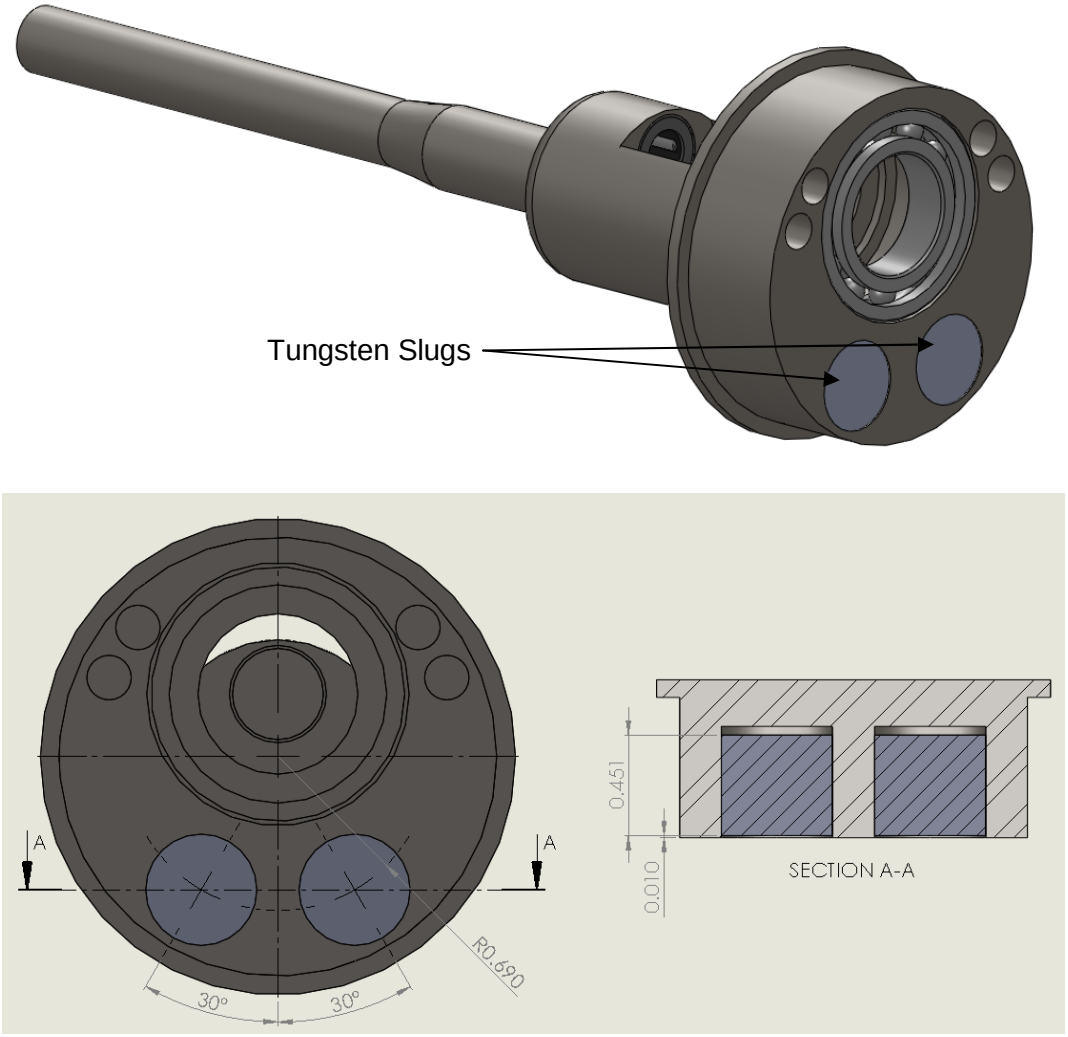

Figure 43 – Carrier Shaft with Tungsten Slugs Installed

With the tungsten slugs in place, the assembly was perfectly balanced in the X and Y direction according to the CAD model. The results of the simulation run again at 3000 rpm with the tungsten slugs in place showed a further improvement over the unbalanced Wiseman engine and stock engine. The final results of the balance analysis after carrier balance (ACB) for the shaking moment and shaking force in X and Y are shown in Figure 44, Figure 45 and Figure 46, respectively.

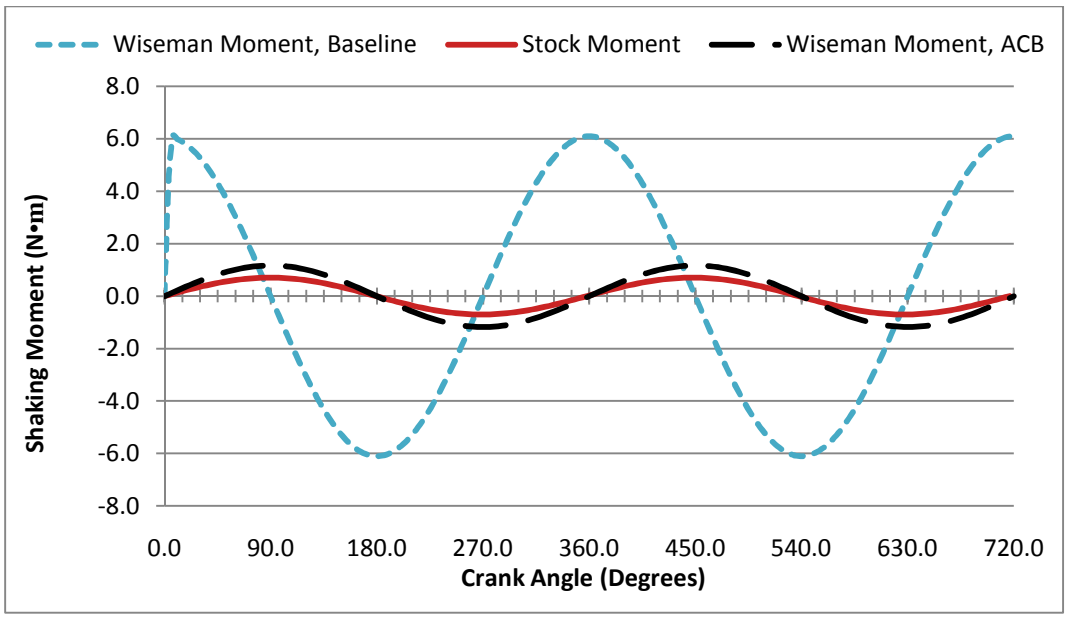

Figure 44 – ACB Wiseman Shaking Moment vs. Crank Angle

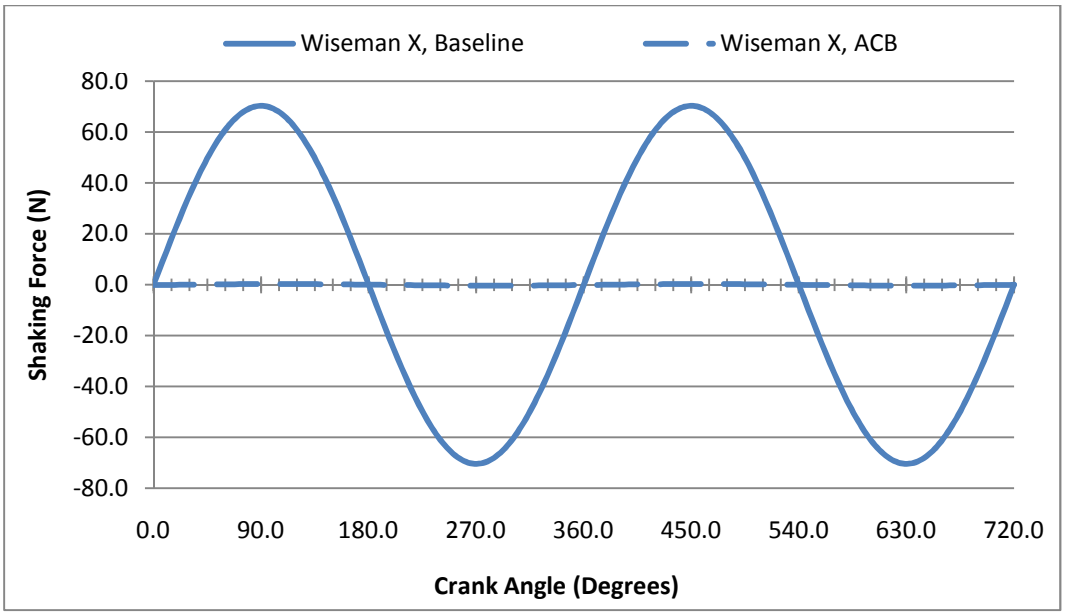

Figure 45 – ACB Wiseman Shaking Force in X vs. Crank Angle

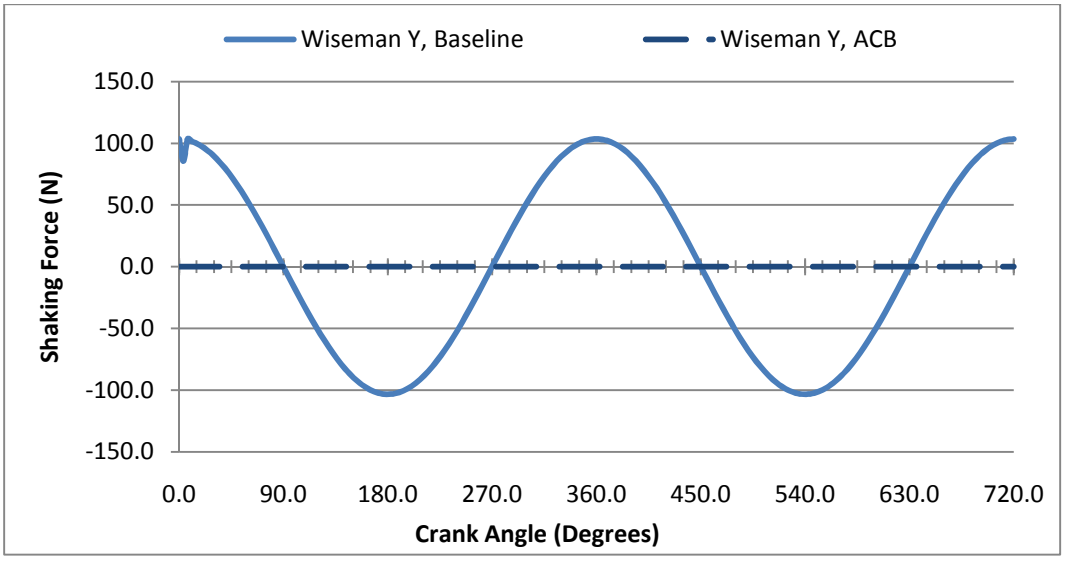

Figure 46 – Balanced Wiseman Shaking Force in Y vs. Crank Angle

The shaking force in X and Y was in fact zero as expected and the Wiseman engine simulation model achieved perfect 2D balance. The shaking moment was also much improved and nearly equaled the shaking moment of the stock engine. Following the balance approach described in (Norton, 2005) the 2D balance was

completed first before attempting full 3D balance in order to minimize the shaking moment first. A proper 3D balance should completely eliminate the shaking moment without affecting the X and Y shaking force.

The remaining imbalanced shaking moment was caused by the off center placement of the carrier and pinion shaft counterweights relative to the piston centerline. To eliminate the remaining imbalanced shaking moment, an additional shaking moment, equal in magnitude but opposite in direction was required (See Figure 47).

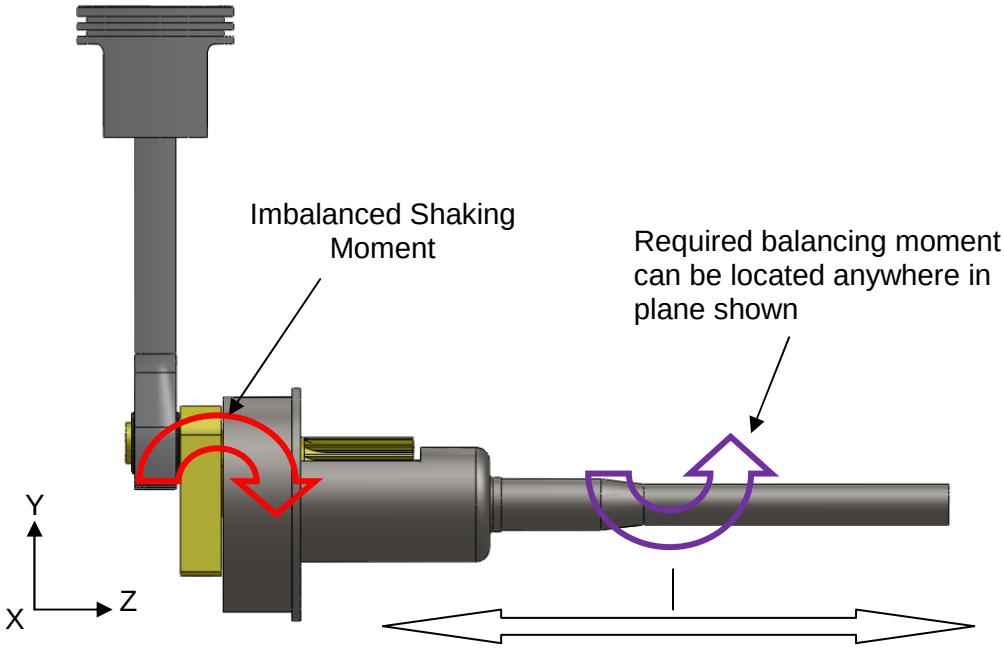

Figure 47 – Shaking Moment and 3D Balance

To generate the balancing moment, the addition of two counterweights offset some distance from each other were required to maintain perfect balance in X and Y. The existing engine flywheel would be an ideal location to implement the offset counterweights. The flywheel width however may limit feasibility. To

determine feasibility, two simple counterweights made of 1045 steel were added (in CAD) to the carrier shaft as shown in Figure 48.

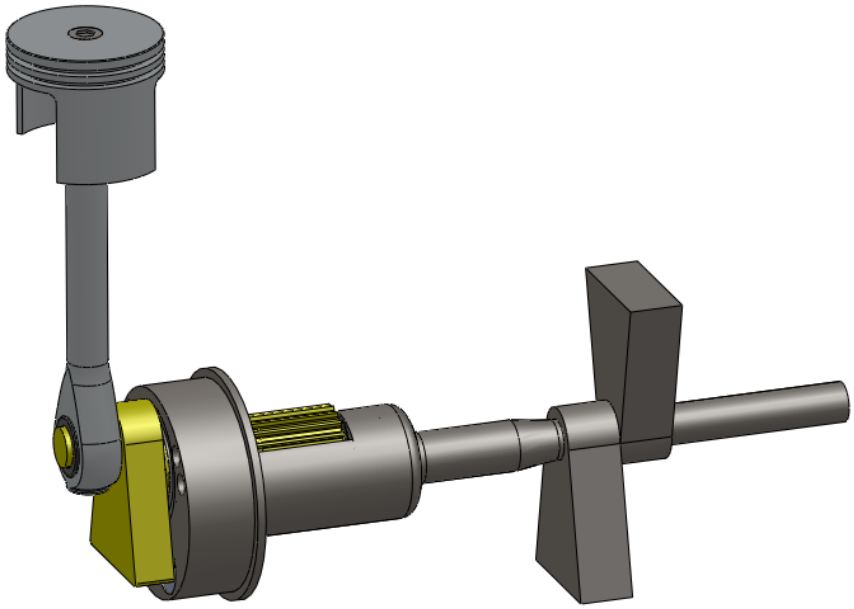

Figure 48 – Shaking Moment Counterweights for 3D balance

The sizes of the counterweights were adjusted using an iterative approach until the minimum shaking moment was obtained. They were located approximately in the same location as the existing flywheel and filled about the same amount of rotating volume. The simulation was run one final time and a minimum shaking moment was observed. The results are shown in Figure 49 where the original Wiseman unbalanced shaking moment is shown for reference.

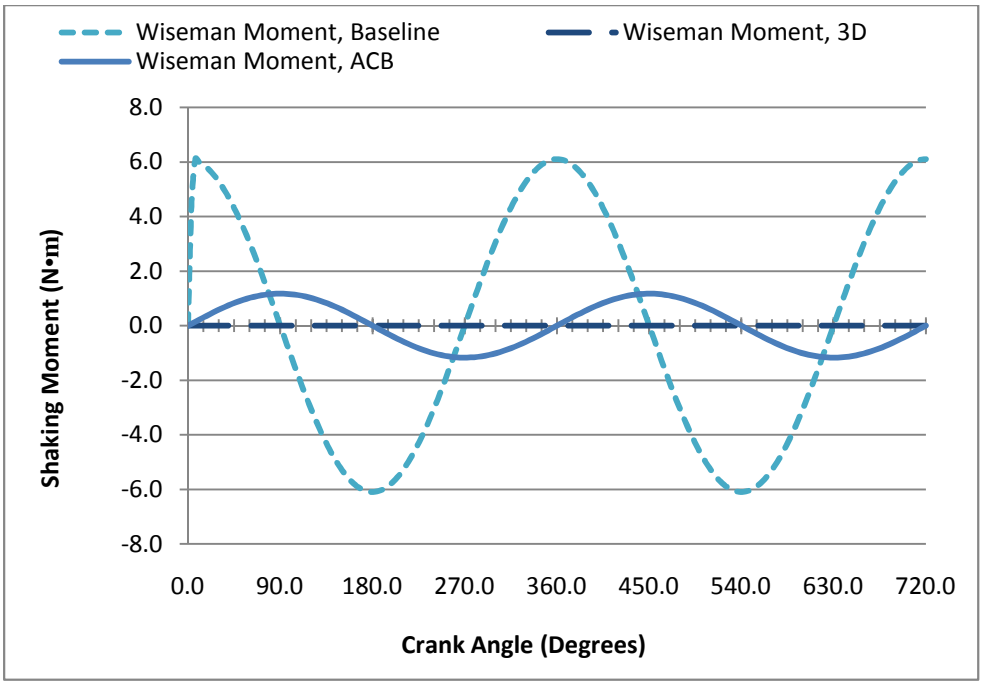

Figure 49 – Shaking Moment vs. Crankshaft Angle with 3D Balance

The shaking moment was reduced to nearly zero and the X and Y shaking forces remain unaffected. The result was a fully balanced Wiseman engine that would produce nearly zero vibration if the following assumptions were made:

- Constant crankshaft speed
- Zero tolerance parts
- Perfectly rigid components
- Lack of combustion forces

Although a nearly zero vibration single cylinder engine is a very interesting study, the amount of mass required for perfect balance did not justify the small improvement from 2D to 3D balance. For this research effort 3D balance was not attempted on the actual Wiseman prototype. With the absence of shaking forces in X and Y and only a slightly higher shaking moment, one can expect a running Wiseman engine to feel more comfortable and impart less harmful

vibration to users in hand held applications. The promising balance simulation results provided enough impetus to fabricate hardware and validate the simulation results for a complete 2D balance.

Piston/Rod Fabrication

The connecting rod was machined from 7075-T6 aluminum due to its excellent strength-to-weight ratio. The starting stock size was Ø19.05 mm (Ø0.750 in) round bar. The first machining operation took place in a Haas SL-20 CNC lathe. A CAM program was created using SurfCam and the imported CAD model of the connecting rod. In the first operation the main section was roughed and finished to Ø9.525 mm (Ø0.375 in) OD in short sections. Roughing the entire length first and then finishing in one pass did not produce a good finish due to long hang out and the small diameter of the part. The OD turn toolpath stopped just beyond the center of the bearing bore. The center of the stock was also spot-drilled and then drilled to Ø4.039 mm (Ø0.159 in) x 12.700 mm (0.500 in) deep. This hole was then tapped to 10-32 UNF-2B. The final toolpath parted off the piece for the next operation. See Figure 50 for the toolpath and verification of OP01.

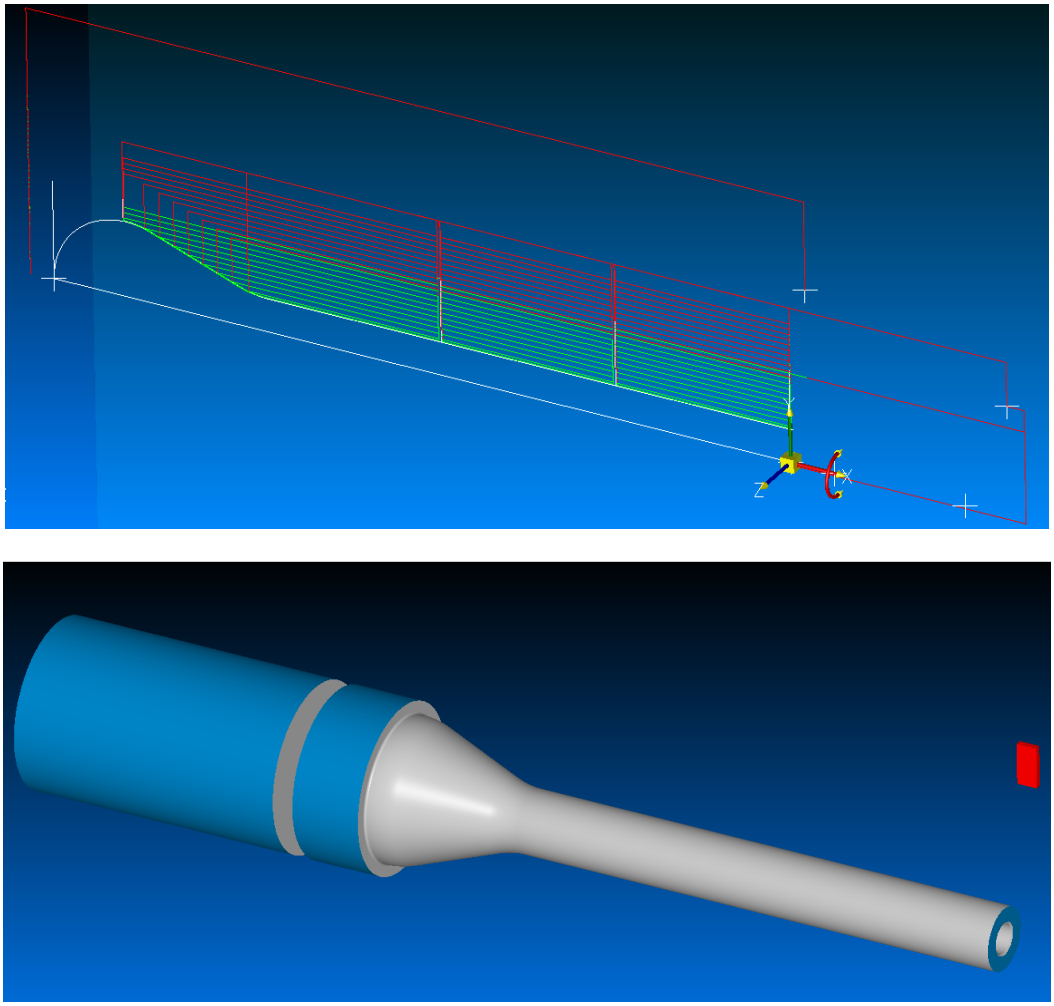

Figure 50 – Connecting Rod CAM OP01

In the second lathe operation the connecting rod was turned around and mounted in the lathe spindle using a collet. The back end was then roughed and finished to just beyond the bearing bore center to avoid any mismatch left from the first operation. Finally, using an extra long parabolic drill, a Ø6.350 mm (Ø0.250 in) hole was drilled until it intersected the Ø4.039 mm (Ø0.159 in) hole drilled in the first operation – about 101.6 mm (4.000 in) deep. The toolpath for OP02 is shown in Figure 51.

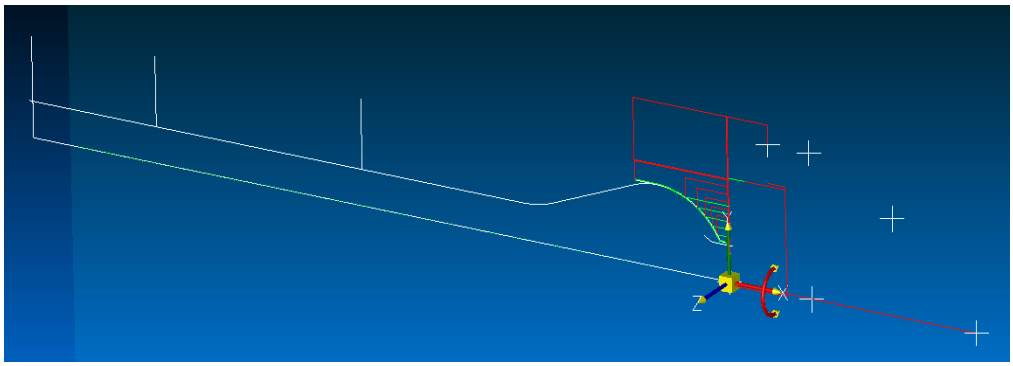

Figure 51 – Connecting Rod CAM Program OP02

In the third operation the connecting rod was transferred from the Haas SL-20 CNC lathe to a Haas VF3, 3 axis mill with a fourth axis rotary table installed. The end of the connecting rod was left approximately spherical in shape by the lathe had to be milled flat on two sides and then bored for a light press fit of the connecting rod needle bearing. The connecting rod was mounted in the three jaw chuck of the rotary table and then supported at the opposite end using the tail stock and custom machined support. The first side was milled flat and then bored (end mill interpolation) to 14.220 mm (0.5600 in) (Figure 52 and Figure 53). The bearing hole was later precision lapped by hand to achieve a light press fit with the connecting rod needle bearing. Finally, the connecting rod was rotated 180 degrees using the fourth axis and then milled flat again on the opposite side.

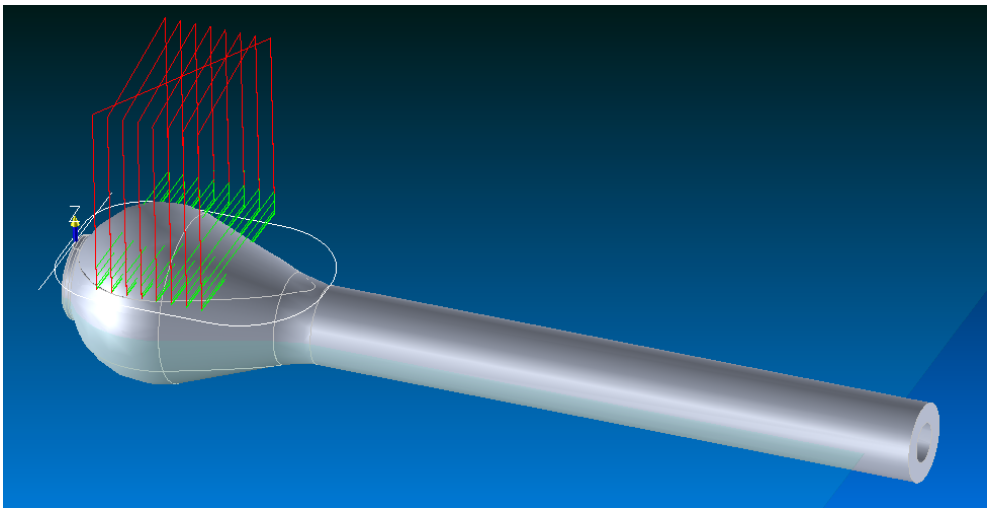

Figure 52 – OP03, Mill Sides Flat

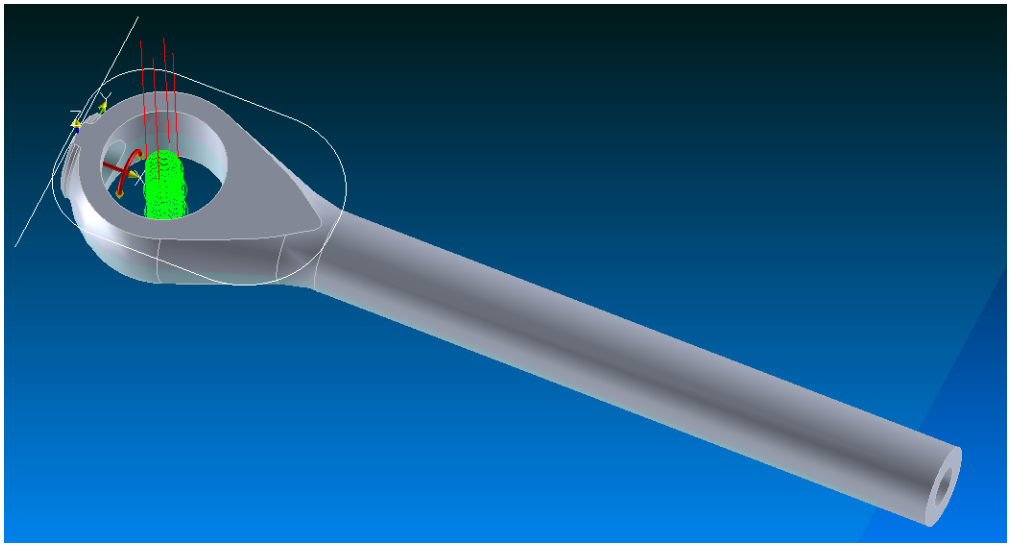

Figure 53 – OP03, Contour Mill Center Hole to Ø0.5600 inches

The machined connecting rod was now complete and ready for lapping and bearing install (Figure 54).

Figure 54 – Machined Connecting Rod

The piston was machined from a high silicon content aluminum alloy known by its trade name as Deltalloy or 4032. Deltalloy was chosen because of its ideal properties for pistons including high wear resistance, a low coefficient of thermal expansion, and excellent machinablity. A piece of 38.100 mm (Ø1.500 in) round bar was the starting stock size.

In the first operation a blank was machined on a manual lathe to a finished Ø36.449 mm (Ø1.435 in) OD by 30.48 mm (1.200 in) long. All remaining operations took place in a Haas VF4 3-axis mill with a 5-axis trunnion installed.

There are two small Ø1.5785 mm (Ø0.0625 in) holes that are located just off center of the ring grooves at 90 degrees from each other. These holes accept dowel pins that locate the piston rings and keep them from rotating into cylinder wall ports where they might cause problems. The pin hole locations on the Wiseman piston were matched to the stock piston design. The piston could have been machined as a 3 axis part but would have required additional operations and fixtures to machine the dowel pin holes.

Mounted to the trunnion plate was a 3-jaw chuck. A set of aluminum soft jaws were bolted to the 3-jaw chuck. A Ø36.449 mm (Ø1.435 in) by 2.540 mm (0.100 in) deep bore was machined into the jaws to securely clamp and locate the piston blank on centerline with the chuck. In the first operation the following features were completed:

- Ring grooves were roughed and finished using a 1.143 mm (0.045 in) thick by Ø19.05 mm (Ø0.75 in) OD, 8 tooth slitting saw.
- A counterbore hole was interpolated in the top of the piston using a Ø4.7625 mm (Ø0.1875 in), 3 flute end mill.
- Two Ø1.5785 mm (Ø0.0625 in) dowel pin holes were drilled using a Ø1.5785 mm (Ø0.0625 in) end mill.

The first dowel pin hole required the trunnion rotate 90 degrees in the A axis. To machine the second hole, the A-axis remained fixed while the B-axis rotated 90 degrees. The toolpaths for the second operation, also programmed in SurfCAM, are shown in Figure 55.

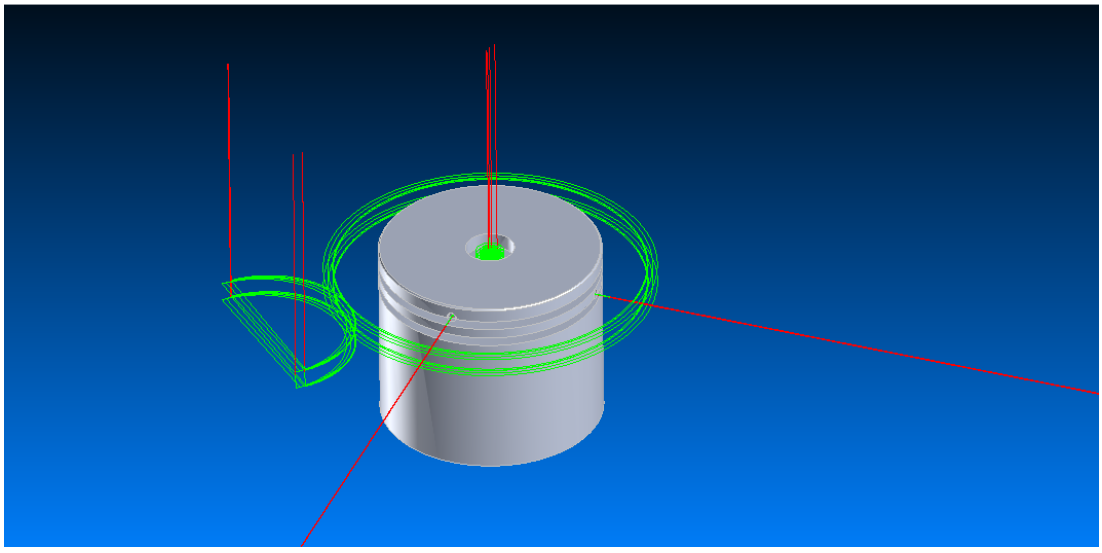

Figure 55 – Piston OP02

For the third and final operation the piston was flipped over and reset in the soft jaws to machine out the bulk of the inner material and create the skirts. A shallow counter bore was also put in to locate the connecting rod when bolted to the piston. A Ø6.350 mm (Ø0.250 in) end mill with a Ø2.362 (Ø.093 in) corner radius was used to finish the interior of the piston. This left a Ø2.362 (Ø.093 in) radius at the base of the skirts and on the underside of the piston to minimize stress concentrations. The third operation finishing toolpaths were also programmed with SurfCam and are shown in Figure 56.

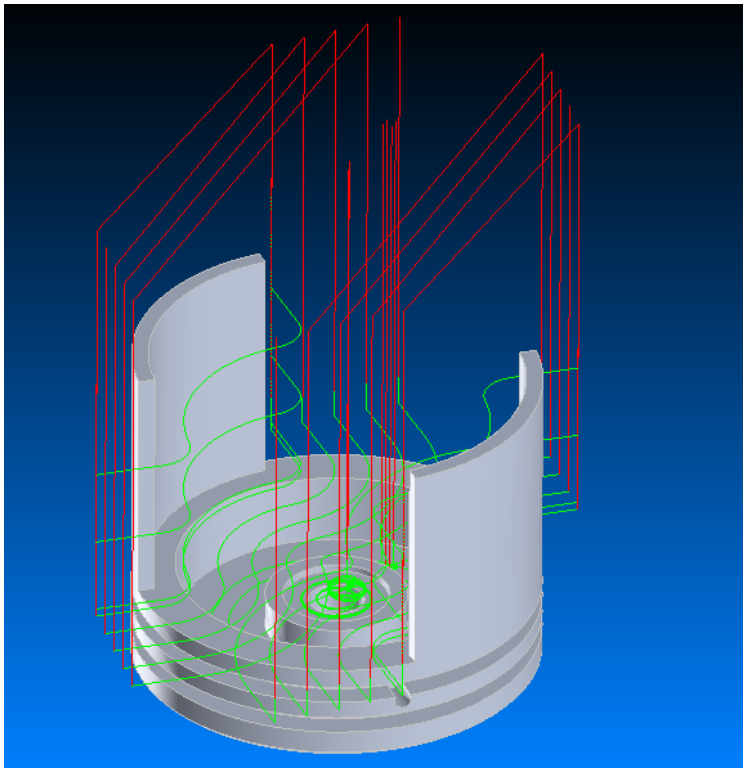

Figure 56 – OP03 Finish Toolpath

Just prior to final assembly, the machined piston and connecting rod are shown together in Figure 57.

Figure 57 – Machined Piston and Connecting Rod

Empirical Vibration Analysis

Before installing the new piston and connecting rod shown in Figure 57 or modifying the pinion shaft and carrier shaft on the actual Wiseman engine it was important to evaluate the two engines empirically to establish baseline vibration data. The empirical data was also necessary to help validate the simulation results.

The primary objective of this analysis was to validate the effectiveness of balancing the Wiseman engine using motion simulation. To quantify the level of imbalance the average intensity of vibration was measured using a dual axis accelerometer as the engines were motored from 1000 to 5000 rpm. This

differed from the simulation analysis where a single direction shaking force/moment was calculated over two rotations at constant speed. To better mirror the simulation test a high resolution encoder could have been used to track acceleration versus output shaft angle. In the empirical vibration test performed here however, a capable encoder was not available and so average vibration intensity was measured instead across a wide range of speeds. The motoring speed was varied from 1000 to 5000 in order to mitigate the effects of harmonic frequencies influencing the results.

To better mirror the software simulations the engines were motored rather than fired. The goal of the vibration test fixture was to evaluate changes to the internal balance of rotating and reciprocating components inside the engine. The absolute output of the tests was not nearly as critical as the relative change before and after changes to the engines.

Mounting the engines for the vibration analysis was an extremely important step in collecting valuable vibration data. Early on soft rubber mounts were attempted to better simulate real world applications but meaningful data could not be obtained. A balancing expert with Raven Engineering recommended the engines be mounted as rigidly as possible to a fixture with a large mass relative to the mass of the engines (Jeffrey, 2011). This mounting technique is desirable when trying to evaluate vibration behavior after changes are made to internal rotating components. Increasing rigidity and mass helps to reduce the effect of resonance by increasing the natural frequencies of the test fixture and engine together. Ideally, natural frequencies of the test fixture should be kept far away from the first few orders of the running engine. Large fixture mass also reduces

the influence of engine mass and this became important because the Wiseman engine is nearly double the weight of the stock engine.

A Tormach 3-axis CNC mill with a continuously variable 5000 rpm spindle was used to achieve the recommended mounting and motoring scheme. At over 1200 lbs the mill provided a heavy and rigid foundation for evaluating engine vibration (Figure 58). The engines were mounted vertically below the spindle and clamped securely in a machine vise. The spindle drove the engine output shaft through two flexible shaft couplers. The two shaft couplers in series provided the following functions:

- Reduced the transmission of vibration from the mill motor and spindle to the engine.
- Accounted for any misalignment between the mill spindle and engine output shaft.
- Accounted for any shaft run-out in the engine output shaft.

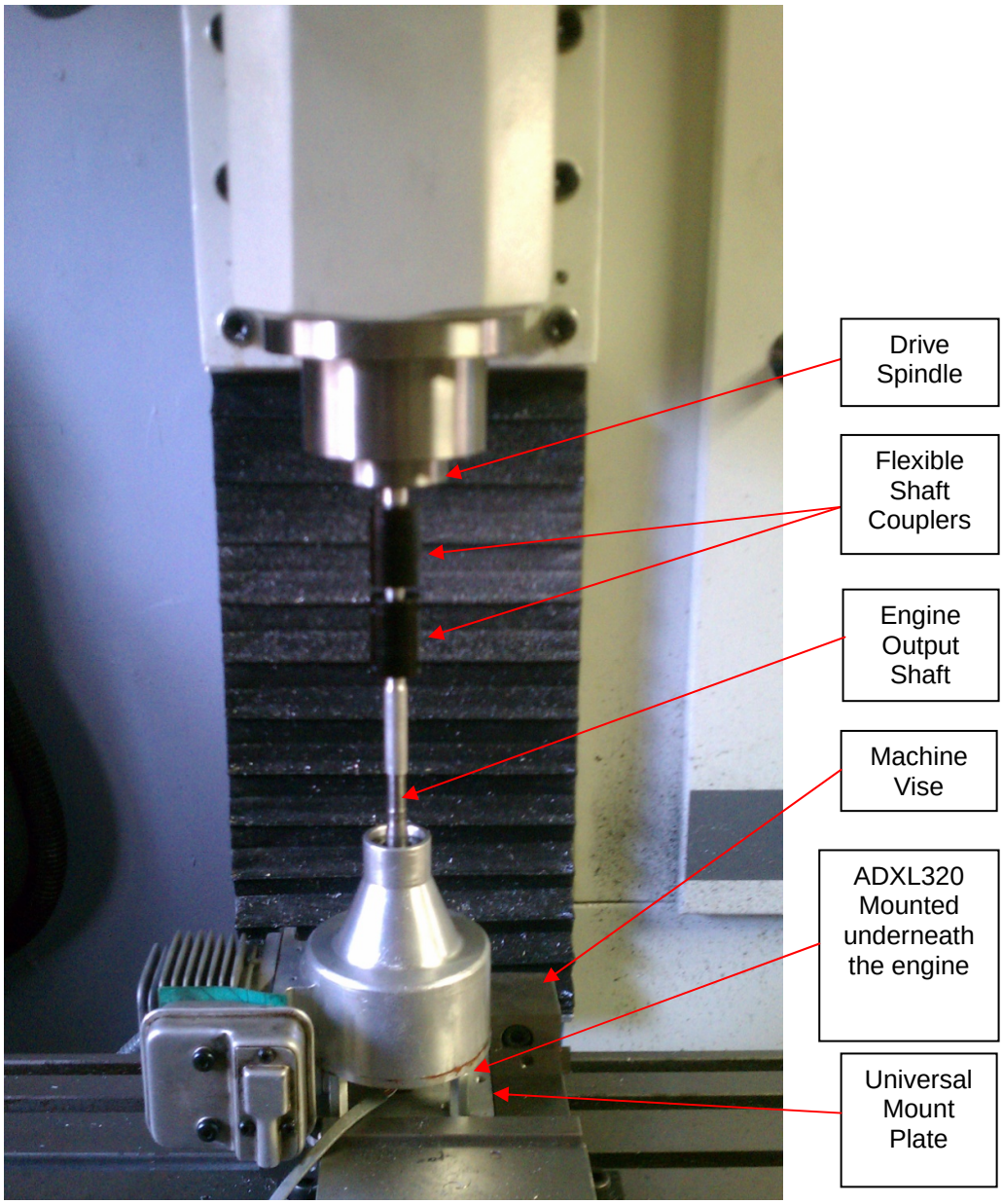

Figure 58 – Wiseman Engine Mounted in Vibration Test Fixture

A dual axis accelerometer was used to measure shaking forces in the X and Y direction only. The accelerometer was a MEMS 5g ADXL320 mounted on a small breakout board. Power supply and filtering capacitors were included with the breakout board unit. The sensor outputs a separate analog voltage for each axis (X and Y) that is proportional to acceleration. The analog voltage was sent

to a NI USB 6009 data acquisition unit connected by USB to a PC. The PC was loaded with Labview Signal Express 2009, a software package that allows for data collection and processing using the USB 6009 DAQ.

The accelerometer output voltage for each axis was calibrated and converted to acceleration in m/s^2. To calibrate the output, a voltage value was recorded while placing the accelerometer so that each axis was vertical up, horizontal and then vertical down relative to gravity. The recorded values are shown in Table 2.

AXIS	Veritcal Up ↑	Horizontal →	Vertical Down ↓
X	2.63 V	2.37 V	2.10 V
Y	2.62 V	2.355 V	2.093 V

Table 2 – Accelerometer Calibration Values

Using the table values and the acceleration of gravity (9.8 m/s^2), Equation 3 and Equation 4 were generated to convert the raw voltage into acceleration (m/s^2) inside the Signal Express program.

$$\boldsymbol{a_x = -37.05V_x + 87.784}$$ Equation 3

$$\boldsymbol{a_y = -37.19V_y + 87.623}$$ Equation 4

where

a_x is the acceleration in the x direction in m/s^2.

V_x is the raw voltage value from the accelerometer x axis.

a_y is the acceleration in the y direction in m/s^2.

V_y is the raw voltage value from the accelerometer y axis.

Once converted to acceleration, each signal is fed through a number of processing steps in Signal Express to obtain useful data. The first step is a bandpass filter that removes frequencies below 10 Hz and above 200 Hz. The second step is an Amplitude and Levels function that calculates an RMS value for the incoming filtered signals. These signal processing steps were chosen based on an ISO standard for testing the vibration of handheld forest machinery (ISO, 2004). This standard stipulates a bandpass filter and a RMS value shall be used to calculate an acceleration value for each axis. This standard also requires a weighted filter that applies a weighting based on frequency. The weighted filter was not used here. The RMS value for each signal is then put through a time-averaging function that takes an average of 10 samples using an exponential weighting mode. The averaged, final signal for each is then plotted vs. time. Each engine vibration test was 50 seconds long during which the mill spindle was accelerated at a linear rate from 1,000 to 5,000 rpm.

Empirical Vibration Results

The first test run was a baseline test that looks at the Wiseman Engine before any balancing modifications were done. Like the balance simulation coordinate system, the accelerometer X direction was oriented perpendicular to the cylinder axis and the Y direction is parallel. The results of the baseline empirical vibration tests are shown in Figure 59.

Figure 59 – Wiseman Baseline Vibration Tests

One might conclude from the results that the vibration was higher in the X direction but it should be noted that the mill table is more rigid in the Y direction and likely influenced the results.

With baseline results recorded, the original 80-gram piston and rod was replaced with the new light-weight 43.2-gram piston and hollow rod assembly. The pinion shaft modification shown in Figure 38 was executed on the physical part to balance it as prescribed by the balance simulation analysis. The engine was placed back in the vibration test fixture for another run to evaluate the improvement of balancing the pinion shaft alone (APB). Following this test the engine was disassembled again to perform the balance modification to the carrier shaft shown in Figure 43 (ACB). As noted previously the final change required for full 3D balance is not carried out on the actual prototype. An additional run was also preformed with the mill running but not driving an engine in order to

understand the contribution of the mill by itself to the results. The results of the described vibration tests are shown in Figure 60 (X-axis) and Figure 61 (Y-axis).

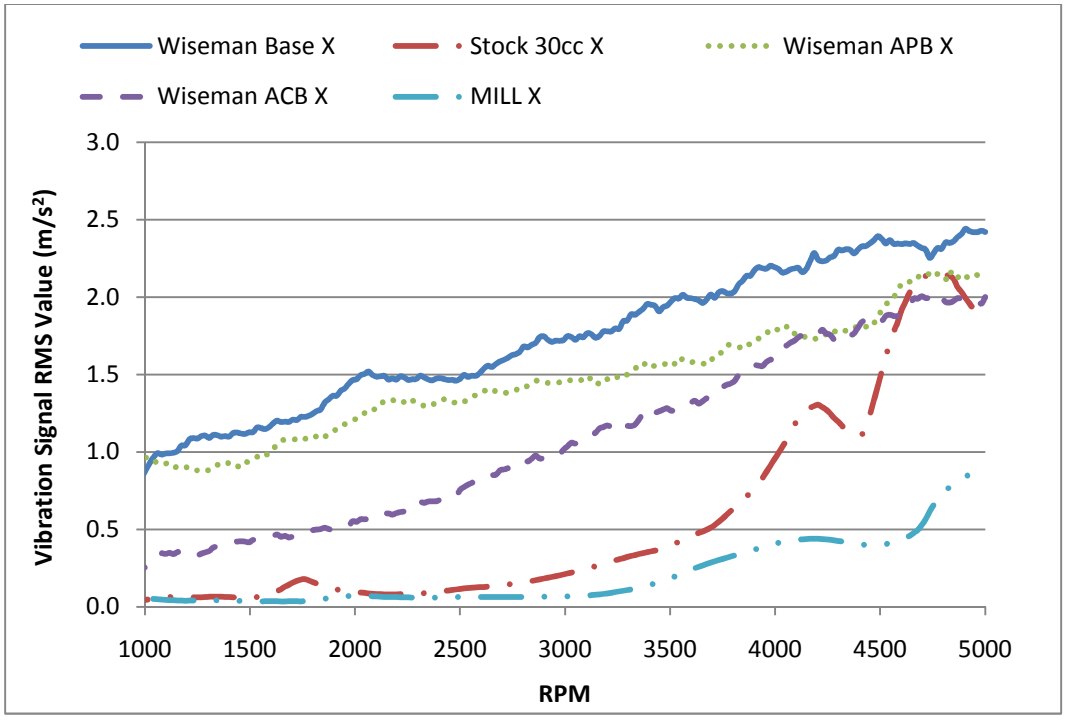

Figure 60 – Vibration in X vs. RPM

In the X direction the Wiseman engine vibration level made a significant improvement from baseline to ACB. The improvement however was less than expected. The reason for this was likely small differences between the CAD models and the physical parts. It is expected that with precision balancing equipment and fine tuning the results would improve. At around 5,000 rpm, even without fine tuning, the vibration was reduced dramatically. It should be noted that the mill vibration and excitation seemed to contribute significantly more to the stock engine vibration than to the Wiseman engine. This is apparent when comparing the vibration of the mill by itself with the stock engine where spikes in vibration level seem to coincide. There may be a resonance effect between the

stock engine and the CNC mill, making it difficult to conclude meaningful information from the stock engine data.

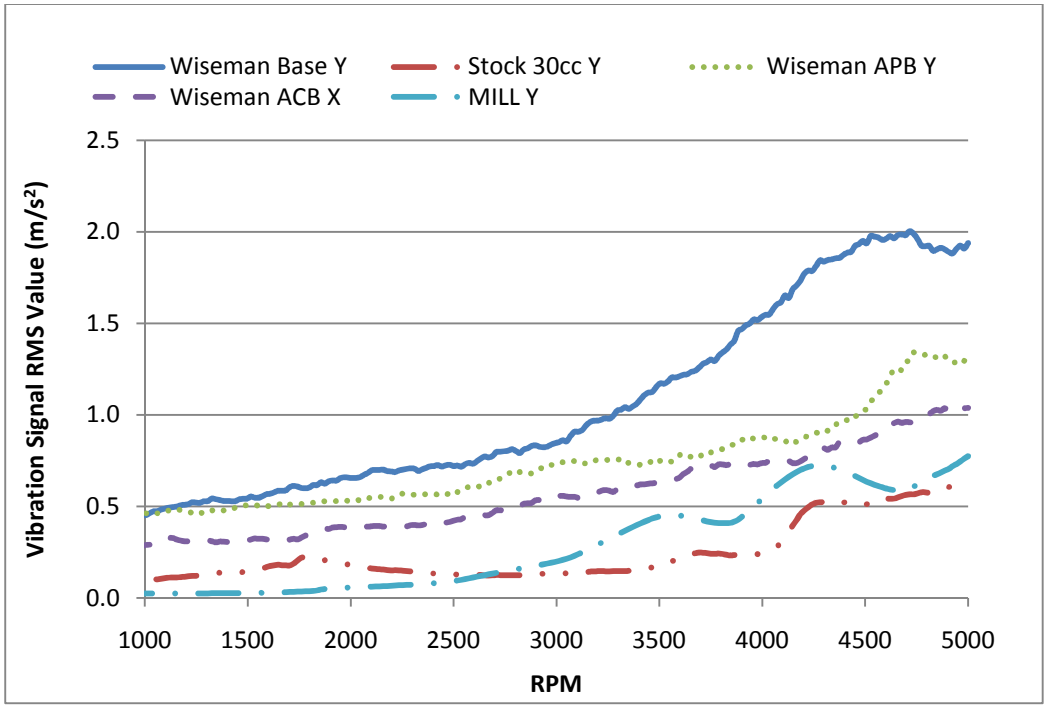

Figure 61 – Vibration in Y vs. RPM

The results in the Y direction were similar to X except an even better improvement was obtained. This is especially true in the APB results for the Wiseman engine. This result was expected because the balance simulation also showed the most significant improvement would come in the Y direction APB (Figure 39). The ACB result showed further improvement as expected. Similar to the X results, a fine tuning with precision balancing equipment would likely yield better results for the Wiseman engine. The stock engine result was actually below what was measured for the mill by itself at speeds above 2,700 rpm. This further proved the existence of an undesirable interaction between the mill and the stock engine. It is difficult to extract meaningful information from the stock

engine results but one can conclude the balancing effort was moderately successful for the Wiseman engine.

Chapter 5

ENGINE PERFORMANCE

This research effort began with an already well running prototype Wiseman engine. As a result the focus was less on design and more on how to evaluate the Wiseman engine and compare it to the stock engine it was constructed from. The major objectives to better understand the performance of the Wiseman engine included:

- Evaluate motored power losses
- Analyze output torque for a given cylinder pressure
- Investigate the effect of primary compression ratio (PCR)
- Determine Brake Specific Fuel Consumption (BSFC) at peak power
- Generate power versus rpm curves
- Compare Wiseman engine to equivalent slider crank engine in all categories.

Methods for testing these engines were developed, designed and constructed as major undertaking in this research effort.

Engine Test Fixture Design

To accomplish the first two objectives above, a special engine test fixture was designed and fabricated. The design specifications for the engine test fixture were as follows:

- Measure driving torque while the engine is being driven electrically (motoring) for losses analysis.
- Allow for variable speed engine motoring up to 3000 rpm.

- Measure static reaction torque of output shaft when pressurizing the cylinder over various crank angles.
- Allow for quick and easy swap of engines by utilizing universal mounting scheme.

To meet the above specifications the test fixture must measure both the torque generated by the engine and absorbed by the engine. There are a number of off the shelf rotary sensors capable of measuring this torque between the output shaft of the engine and the output or input, however, many do not handle high speeds/torque and the ones that do were cost prohibitive. It was decided instead to utilize a strain gauge load cell that could measure a linear force in compression or tension (See Figure 62) and mount it to measure engine torque.

Figure 62 – Omega Strain Gauge Load Cell and Meter

The challenge was how to measure the rotary torque of the engine shaft using a linear device that remains static. The solution has the engine mounted so it is free to rotate about the same axis that passes through the center of the output shaft. This is accomplished using a set of low friction pillow block bearings on which the engine and mount shaft is free to rotate (See Figure 63). The engine mount shaft is tubular and encloses an internal flex shaft that couples

to the engine output shaft. The internal flex shaft is supported by the tubular outer shaft and is free to rotate at high speed with very little friction.

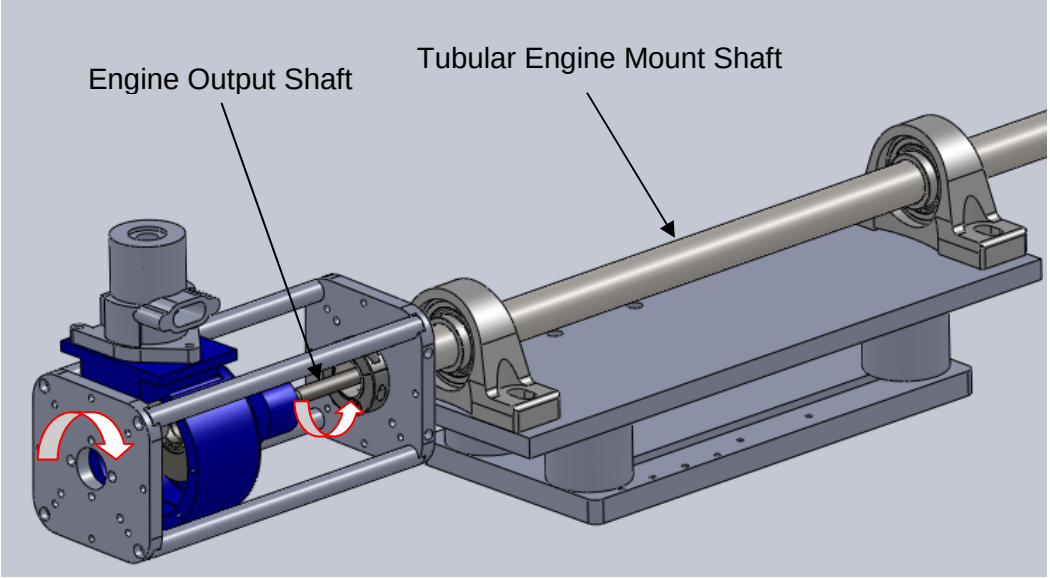

Figure 63 – Engine Test Fixture and Reaction Torque Concept

In this mounting configuration it was possible to measure the torque of the crankshaft by simply measuring the equal and opposite torque of the engine itself. In addition, the measurement of both the torque being generated by the engine or being sent into the engine is possible. This design feature allowed the test fixture to measure motoring resistance torque due to friction and static compression torque all in one setup. To measure reaction torque using the load cell, an arm was attached to the engine mount shaft to convert the torque into a linear force (See Figure 64).

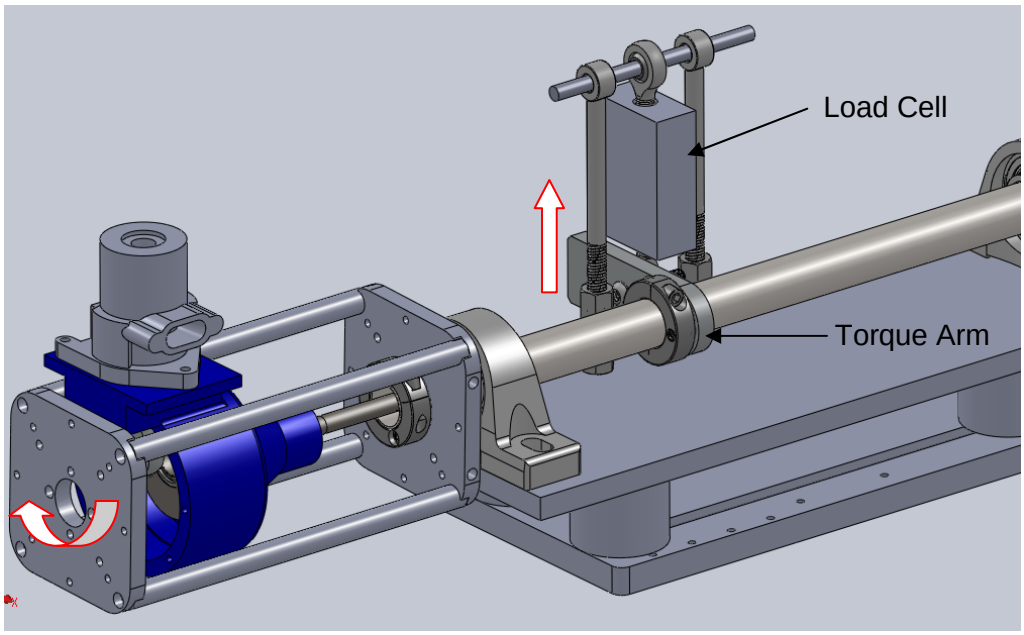

Figure 64 – Load Cell Measuring Engine Reaction Torque

Once the test stand was assembled the final step was to calibrate the load cell and convert the load cell voltage output to a usable torque value. A precision scale (0.1 gram resolution) and weights were used at the end of a long arm temporality installed on the engine mount shaft. A precision scale was temporarily placed under the end of the long arm. By taking the known distance between the end of the arm (where the scale is placed) and the center of rotation one can easily convert this into a known torque. The scale was then removed and the load cell reattached while keeping the weights in place. The load cell then measured the same load previously applied to the scale. Repeating this procedure multiple times with varying weights allowed a curve to be generated for multiple data points. From this linear curve an equation was extracted to convert the output voltage of the load cell directly to a torque value.

Motored Power Loss Test

Many previous research efforts on hypocycloid engines predict that engine friction may be lower due to the elimination of side load on the piston and high gear efficiencies (Karhula, 2008) (Andriano, 1998). However, it can also be argued that some friction is added back in through the gear train and the two additional bearings required in the bottom end. The fact that these two extra bearings are also subjected to twice engine RPM must be noted and considered.

A motoring friction test was performed on the now balanced Wiseman engine and then the stock engine for comparison. The test fixture described previously was used to carry out this test by attaching a DC electric motor to drive the flex shaft coupled to the engine output shaft. The engines were driven by the electric motor while measuring the torque required to maintain a particular engine speed. A variable speed pulse width modulated (PWM) controller was used to vary the voltage to the electric motor and adjust its speed.

The engines were first brought up to normal operating temperature by firing them under load. The spark plug and muffler were removed and the variable speed electric motor was attached at the end of the test fixture to drive the engines at the prescribed speed. The carburetor, held at wide open throttle, was left attached allowing fresh oil (and fuel) to enter the engine and maintain lubrication. Motoring the engines and measuring the required torque to maintain a certain speed provided some indication of the friction and pumping losses inside each engine. Knowing rpm, the power losses were also calculated. It should be noted however, that because the spark plug was removed and there are no combustion forces, the load on top of the piston is negligible. Without pressure loads on the piston the stock engine does not develop the same side

load it does while being fired. The Wiseman engine did not develop side load during this test or while being fired but the gears did not see the same loads they would during firing either. The bearings in both engines were also not subjected to the same level of loading during this motoring test as they would if the engines were being fired. That said, there was still value in measuring the motoring friction to see if there was a substantial difference in friction between the two engines in the unloaded state. The exhaust and spark plug were all removed to minimize pumping losses. However it should be noted that pumping losses were not completely eliminated because the piston was still pulling air in through the carburetor and pushing it out of the cylinder through various openings, including the spark plug hole.

Each engine was motored up to a particular speed on the test fixture and held constant for five seconds to provide enough time for the torque and rpm value to stabilize and eliminate any inertial effects. A torque and rpm value was then recorded and the electric motor (and engine) was returned to zero rpm. A number of data points between 500 and 3000 rpm were collected in order to generate a curve. The results of these tests are shown in Figure 65.

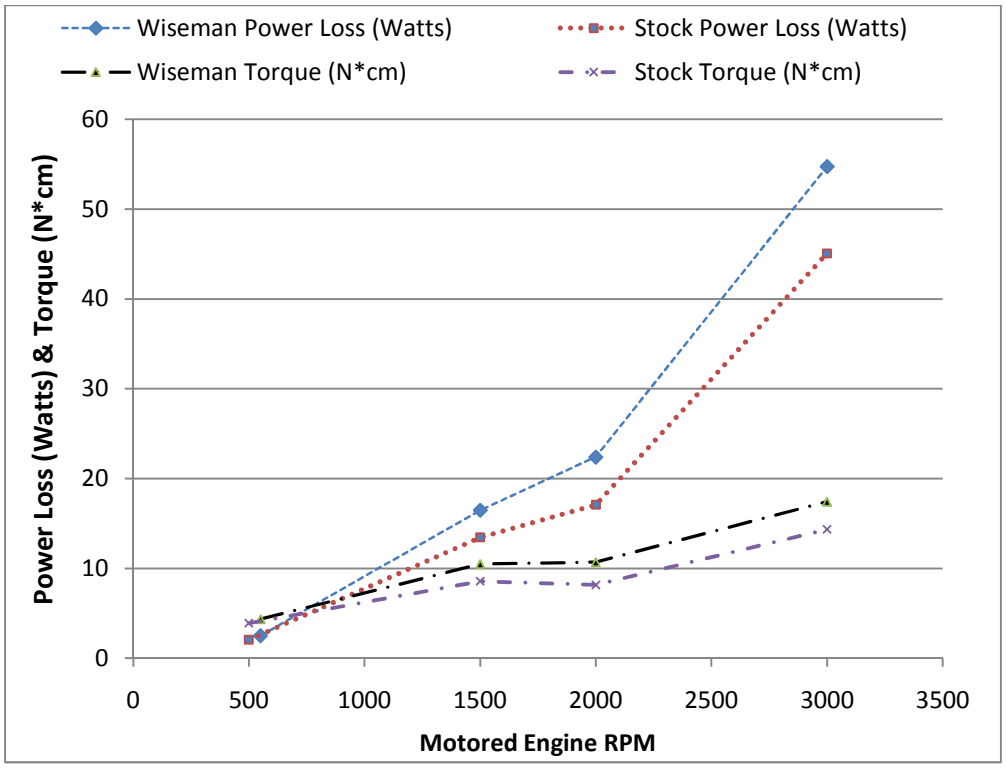

Figure 65 – Motored Friction Power Loss & Torque vs. RPM

The Wiseman Engine measured slightly higher torque and power loss during the tests. As speed increased the power loss gap between the two engines increased slightly in favor of the stock engine. At 3,000 RPM the measured frictional power loss of the Wiseman engine was 23% higher than the stock engine. Motoring the engines closer to their true design speed of 7000 rpm would have provided better empirical data but the electric motor was not capable of reaching these speeds. It was possible though, to fit a second order polynomial to each engine curve and extrapolate out to 7,000 rpm. It should be noted that the extrapolated results were only a prediction and should be proven empirically with a more powerful electric motor in future work. The extrapolated results on top of the original empirical results are shown in Figure 66.

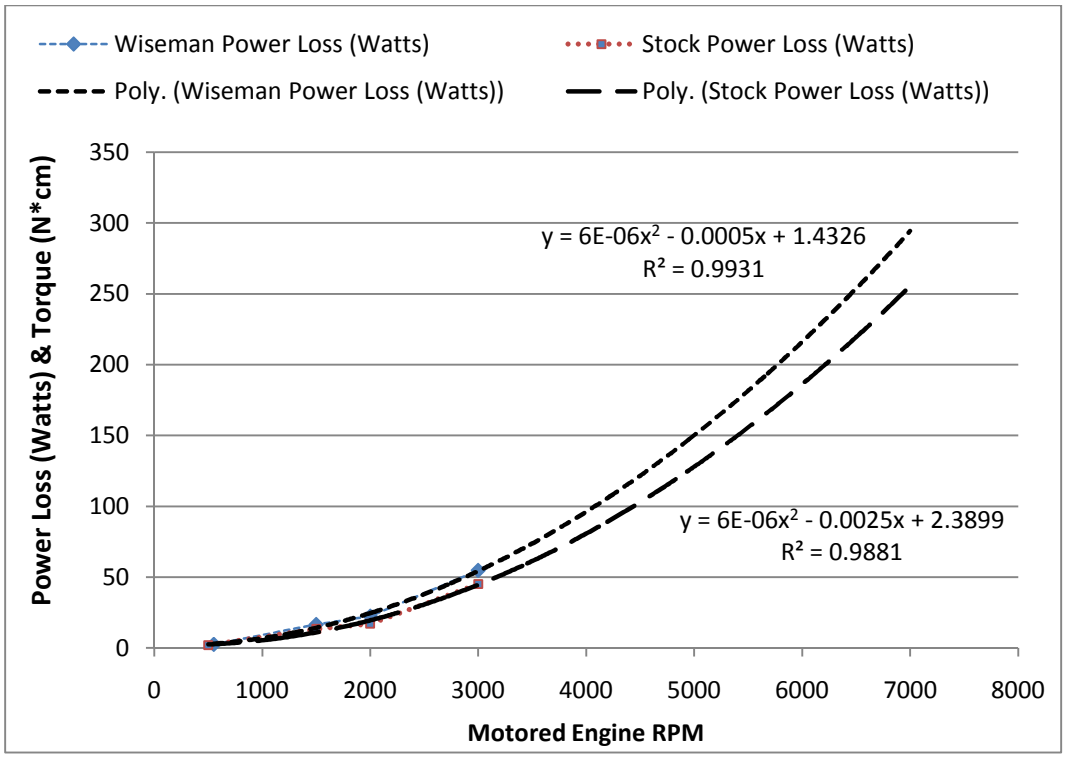

Figure 66 – Power loss vs. RPM Extrapolated to 7000 RPM

The extrapolated results, although only a prediction, provide some interesting insight into small engine performance. At 7,000 rpm, where the stock engine is designed to produce peak power, the results indicate that 278 W (.37 hp) is being dissipated to friction and other losses. The addition of true firing loads would likely increase friction losses in both engines but possibly less so in the Wiseman. For an engine that only produces about 746 W (1.0 hp), losing 278 W (37%) to friction and other losses is significant. According to the predicted curve, at 7,000 rpm, the Wiseman engine looses 292 W (.39 hp) to friction and other losses. At 7,000 rpm the predicted Wiseman engine power loss is about 5% higher than the stock engine.

Output Torque vs. Crankshaft Angle

Prior research efforts looked in depth at the kinematics and equations of motion for a hypocycloid engine (Karhula, 2008). Because a well running hypocycloid engine and a very similar slide crank engine (stock) was available for this research effort it was of value to apply some of the analytical results of past research efforts to the actual engines. Of particular interest was the instantaneous output torque of the engines for a given pressure (converted to a force) on top of the piston.

Equation 5 was used to convert linear force on the piston (gas force) to an output torque (gas torque) of the crank shaft for a single cylinder slider crank engine (Norton R. L., 2005).

$$\boldsymbol{T = F_g r \sin \omega t \left(1 + \frac{r}{l} \cos \omega t\right)} \qquad \text{Equation 5}$$

where:

T is gas torque of the output shaft.

F_g is the linear force generated the gas pressure on top of the piston.

r is the radius of the crankshaft.

ωt is crank angle in radians with 0 being TDC.

l is the length of connecting rod.

Equation 5 does not find the exact solution but it was sufficient for this analysis.

Calculating output torque for a given gas force of a hypocycloid engine is more simple and an exact solution. Rearranging Equation 6 and Equation 7 (Ruch, Fronczak, & Beachley, 1991) it is possible to calculate output torque for a given gas force and crank angle using Equation 8.

$$\boldsymbol{W_t = F_g \sin \theta_c}$$ Equation 6

$$\boldsymbol{T = W_t \frac{L}{2}}$$ Equation 7

$$\boldsymbol{T = F_g \sin \theta_c \frac{L}{2}}$$ Equation 8

where:

W_t is the tangential gear tooth load exerted on the pinion gear.

F_g is the linear force generated by the gas pressure on the piston.

L is the stroke of the engine.

T is torque of the output shaft.

θ_c is the angle of output shaft with 0 being TDC.

Using Equation 5 and Equation 8, one can compare the gas force conversion to output torque for a full half rotation (180º) by applying the same force (F_g) to the Wiseman and stock engine piston. Note that a firing engine gas force (F_g) varies dramatically with crank angle but in the following analysis it was first assumed constant for the purposes of comparison. The stock engine connecting rod length (l) measured 56.007 mm (2.205 in). The measured stroke is used to find the crank radius (r) for the stock engine and the $\frac{L}{2}$ term for the Wiseman engine. The Wiseman engine stroke is slightly longer at 28.575 mm (1.125 in) than the stock engine at stroke at 28.296 mm (1.114 in).

The constant gas force (F_g) was calculated by assuming a 1.0 bar (14.5 psi) pressure is applied to the top of the piston over the entire half rotation. The bore in both engines measured Ø36.450 mm (Ø1.435 in) in diameter resulting in an area of 1043 mm^2 (1.617 in^2). The resulting gas force is simply pressure times area and is thus 104.4 N (23.46 lbf). Plugging in the described values, the output torque was calculated for every five degrees of crank rotation producing the plot shown in Figure 67.

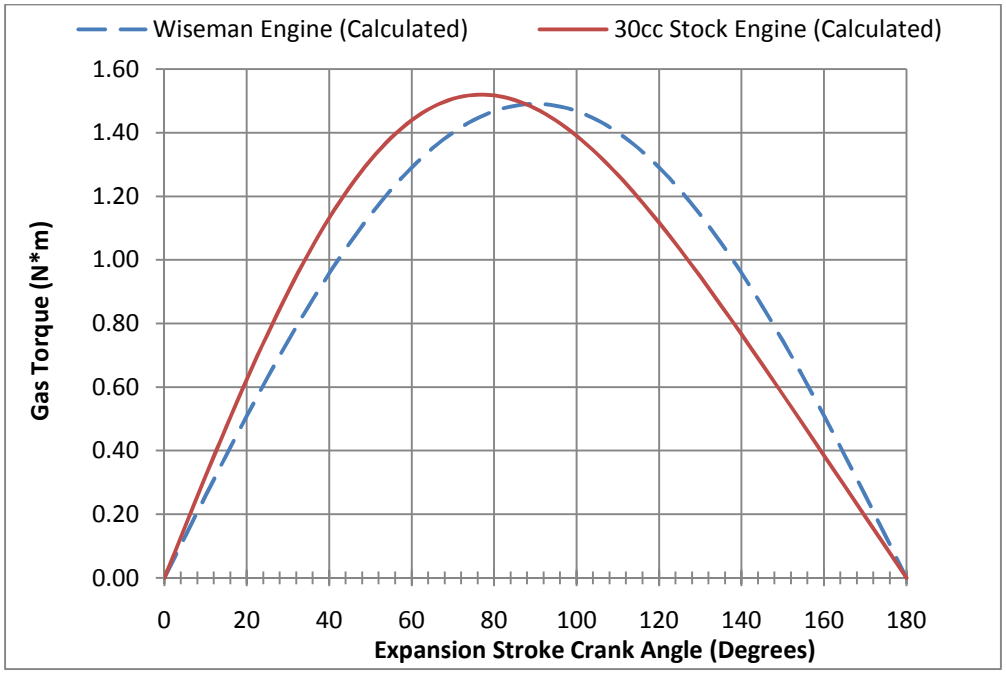

Figure 67 – Gas Torque vs. Crank Angle @ 1.0 bar Pressure on Piston

The results show a 1.9% higher peak output torque for the stock engine over the Wiseman engine even though the stock engine stroke is shorter. If the two engines had the same stroke of 28.575 mm (1.125 inches), the calculated stock engine peak output torque is 3.0% higher than the Wiseman engine for the same 1.0 bar applied pressure. The results also show the peak output torque for the stock engine occurs at 75º ATDC as opposed to 90º ATDC for the Wiseman

engine. The stock engine earlier peak and higher output torque early in the stroke is important because a fired engine typically produces peak cylinder pressures at 10º to 20º ATDC. The stock engine appears to convert gas pressure to torque in a manner better suited to typical combustion pressure behavior. These result indicates the Wiseman engine's optimal ignition timing might be less advanced (delayed ignition) than the stock engine in order to delay peak pressure in the cylinder. After 85º the Wiseman engine begins producing more torque for the same gas pressure but at this point the combustion pressure is substantially reduced.

Although the above equations are well proven and fairly simple it was worth validating them on the actual engines to reaffirm their accuracy. The engine test fixture developed provided a simple and effective way of validating the above equations using empirical data. Each engine was mounted to the test fixture and a degree wheel was attached to the flywheel (See Figure 68) for crankshaft angle resolution. A compressed air tank and regulator provided a constant air pressure of 1.0 bar (measured with a gauge) that was applied to the top of the piston via the spark plug hole. A plumbing schematic of the test setup is shown in Figure 69. The piston was forced down by the applied air pressure which generated a torque at the output shaft via the slider crank or hypocycloid mechanism. The output shaft (via flywheel) was fixed resulting in an equal and opposite torque applied to the engine mount shaft on the test fixture. The only constraint preventing the engine from rotating was the load cell attached to its arm, which is fixed to the engine mount shaft. The load cell and Signal Express software could then output a torque value for a given gas pressure and output shaft angle.

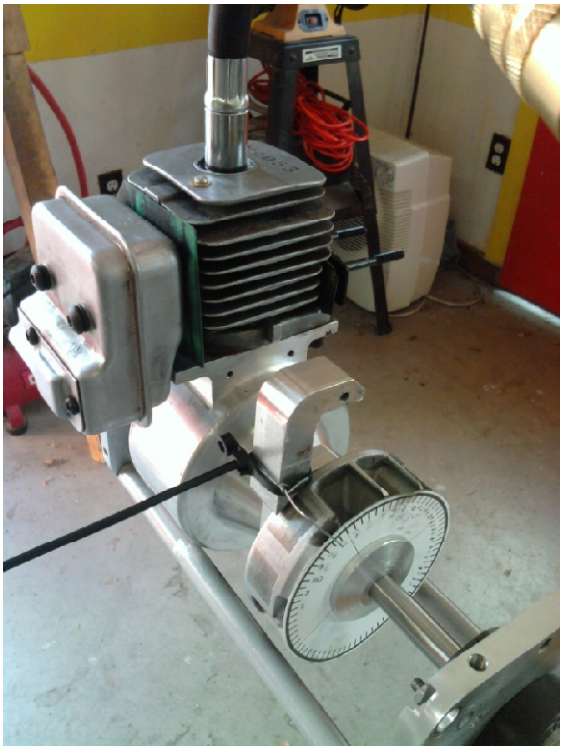

Figure 68 – Degree wheel Attached to Flywheel

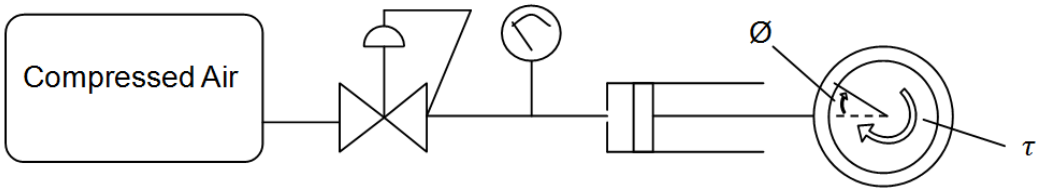

Figure 69 – Pressure Torque Test Fixture Plumbing Schematic

The regulator was adjusted to1.0 bar (14.5 psi) pressure applied to the cylinder via the spark plug hole and the flywheel was manually held fixed for a torque measurement. A measurement was taken every 10 degrees starting at TDC (0º) and ending when the upper piston ring just passed the exhaust port opening. Once the upper piston ring just passed the exhaust port, significant leakage started to affect the pressure reading and the results. The result of the

performed test for the Wiseman and stock engines are shown in Figure 70 and Figure 71, respectively.

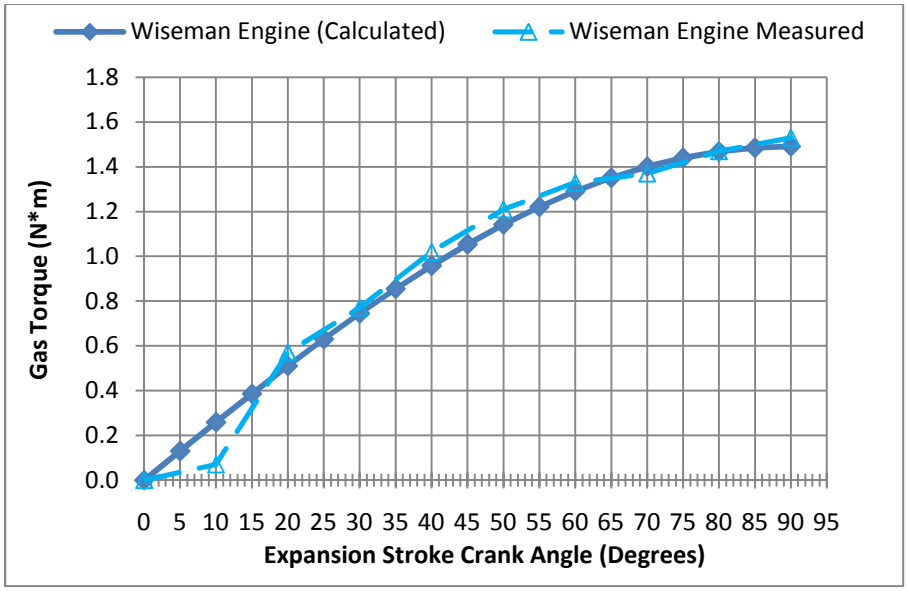

Figure 70 – Wiseman Gas Torque vs. Crank Angle at 1.0 bar

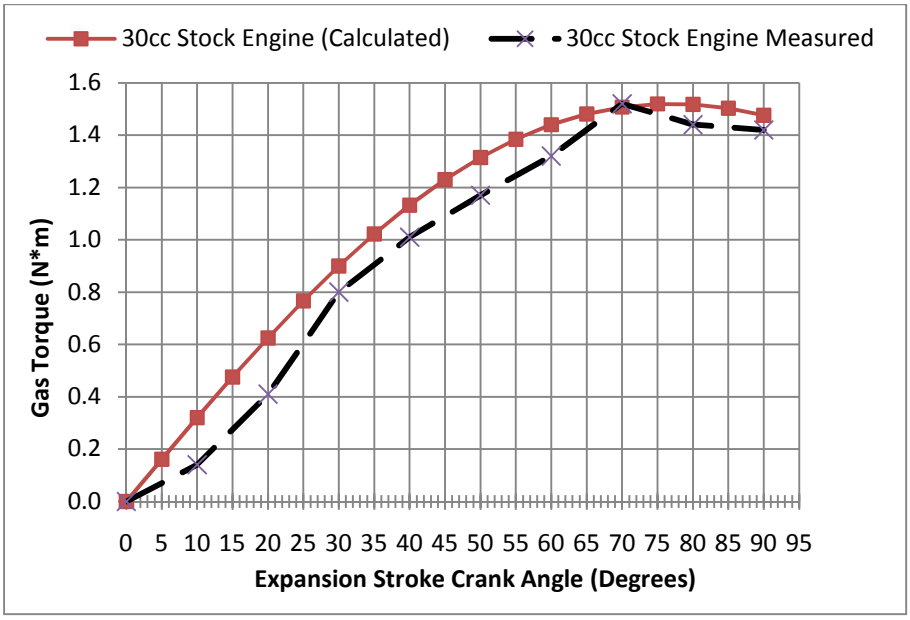

Figure 71 – Stock Gas Torque vs. Crank Angle at 1.0 bar

The results of the measured torque experiment using the load cell test fixture correlate well to the calculated values for both engines. The empirical test results conclusively validate the equations used to calculate torque for both engines. The error is likely attributed to the inexact calibration of the load cell and static friction causing the piston to stick and slip. In the stock engine the measured values were consistently lower than calculated. This can be explained by the existence of piston side load in the stock engine (absent in Wiseman) causing higher static friction and reduced output torque. The lack of piston side load in the Wiseman engine and lower piston friction results in better correlation to the predicted results. The measured data for each engine is plotted in Figure 72 which shows that although the stock engine has higher mechanical advantage, the higher friction places the two curves almost equivalent to each other. Note these results are influenced by static friction because the readings were taken while the piston was at rest. A moving piston in a running engine experiences dynamic friction (lower than static) except at TDC and BDC.

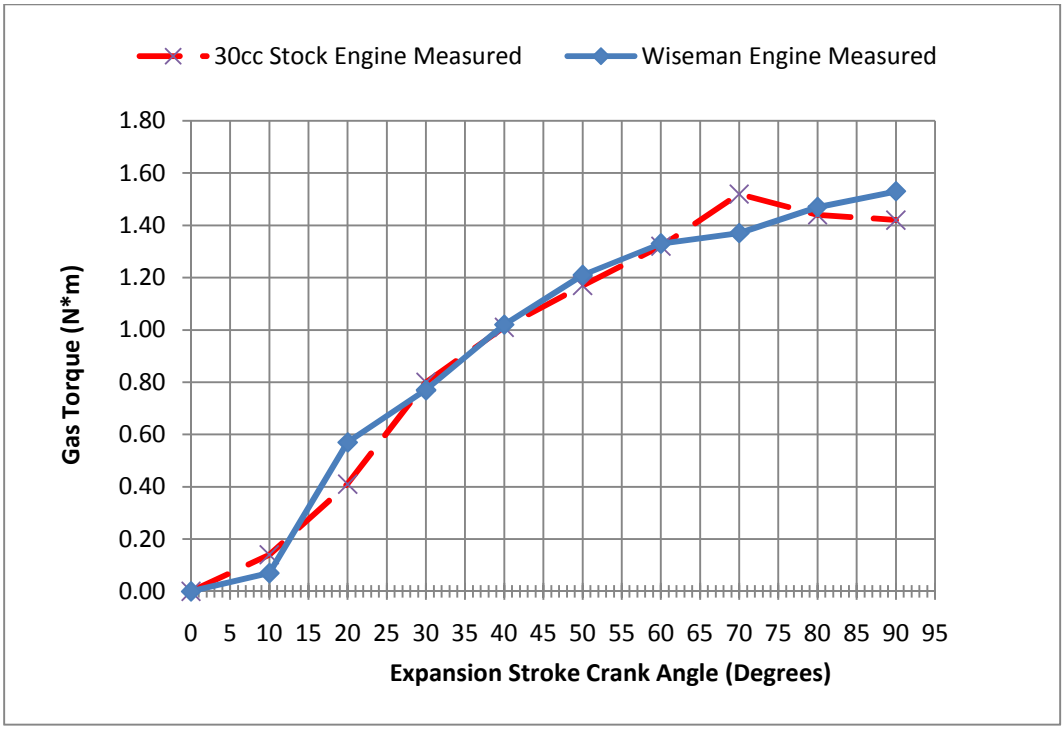

Figure 72 – Wiseman and Stock Gas Torque vs. Crank Angle

The next logical step was to plug in an actual gas pressure curve into Equation 5 and Equation 8 instead of a constant pressure to see the effect of higher torque conversion by the stock engine during the first half of the expansion stroke. Unfortunately, a complete gas pressure curve could not be obtained on the test engines. In lieu of actual data, a curve was borrowed from another two-cycle engine that produces 10 horsepower at 8000 rpm (Blair, 1996). Because the stock engine produces closer to 1.0 horsepower the curve was scaled down by a factor of 0.21 to generate a new curve whose maximum pressure was more appropriate to this engine type and power. Typical peak pressure for this style of piston-ported two-stroke engine is around 300 psi (20.7 bar) (Payne, 2011). The resulting scaled gas pressure used to continue this analysis is shown in Figure 73.

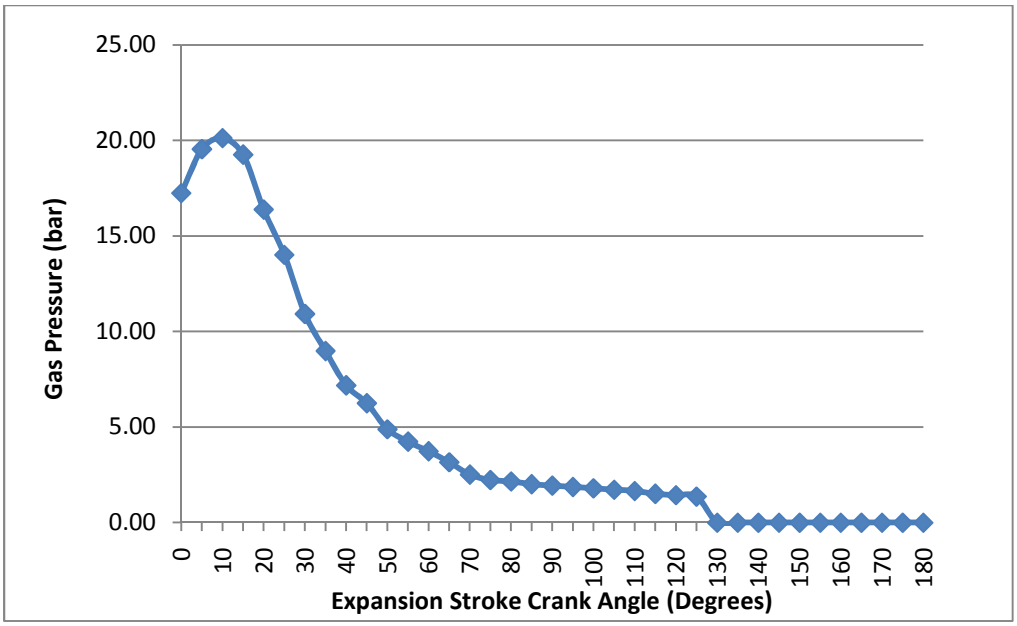

Figure 73 – Scaled Gas Pressure vs. Expansion Stroke Crank Angle Curve

Peak pressure occurs at 10 degrees ATDC in this curve. The exhaust port starts to open at 125 degrees (ATDC) at which point the pressure rapidly drops to zero. It should be noted that this curve is not indented to accurately represent the expected curve for the test engines and is only a rough approximation. The peak pressure may occur at a different angle and behave differently. In addition the exhaust port on each engine does not start to open at 125 degrees ATDC. The exhaust port for the Wiseman engine starts to open at 122 degrees ATDC while the stock engine port starts to open at 108 degrees. Despite these differences the intent here was only to gain a better understanding of how the torque output of the two engines is different assuming the same pressure curve is applied to each engine. It should be understood the analysis deviated somewhat from the physical engines in order to remove the influence of so many different variables.

The output torque calculated is the lossless torque at the output shaft of each engine. Friction and compression losses are assumed zero. Plugging the

pressure curve into the appropriate torque equation for each engine produces the plot shown in Figure 74.

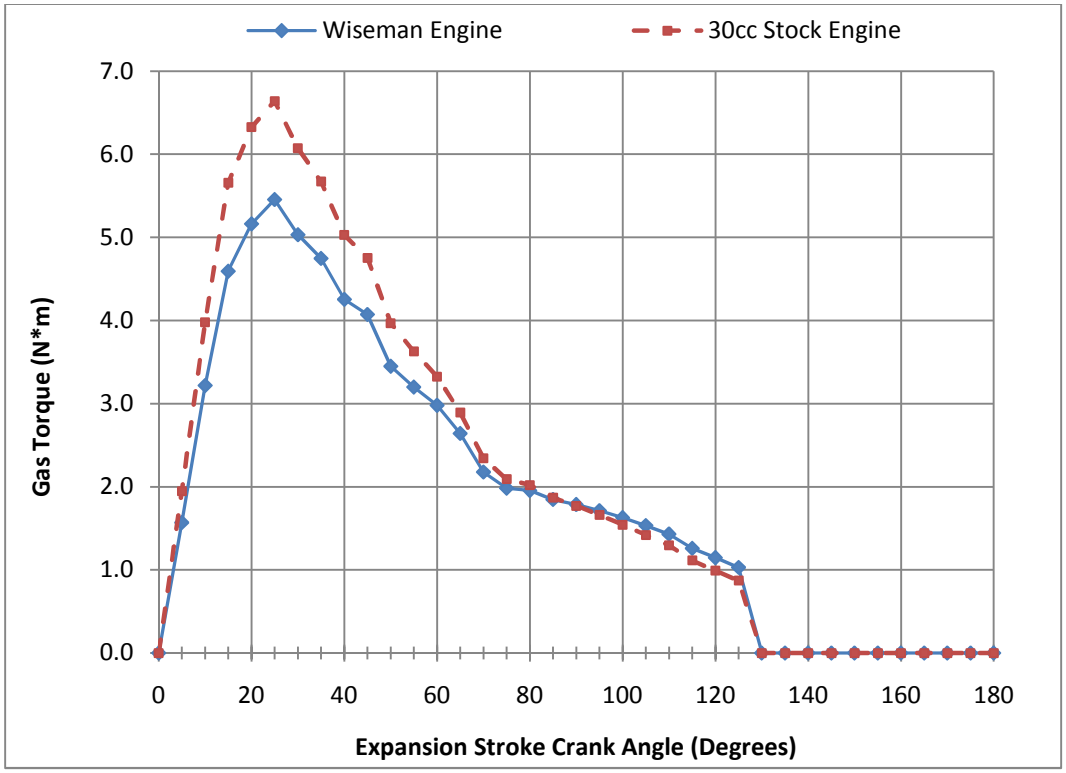

Figure 74 – Gas Torque vs. Crank Angle for Scaled Pressure

The results provide some insight into comparing the performance of both engines. Although the difference in torque output for a constant pressure is only a few percent in favor of the stock engine in Figure 70, the difference calculated when using an actual pressure curve is significant. The stock engine torque output is higher starting from zero degrees until about 90 degrees where the curves intersect. From 90 degrees until 125 degrees ATDC, the Wiseman output torque is slightly higher, but at this point, the pressure has significantly dropped. The maximum difference occurs at 25 degrees ATDC at which point the stock engine output torque is 6.64 N•m compared to 5.46 N•m for Wiseman, or 22% higher. The average torque over the entire expansion stroke is 2.13 N•m for the

stock engine and 1.88 N•m for the Wiseman engine. If the same pressure curve is applied to each engine, and all else being equal, the Wiseman engine would produce lower torque and power at the same rpm. Using the average torque of each engine and assuming peak pressure occurs at 7,000 rpm (peak pressure typically occurs at a lower rpm than peak power and near peak torque but 7000 rpm was chosen for consistency here) the lossless power output of the stock engine is 1.56 kW (2.12 hp) while the Wiseman engine produces 1.38 kW (1.87 hp). The quoted power figures are for the lossless case, which does not include power lost to pumping and friction.

The preceding results indicate that the hypocycloid geometry and resulting sinusoidal motion of the Wiseman piston is not quite as effective in converting gas pressure to torque when stroke and displacement are equal. Note that the Wiseman engine stroke is longer by .280 mm (.011 in) giving it a slight advantage in this analysis. Still assuming the same pressure curve the Wiseman engine would require an increase in stroke to 31.75 mm (1.27 in) to equal the 2.13 N•m average torque output of the stock engine. The resulting plot for output torque in which the two engines have the same average torque is shown in Figure 75.

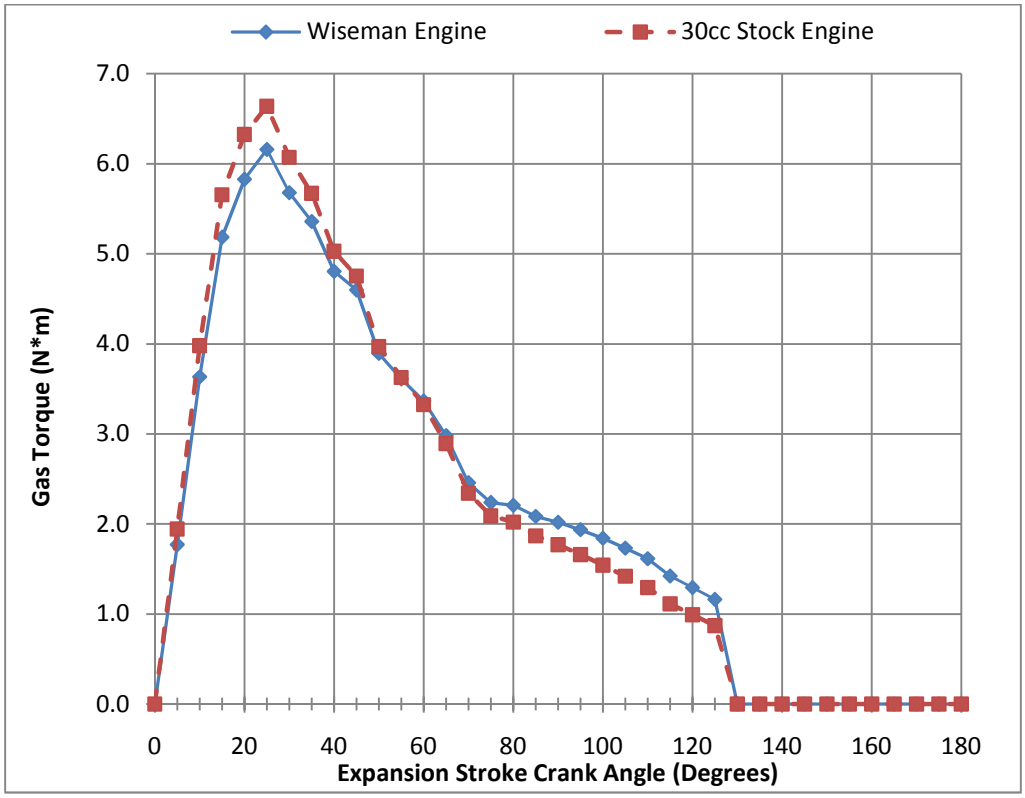

Figure 75 – Gas Torque vs. Crank Angle for Wiseman stroke = 1.27 in

Figure 75 shows that although it requires a longer stroke and larger displacment to achieve the same average torque, the Wiseman engine peak torque is lower. This results from both the longer stroke of the Wiseman but also better pressure to torque conversion after 90 degrees ATDC.

In the preceeding gas output torque calculations the same pressure curve versus crank angle is used in all instances. In reality the Wiseman piston sits higher in the cylinder for a given crank angle except at TDC and BDC. This means the volume available for combustion gasses to expand is also less. It was worthwhile then to investigate volume versus crank angle for both the Wiseman and stock engine. The volume above the stock piston (zero volume origin

occuring at TDC, does not include clearance volume) for a given crank angle can be found using Equation 9 and Equation 10 (Heywood, 1988).

$$s = a\cos\theta + (l^2 - a^2 - \sin^2\theta)^{\frac{1}{2}} \qquad \text{Equation 9}$$

$$V = \frac{\pi B^2}{4}(l + a + s) \qquad \text{Equation 10}$$

where:

- s is piston posistion, maximum at TDC
- a crankshaft radius or stroke divided by 2
- θ is crankangle with 0º being TDC
- l is the length of the connecting rod
- V is the volume above the piston, and is equal to 0 at TDC
- B Is the diameter of the cylinder diameter (bore)

The equations for finding the volume above the Wiseman piston were not readily available and are dervied here using Figure 76. The origin or zero point is definded to occur when the piston is at TDC and crankangle, θ is zero.

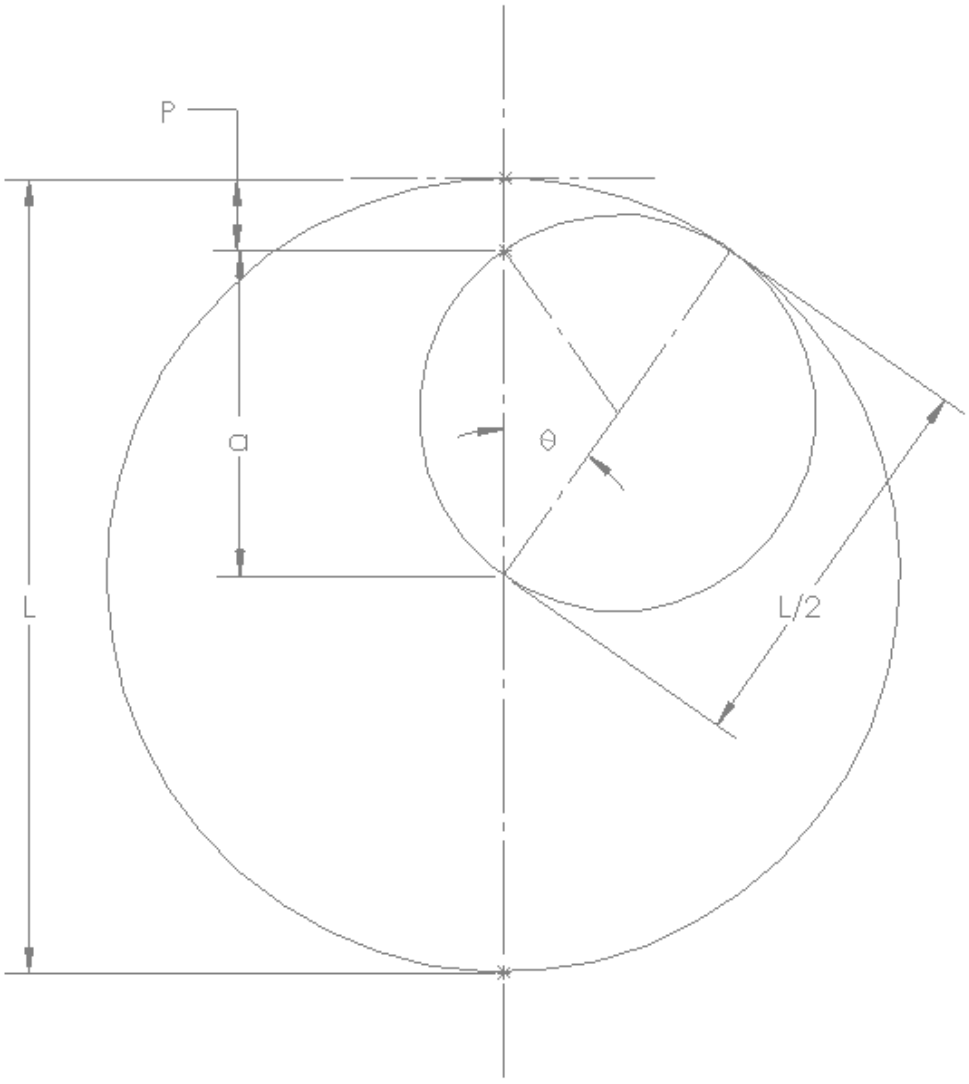

Figure 76 – Wiseman (Hypocycloid) Piston Position Diagram

The distance P or piston position relative to TDC can be found using Equation 11, from θ = 0 to 90º and Equation 12 from θ = 90º to 180º. Knowing piston postion, volume is found using Equation 13.

$$\boldsymbol{P = \frac{L}{2} - \left(\frac{L}{2} cos\ \theta\right)}$$ Equation 11

$$\boldsymbol{P = \frac{L}{2} + \left(\frac{L}{2}\, cos\, (\pi - \theta)\right)}$$ Equation 12

$$\boldsymbol{V = P\left(\frac{\pi B^2}{4}\right)}$$ Equation 13

where:

L is the stroke length of the engine.

θ is crankangle with 0 being TDC.

V is the volume above piston, equals 0 at TD.

B is the diameter of the cylinder (bore).

P is the postion of the piston with the origin being TDC.

Plotting Equation 10 and Equation 13 from 0º to 180º results in the graph shown in Figure 77.

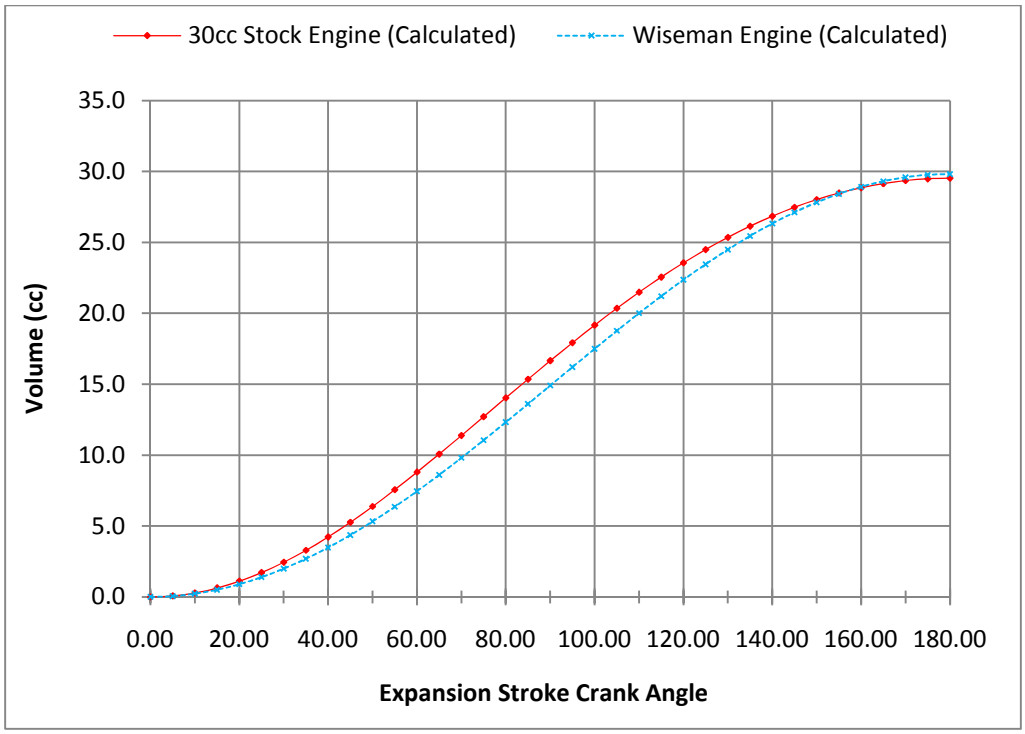

Figure 77 – Expansion Stroke Crank Angle vs. Volume above Piston

The results shown in Figure 77 indicate the volume is less for the Wiseman engine for most of the expansion stroke. The difference in volume starts at zero and gradually increases until about 90º ATDC at which point the difference starts to decrease. With less volume for combustion gasses to expand in the Wiseman engine, higher combustion pressures would likely result. Higher combustion pressures would generate increased torque output and may earn back some or all of the torque output defficiency below the stock engine. However, there are practical limits to peak combustion pressure in order to avoid preignition (in spark-ignition engines) and excessive NO_x emissions. Investigating how the reduced expansion volume behavior of the Wiseman engine affects combustion pressure would be of great value but is outside the scope of this research effort.

Baseline Performance Evaluation

A better understanding of the peak performance and fuel efficiency of the actual Wiseman Engine was gained through extensive dynamometer testing. The Wiseman engine was tested on two different dynamometers with different objectives and desired outcomes for each test:

- MTD Dynamometer and BSFC: This series of testing took place on a calibrated, EPA certified dynamometer made available by MTD Southwest Inc. in Tempe, Arizona. The test objective on the MTD dynamometer was to determine brake specific fuel consumption (BSFC) for the Wiseman engine while tuned for best emissions at peak power. Only the Wiseman engine was run on the MTD dynamometer and not the stock engine. However data from a similar MTD brand 31cc two-cycle, piston-ported engine was available and used for comparison against the Wiseman.
- Land and Sea Dynamometer and Peak Power: The second series of tests took place on a custom dynamometer test stand using a Land and Sea water brake. The test stand was specifically designed to test high speed and low torque engines. The test objective on the Land and Sea dynamometer was to evaluate peak performance while the Wiseman and stock engine were tuned for maximum power. The majority of testing in this research effort took place on the Land and Sea dynamometer.

MTD dynamometer and BSFC

The Wiseman engine was tested on the MTD dynamometer in a mode where the operator selects a desired engine speed. The dynamometer then applies the

necessary load to maintain that speed regardless of throttle position and engine output (assuming it's above a minimum threshold).

The Wiseman engine was brought up to normal operating temperature and then multiple setup runs were taken at wide open throttle. Data was displayed live at this time but not recorded during the first few setup runs. The first setup run was set for 7,000 rpm and then followed by successive setup runs at 6,500, 6,000, and finally 5,500 rpm. During each run, the dynamometer technician adjusted the Wiseman carburetor mixture settings until an optimal air fuel ratio and emission levels (according to typical MTD production engines) were obtained. The air fuel ratio and emission output of the engine (including CO, CO_2, HC and NO_x) were all measured and displayed in real time. Of all the runs, 6000 rpm produced the most power and was therefore selected for an official recorded run. On this run the ideal air fuel ratio for best emissions at 6,000 rpm was lambda =.89.

The recorded 6,000 rpm run lasted 3 minutes and 20 seconds, all at wide open throttle. The air-fuel ratio remained steady and averaged a lamda = 0.89 over the run. The average power was 0.60 hp (.44 kW) and the average BSFC was 410.1 g/hp•hr over the run. Although the stock engine was not available for identical testing at MTD, data from a similar 31cc production string trimmer engine was provided by MTD for comparison. The Wiseman results compared with a similar run for the MTD 31cc are shown in Figure 78, Figure 79, and Figure 80.

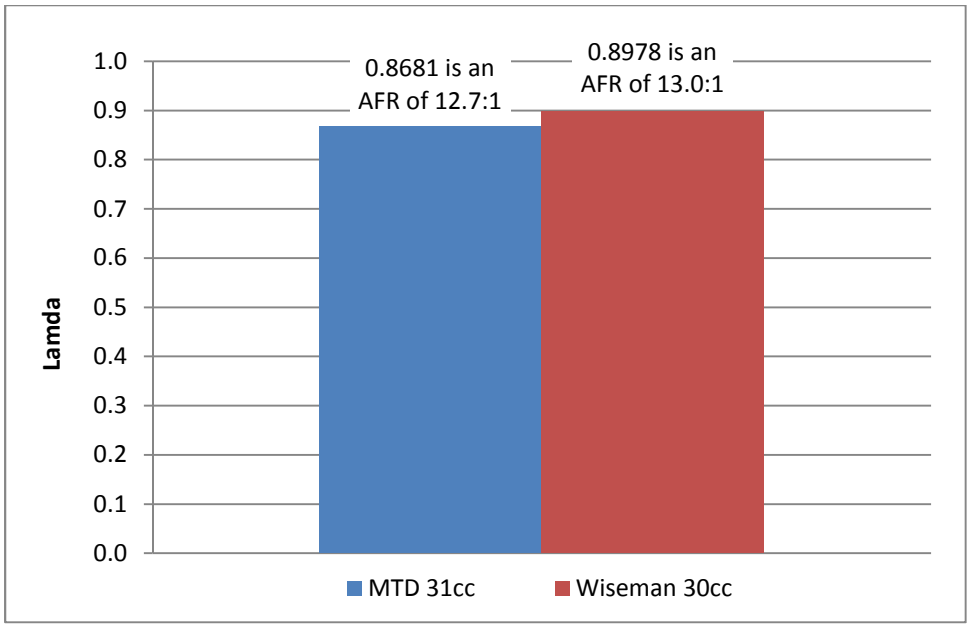

Figure 78 – Average Lamda During Peak Power Runs

The Wiseman engine ran with best emissions at a slightly leaner setting than the 31cc MTD engine. The MTD technician noted that different engines often require a different air fuel ratio to achieve best emissions performance.

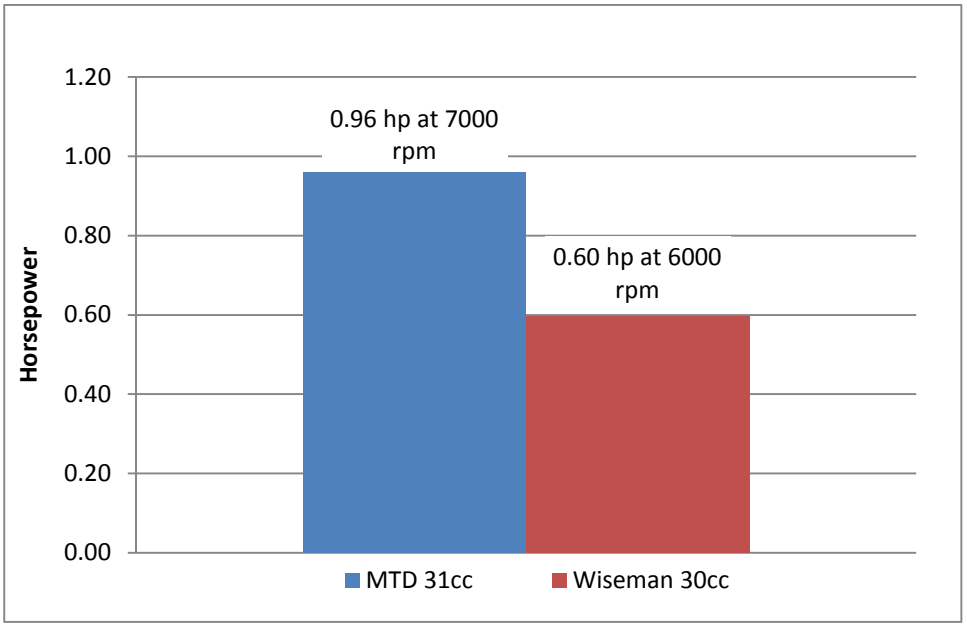

Figure 79 – Average Horsepower During Peak Power Runs

During this run the Wiseman engine made 38% less power than the MTD 31cc. The MTD 31cc is slightly larger in displacement and peaks at a higher rpm so normalizing to brake mean effective pressure (BMEP) is prudent. BMEP in kPa was found using Equation 14 (Heywood, 1988) and then converted to bar and psi.

$$\boldsymbol{BMEP} = \frac{\boldsymbol{P n_r}}{\mathrm{V_d N}} \qquad \text{Equation 14}$$

where:

P is the power output measured on a dynamometer in Watts.

n_r is the number of crank revolutions for each power stroke.

V_d is the displacment volume of the engine.

N is rotational speed of the output shaft in revolutions per second

The MTD 31cc has a 1.378 in bore and a 1.284 in stroke resulting in an exact displacement of 31.38 cc (1.915 in^3). The resulting MTD 31cc BMEP is 1.96 bar (28.4 psi) while the Wiseman BMEP for the 6,000 rpm run is 1.50 bar (21.8 psi). The BMEP for Wiseman engine is 23.2% lower than the MTD 31cc which indicates its lower performance cannot be entirely attributed to smaller displacement and lower peak rpm power. Calculating BMEP in this case was useful for making a valid comparison of engines with unequal displacements and different peak output rpm.

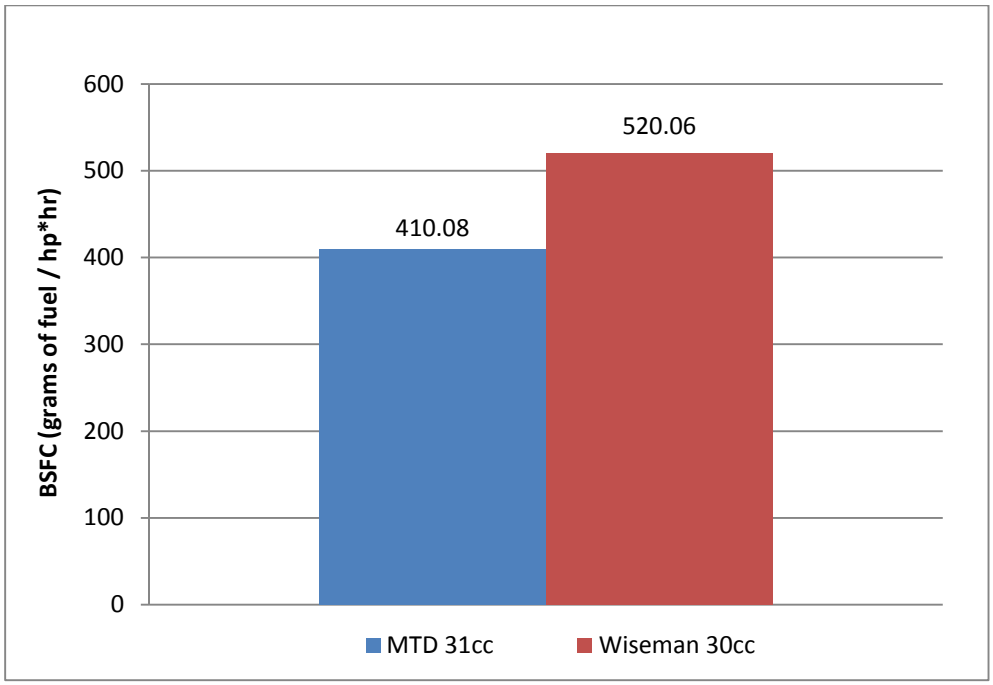

Figure 80 – BSFC Wiseman and MTD 31cc

BSFC for the 6,000 rpm run showed the Wiseman engine was 21% less fuel efficient on this test run. The Wiseman air-fuel ratio was slightly leaner (but still rich of stoichiometric) than the MTD 31cc. Assuming all else equal, one might expect a better BSFC for the Wiseman engine with a leaner AFR but this was the case. An even leaner setting might improve BSFC for the Wiseman but at the expense of lower peak power and increased NO_x emissions.

Land and Sea Dynamometer and Peak Power

All other dynamometer testing on the Wiseman and stock engine were done with the Land and Sea dynamometer setup. It is critical to note that the data from the MTD dynamometer cannot be directly compared to data from the Land and Sea dynamometer. The Land and Sea dynamometer is not calibrated and the transmission losses are not exactly known or accounted for in the results.

The assumption was that all results from the Land and Sea dyno stand were probably low by 10-20 % but equally low for all engines tested.

The five inch water brake from Land and Sea is not well suited to measure below 1.0 horsepower. In order to properly measure low torque at high rpm and below 1.0 horsepower, a 4.8:1 ratio chain drive multiplies the torque of the engine into the water brake. The Land and Sea dynamometer includes a weather station that measures temperature, humidity, and barometric pressure in real time and automatically compensates according to SAE standard J1349 (SAE International, 2008). A photo of the Wiseman engine mounted to this dynamometer is shown in Figure 81.

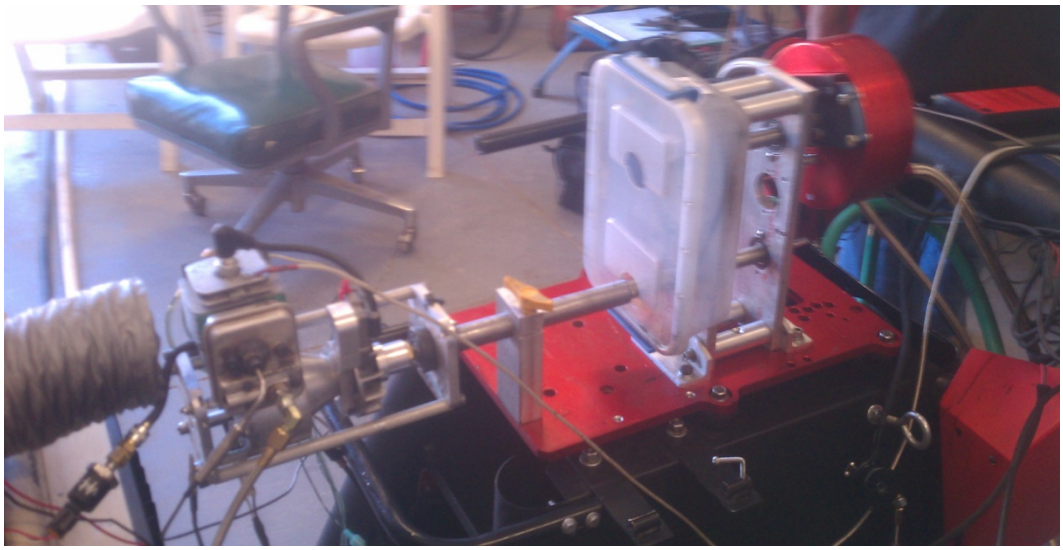

Figure 81 – Wiseman Engine Mounted to Land and Sea Dynamometer

The objective on the Land and Sea dynamometer was to tune and collect data for each engine at maximum power rather than best emissions. The tuning variables included carburetor mixture settings, cylinder head temperature (cooling air flow), and ignition timing (Wiseman only). These variables were adjusted independently and together until a consistent maximum power run was

achieved for each engine. The resulting maximum power runs for each engine are shown in Figure 82.

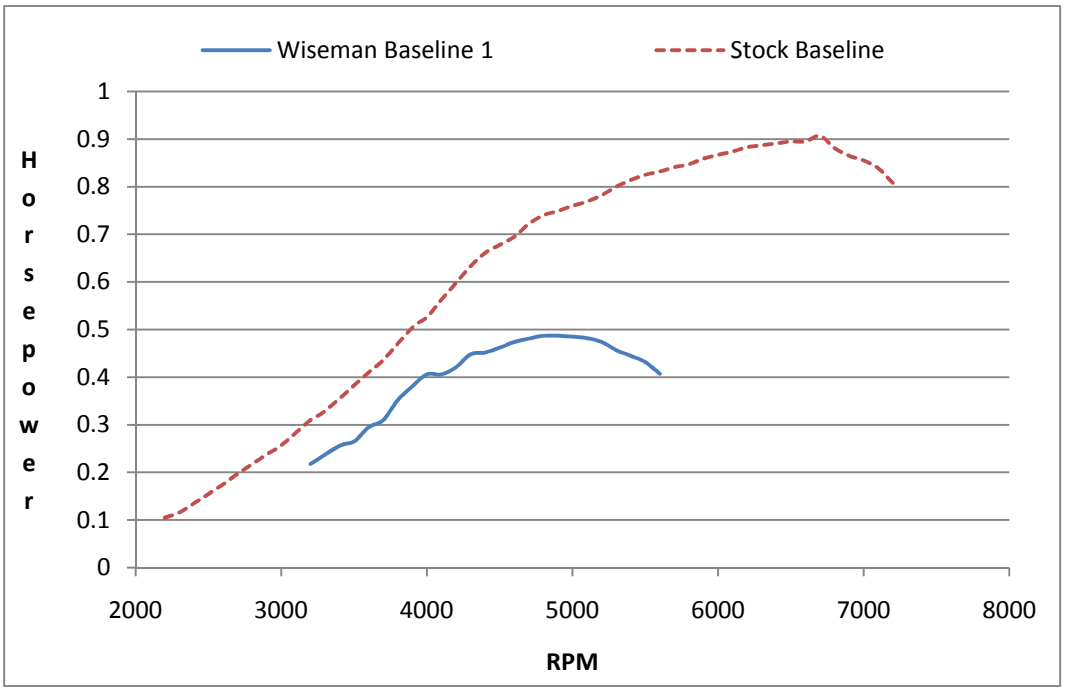

Figure 82 – Baseline Peak Power Dynamometer Runs

The result of the tuned for maximum power runs show the stock engine was able to achieve just above 0.90 hp (.67 kW) at 6800 rpm giving it a BMEP of 29.25 psi (2.02 bar). The Wiseman engine peaked at 0.49 hp (.37 kW) at 4800 rpm giving it a BMEP of 22.22 psi (1.53 bar). The peak power results found here showed the Wiseman engine produced 46% less power and had 24% lower BMEP than the stock engine.

Primary Compression Ratio (PCR)

A possible contributor to the lower power output of the Wiseman engine was its larger crankcase and internal volume. Like most two cycle engines the crankcase serves as a working chamber to pull in each fuel air charge, compress it, and then pump it through the transfer ports. The ratio of engine displacement

to the total volume under the piston at TDC (including the crankcase) is called the primary compression ratio (PCR). This ratio is critical in two cycle engines and if too low (Wiseman Engine) or too high, this ratio can have a negative impact on peak power output. (Ortiz, 2011).

The PCR for both the stock and Wiseman engine was calculated using the same CAD models developed for the balance analysis and Equation 15.

$$\boldsymbol{PCR = \frac{V_i}{V_i - D}} \qquad \text{Equation 15}$$

where:

PCR is the Primary Compression Ratio.

V_i is the total volume under the piston (including crankcase) at TDC.

D is the volumetric displacement of the piston from TDC to BDC.

The input values and results of the calculations using Equation 15 are shown in Table 3.

Engine	Displacement	Volume under Piston at TDC	Primary Compression Ratio
Wiseman	1.819 in^3 (29.81 cc)	14.82 in^3 (242.5 cc)	1.14
Stock	1.802 in^3 (29.53 cc)	6.10 in^3 (100 cc)	1.42

Table 3 – Primary Compression Ratio of Wiseman and Stock Engine

The difference in PCR between the two engines was of interest and worth further analysis to determine if peak power and BMEP could be improved for the

Wiseman engine. Ideally, the Wiseman engine should have been modified so that its PCR equaled that of the stock engine and then retested on the dynamometer. Unfortunately, decreasing the volume of the Wiseman crankcase enough to approach the stock engine was not easily accomplished without a complete redesign of the crankcase.

Lotus Engine Simulation (LES)

Without a simple way to match the PCR of the stock engine another method was desirable to investigate if the lower PCR of the Wiseman engine was a major contributor to its lower power output. Lotus Engine Simulation (LES) software is a tool capable of investigating the effect of PCR on power without building or modifying any hardware. LES software allows users to build and simulate a complete engine from intake to exhaust and then output useful data including power curves versus rpm. It was not possible to model the alternative (sinusoidal) motion of the piston in the Wiseman engine and therefore only the stock engine was considered in this study. The software assumes a slider crank mechanism and calculates piston kinematics using stroke, crank radius, and connecting rod length. It was expected that the affect of PCR on performance of the stock engine would be very similar in the Wiseman engine. LES can simulate a large number of input variables and output a wide variety of useful engine data. However, in this analysis the objective was only to understand the effect of PCR on peak power.

The starting point used to model the stock engine was a model of a 125cc two-cycle engine provided as a training tool from Lotus (Lotus Cars Ltd., 2001). The 30cc stock engine dimensions and design parameters were then used to modify the 125cc model to fit the stock engine. The assumption was that,

although larger in displacement, the 125cc two-cycle model provides a solid baseline to build the stock (30cc) model from. As a result, a number of inputs not specific to the stock engine, were borrowed from the 125cc model. These inputs included various temperatures, combustion, heat transfer, and scavenging models. It should be noted that the objective of this effort was not to accurately predict performance but rather to make relative performance comparisons of the stock engine simulated with different primary compression ratios.

LES uses a simple drag and drop type graphical interface. Engine components were brought into the model and then connected together. Each component dropped into the model required a number of inputs to fully define its properties. The completed model for the stock engine is shown in Figure 1Figure 83.

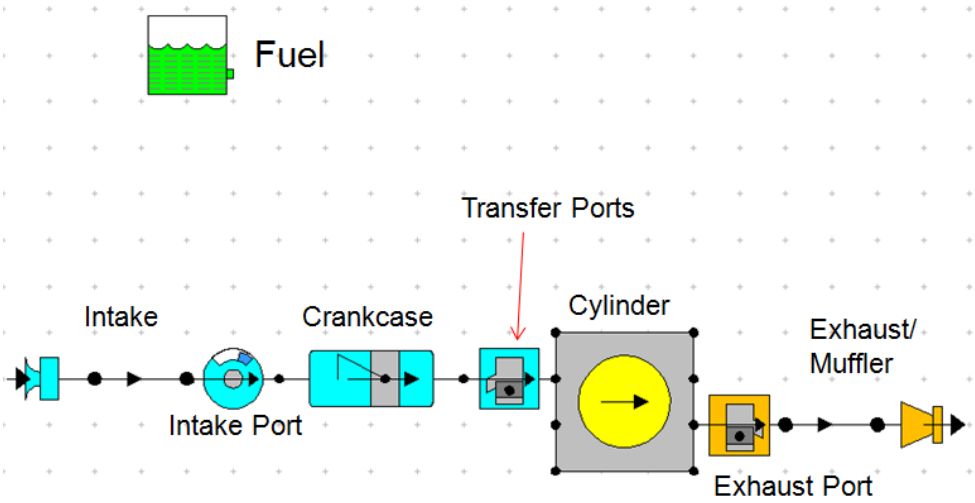

Figure 83 – LES Engine Simulation Model

The intake system was modeled as a simple tube that approximates the dimensions of the carburetor with a wide open throttle. A piston ported intake valve was not available in LES and in its place a rotary disk valve was used. The

piston port diameter and port timing angles from the stock engine were used to populate the inputs of the rotary disk valve.

The crankcase was simulated by a variable volume inlet plenum that is 180 degrees out of phase with the engine piston and cylinder. In other words minimum volume in the crankcase occurs at maximum volume in the cylinder and vice versa. The compression ratio of the variable volume inlet plenum was set equivalent to the PCR. Next in line is the transfer ports modeled as a single, rectangular opening whose total opening area is equal to the combined opening area of the two transfer ports on the actual engine. Transfer port open and closing angles were defined according to the stock engine dimensions.

The cylinder immediately follows the transfer ports and was defined based on the stock engine. Bore, stroke, connecting rod length, and clearance volume make up the primary inputs. Additionally, combustion, heat transfer, and scavenging models were defined for the cylinder. A Single Wiebe type combustion model with coefficients A = 10 and M = 2 were used. An Annand heat transfer model along with a Perfect Mixing Scavenging model was used. The selection of these models and coefficients were borrowed from the 125cc model. It was expected these parameters are also appropriate for the smaller displacement, 30cc stock engine.

At the outlet of the cylinder is a piston ported exhaust, approximated as a rectangular opening, equal in size to the actual port in the stock engine cylinder. The port opening and closing angles were also made equivalent. The final component is the exhaust outlet or muffler. The muffler on these engines is not a tuned profile that is designed for performance. It is essentially a rectangular box and was not easily represented in the LES software. As a result the model does

not accurately represent input dimensions for the exhaust. Instead, a simple straight tube was defined equal in length and diameter to the outlet of the muffler.

A tabulated and detailed summary of all described engine data used to build the model can be found in Appendix A. The model calculated steady state brake power starting at 4000 rpm and then every 500 rpm until a comprehensive power curve was obtained. The model was initially run twice to generate a power curve for a PCR equal to 1.14 (Wiseman equivalent) and then 1.42 (stock). The resulting power curves from the model with PCR = 1.14 and PCR =1.42 are shown in Figure 84 and Figure 85, respectively.

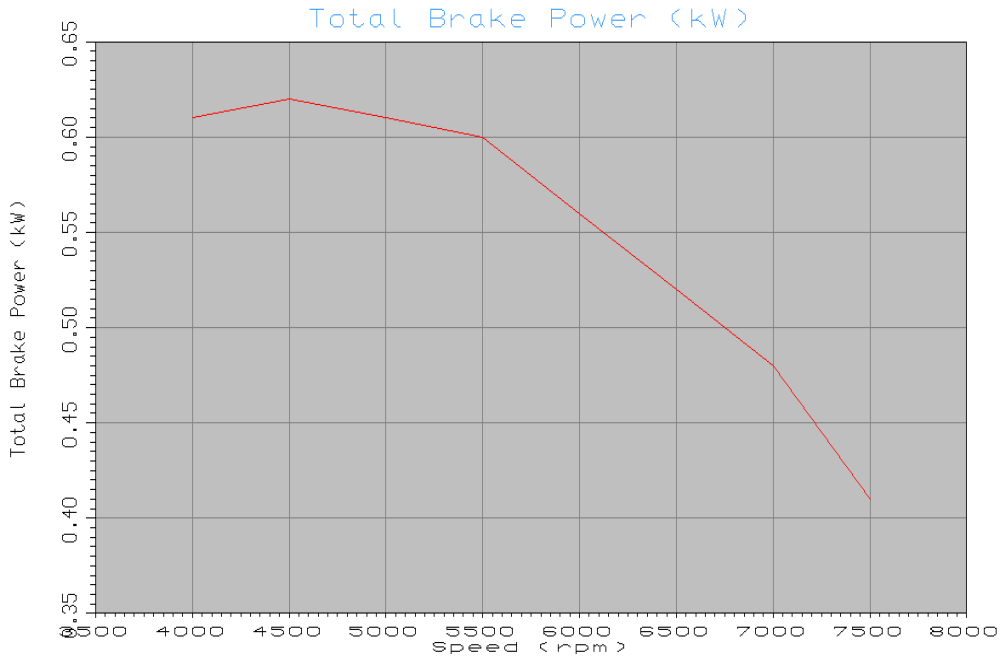

Figure 84 – Power Curve at PCR=1.14

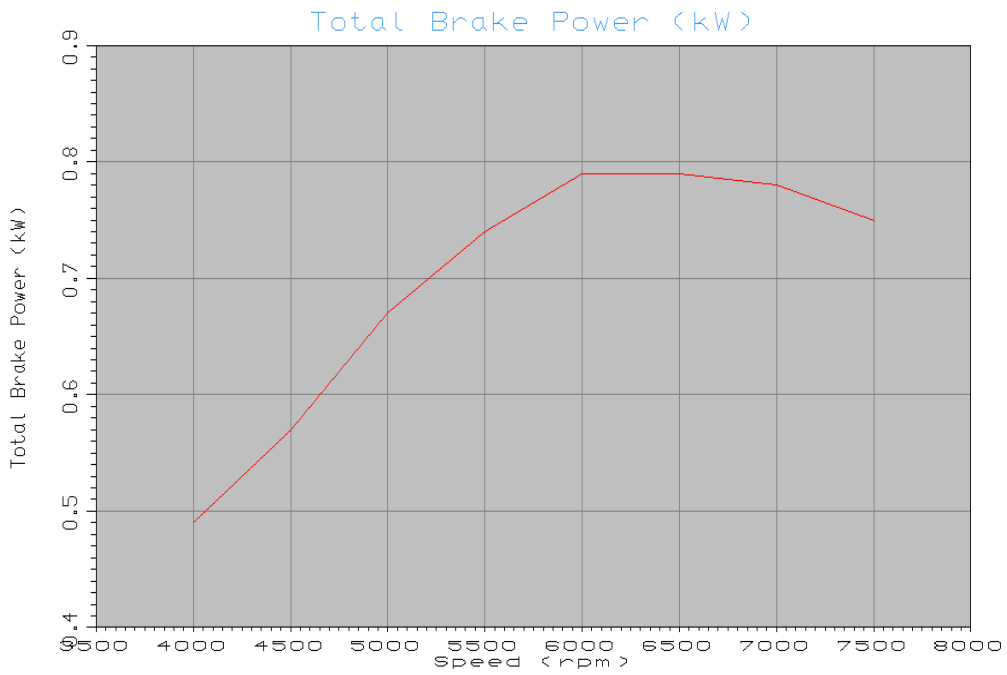

Figure 85 – Power Curve at PCR=1.42

With a PCR of 1.14 the model predicted a peak power of .84 horsepower (.62 kW) occurring at 4500 rpm while a PCR of 1.42 produced 1.06 horsepower (.79 kW) and held steady between 6000 and 6500 rpm. The LES model predicted the stock engine with a PCR of 1.14 would produce 21% less power than the same engine with a PCR of 1.42.

A PCR of 1.42 produced a more desirable power curve because near peak power was maintained across a wider range of engine speed. These curves when compared with the baseline dynamometer results from Figure 82 show some encouraging correlation. The model predicted higher power than found on the dynamometer in both cases (possibly due to the perfect scavenging assumption and rotary valve substitution) but peak power rpm correlates well. The conclusion from the LES model results is at least some of the reduced performance by the Wiseman engine can be explained by a less than ideal PCR.

These results provided enough impetus to experiment with PCR on the Wiseman engine to seek out increased power at higher operating speeds. One common method to increase PCR (decrease crankcase volume) is to add a case stuffer or material inside the crankcase to displace volume.

A case stuffer was designed and machined to fit inside the Wiseman case and displace as much volume as possible without obstructing moving engine components. The resulting design is shown in Figure 86. The volume of the case stuffer is 48.34 cc (2.95 in^3) and increased the PCR from 1.14 to 1.18 once installed on the Wiseman engine. Not enough to equal the stock engine but still an increase in the right direction. The machined case stuffer was installed on the Wiseman Engine and then tested again on the dynamometer. Unfortunately, the case stuffer did not generate a strong enough improvement to conclude a gain in peak power.

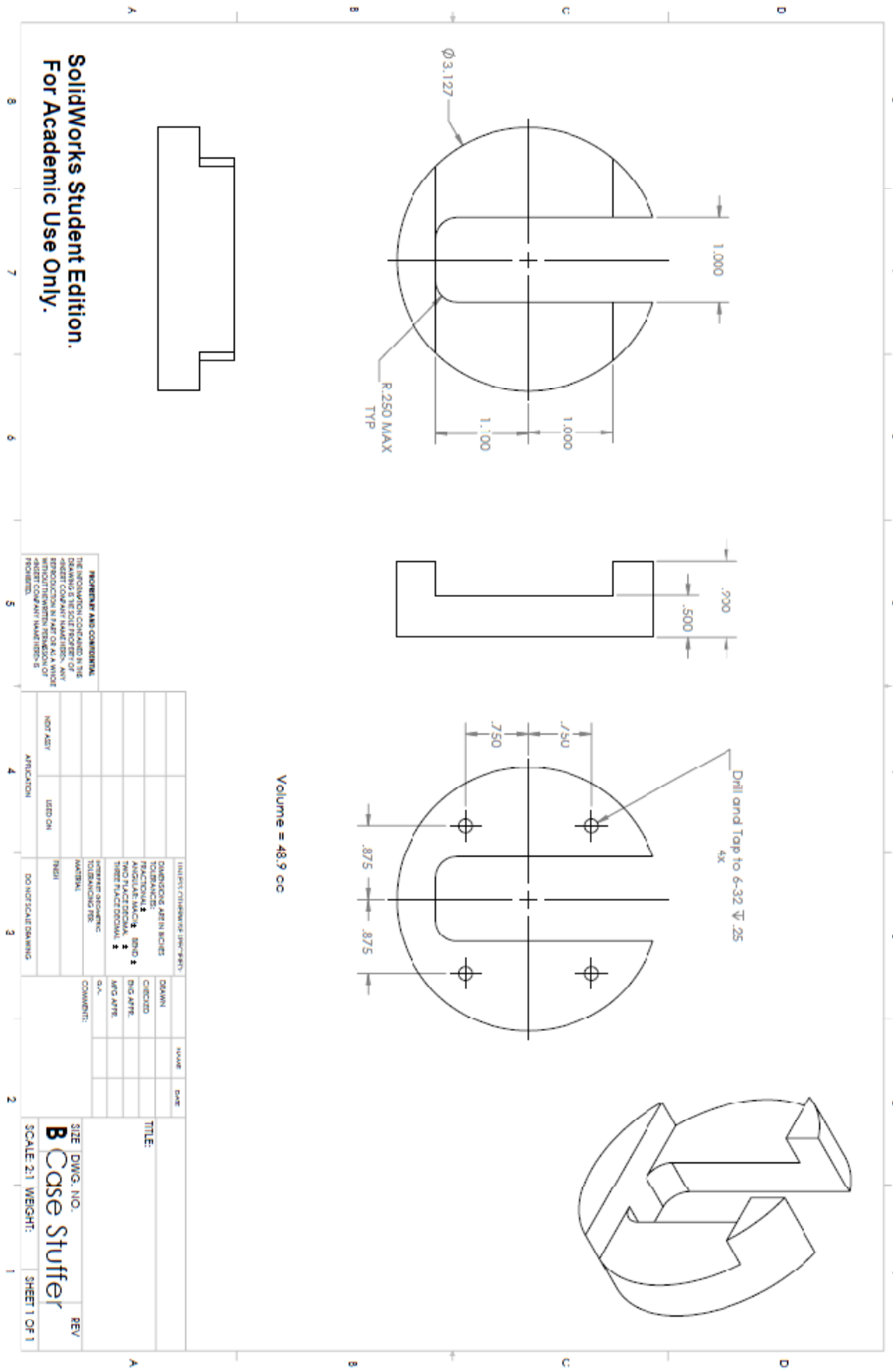

Figure 86 – Case Stuffer Drawing

Connecting Rod Seal

The case stuffer was a simple experiment but did not make a significant impact on PCR relative to the target. Unfortunately a major case redesign would be required to achieve the desired 1.42 PCR in the Wiseman engine. An attractive alternative to a case redesign for increasing the PCR was to add a seal around the connecting rod to completely eliminate the volume of the crankcase. The only remaining volume is between the underside of the piston and the base of the seal.

The design of a connecting rod seal was carried out with careful consideration for minimizing friction. The material of choice was a low friction, mechanical grade PTFE. The seal assembly comprises three components; the seal plate, which seals around the connecting rod and two identical support plates. The two support plates were designed to allow some freedom of movement to the seal plate. The floating design allows for some non linearity of connecting travel due to gear backlash and avoids any binding as a result. The connecting rod surface finish became critical and fortunately it was quite good. The connecting rod seal assembly mounted in the Wiseman engine is shown in Figure 87.

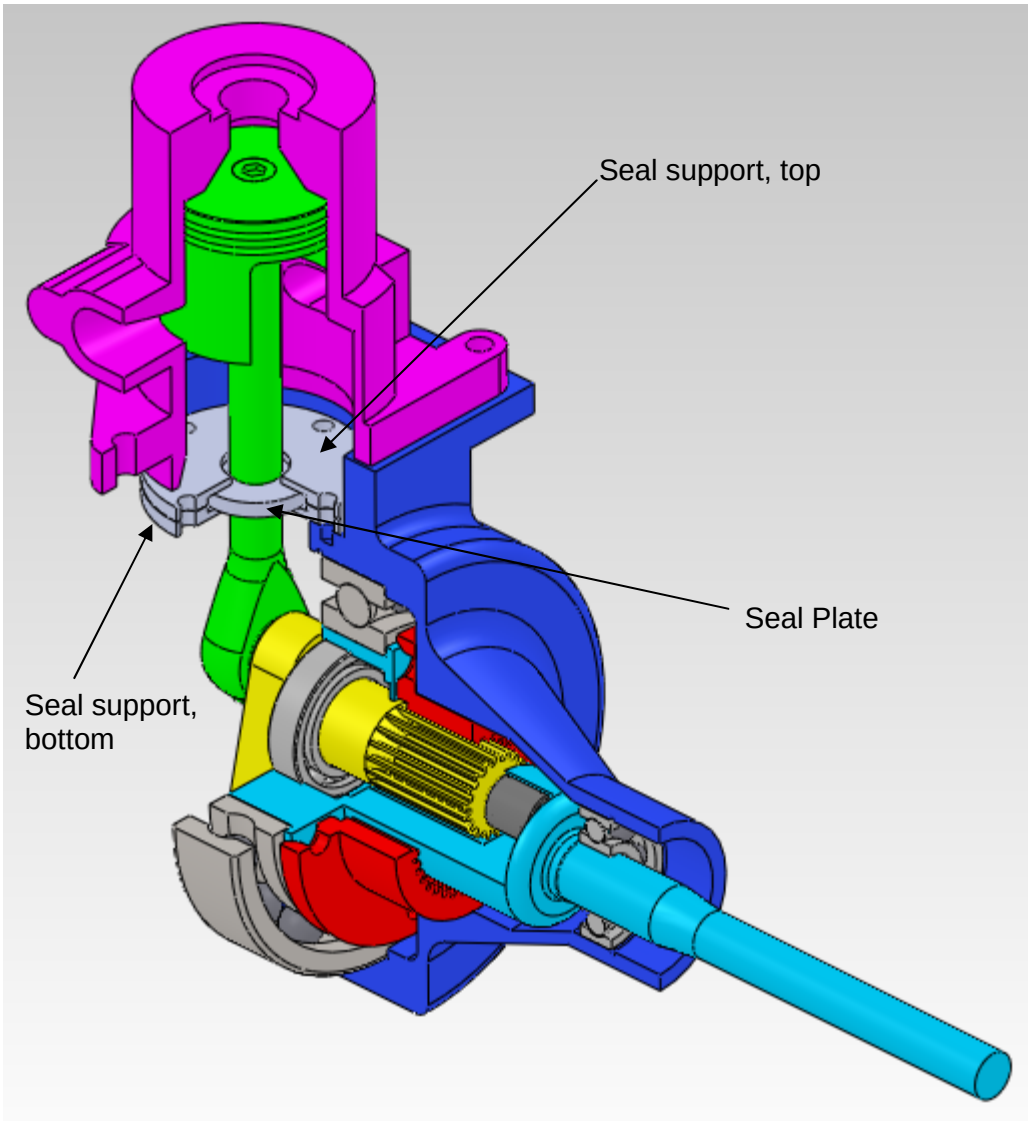

Figure 87 – Connecting Rod Seal installed in Wiseman Engine

The resulting PCR with the connecting rod seal installed on the Wiseman engine was 2.17 and significantly higher than the target of 1.42. Before building any hardware a PCR of 2.17 was plugged into the LES model to try and predict possible gains. The resulting power curve for a PCR of 2.17 is shown in Figure 88.

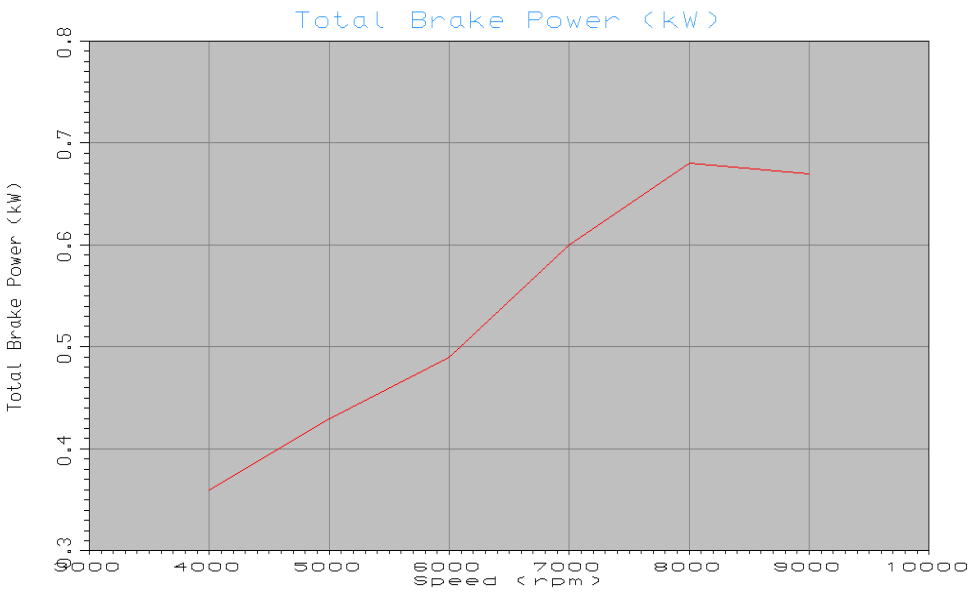

Figure 88 – Power Curve for PCR = 2.17

The LES model predicted an increase in peak power of 7.7% to .91 horsepower (.68 kW) that occurs at 8000 rpm. This result indicates a PCR of 2.17 is too high since higher peak power and a flatter power curve was predicted with a PCR equal to 1.42. Also notable in Figure 88 is the dramatic shift in peak power rpm from only 4800 (PCR = 1.14) to 8000 rpm (PCR = 2.17). Although not an ideal PCR, the seal appeared to provide an improvement that justified building and testing the seal on the Wiseman engine.

The seal assembly parts were machined on a manual lathe and assembled into the Wiseman engine. The seal plate ID was machined to .0254 mm (0.001 in) undersize relative to the OD of the connecting rod providing a tight seal without excessive drag between the sliding parts. It was expected that the seal would require some break-in period where an ideal balance between effective sealing and low drag occurs. After this point, sealing effectiveness would decline at an unknown rate. To ensure the seal increased the PCR well above that of

the stock engine, a simple motored test was carried out on both engines before after each run. Each engine was motored at 3500 rpm with a pressure tap and gauge installed in one of the transfer ports to measure maximum pressure. The stock engine at 3500 rpm measured below 1.0 psi (lower reporting limit of gauge) while the Wiseman engine with the seal installed consistently measured 2.0 psi. The blow by rate of the seal is unknown and the actual PCR was probably somewhat lower than 2.17 but this simple motored test confirmed the seal was effective.

The Wiseman engine was put back on the dynamometer for another run to determine the change in performance with the seal installed and functioning. It should be noted that while running, the Wiseman crankcase was open to atmosphere via the removal of a 1/8" NPT pipe plug from the case cover. Removal of the plug provided a port for adding oil to the bottom end while running but after numerous runs the case temperature remained stable and frequent oiling was not required. The resulting power curve is shown in Figure 89 along with the original baseline runs for reference.

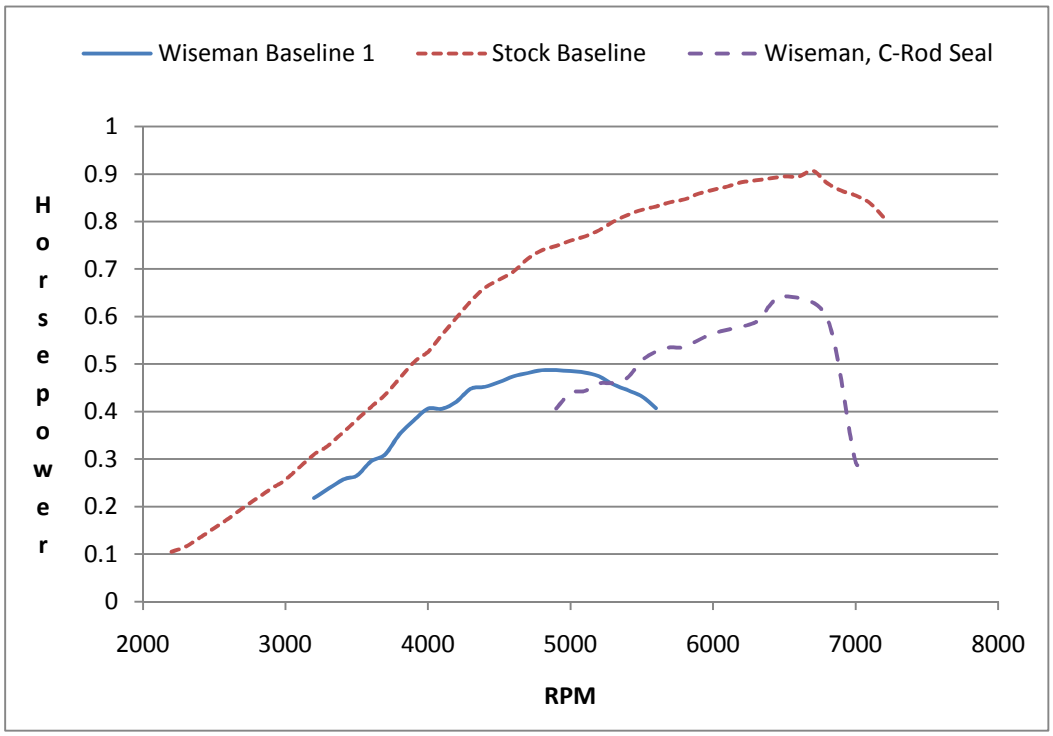

Figure 89 – Connecting Rod Seal Run with original baseline runs

The original tuning parameters, including timing and mixture settings were not adjusted prior to running the Wiseman engine with the new seal installed. The resulting run with the connecting rod seal installed showed a significant improvement beyond that predicted by the LES model. The peak power increased 31% to 0.64 horsepower and at a much higher rpm of 6500. One possible explanation for the higher-than-predicted gain is seal blow-by causing an actual PCR below 2.17. Similar to the LES model prediction, the curve is slightly steeper and peak power is available in a small rpm range. The improvement is substantial both in peak power and operating speed. The peak power rpm actually aligns well with the stock engine run. However, because peak power was achieved at much higher rpm, BMEP went down from 1.532 bar

(22.22 psi) to 1.412 bar (20.48 psi). The connecting rod seal actually had a negative impact on BMEP because peak power was achieved at a much higher rpm. Additional runs were carried out in an attempt to maximize peak performance by adjusting and tuning the following:

- Leaner and richer carburetor settings
- Higher cylinder head temperature
- Lower cylinder head temperature
- More and less advanced ignition timing

The above changes produced lower peak power in all cases. The ideal settings for the Wiseman engine without a connecting rod seal also produced peak power when the seal was installed.

Wiseman Power and Efficiency Conclusions

The combined results of the dynamometer testing on the Wiseman engine showed it produced 30-46% less power (depending on configuration and tuning), had a 30% lower BMEP, and 26% higher BSFC when compared to a similar slider crank engine tested under similar conditions. Other researchers have predicted that a GHE should be more efficient and produce more power than an equivalent slider crank engine (Karhula, 2008). The remaining question to be answered is: Was the reduced performance of the Wiseman engine in this study strictly due to its alternative hypocycloid bottom-end mechanism or are there other unrelated variables that influenced the results negatively on behalf of the Wiseman engine? The results of the motored friction test predicted only 5% higher losses in the Wiseman engine, which does not fully account for the reduced performance but is also not negligible. The LES model predicted a power gain of 26% going from a PCR of 1.14 to an ideal 1.42. The connecting

rod seal and a PCR of 2.17, although not ideal, showed PCR has a strong influence on peak power. The combined effect of higher friction (5%) plus a less than ideal PCR (26% reduced power) may fully explain the delta in performance by the Wiseman engine but this is not conclusive. The higher friction in the Wiseman engine is not a fundamental issue that cannot be overcome. Improved bearings, higher precision component fabrication, and better gear finish could make up this gap in the motored friction test and perhaps surpass the stock engine in fired friction losses when side load becomes significant. The PCR is also not a fundamental flaw of the Wiseman hypocycloid mechanism and is easily solved with a new design of the crankcase.

The final variable studied was the reduced output torque of the Wiseman engine for a given gas pressure curve. Karhula predicted that for the lossless engine case, a hypocycloid and slider crank engine would produce nearly the same torque and power (Karhula, 2008). However, this result assumes higher combustion pressures as a result of slower piston speed (reduced volume) on the expansion stroke. This conclusion is in line with the findings here that equivalent pressures produce lower power and torque in a hypocycloid (Wiseman) engine.

Chapter 6

SUMMARY AND FUTURE WORK

The slider crank mechanism dominates the internal combustion engine industry and very few alternatives have had much commercial success. The hypocycloid concept when applied to an ICE using gears is one possible alternative that has shown promise in some applications, particularly single cylinder engines where minimum vibration is paramount. Prior researchers have shown full crank geared hypocycloid engines can achieve theoretical perfect balance. Prototype engines have been constructed and proved empirically that much improved vibration behavior is possible compared to a conventional slider crank engine.

The piston and connecting rod assembly mass plays a major role in balancing the Wiseman engine in a reasonably small package. To balance the Wiseman engine required a new design for the piston and connecting rod constructed using advanced machining techniques including a 5-axis CNC mill and CNC lathe. The new piston and connecting rod weight was nearly cut in half compared to the original. The lightweight design ran many hours at high loads and rpm without any signs of premature wear of failure. The lightweight design allowed for material removal on the pinion shaft counterweight and made balance of the carrier shaft feasible with a simple modification. The carrier shaft modification required displacing its native steel construction with two heavy metal slugs (tungsten alloy) to achieve theoretically perfect 2D balance. To complete the balance effort in three dimensions and completely eliminate the shaking moment a novel concept of offset counterweights at the flywheel was proposed and tested in motion simulation. The motion simulation showed theoretically

perfect balance in three dimensions is possible even in a half crank hypocycloid engine. The gain in vibration reduction over 2D balance did not justify its construction due to a significant increase in overall engine weight.

To validate the motion simulation results a custom designed vibration test fixture and data acquisition system was developed. The test fixture consists of a 3-axis CNC mill where a variable speed spindle was used to motor the engine while it was fixed to the mill table. The high rigidity and mass of the mill provided a sound foundation for obtaining meaningful results. A dual-axis accelerometer mounted to the engine fed a data acquisition program designed to collect and process the vibration data. The data processing flow, completed in Labview SignalExpress, was constructed following the guidelines provided by an ISO standard for testing vibration of handheld power equipment. The Wiseman engine showed a significant improvement on the vibration test fixture once properly balanced and partially validated the motion simulation results. However, further improvements are likely possible using professional grade balancing equipment.

Once the Wiseman engine was well balanced it was better suited for high speed and high load testing. This type of testing had not been thoroughly researched nor tested until completion of this research effort. Settings including carburetor adjustments, cylinder head temperature, and ignition timing were adjusted independently and together in an attempt to seek out maximum efficiency and then maximum power. Maximum efficiency testing on a calibrated MTD dynamometer showed the Wiseman engine achieved good results at only 21% lower than modern MTD 31cc. Higher friction and poor PCR are partially to blame for the lower efficiency of the Wiseman engine.

The Wiseman engine was also tuned for maximum power on another dynamometer, specially modified for testing small, high speed engines. Once consistent maximum power was achieved, many recorded runs were completed. Baseline dynamometer results on the balanced Wiseman engine showed the Wiseman made 46% less power than the stock engine at a lower operating speed. These results drove the remaining research effort to investigate possible reasons for lower performance. The three aspects studied here that have a strong influence on peak performance of the Wiseman engine include:

- Higher friction losses
- Gas pressure to gas torque conversion effectiveness
- Primary Compression Ratio (PCR)

Mathematical models and empirical data collection were used to determine if and to what degree each of these aspects explain the lower power output of the Wiseman Engine. Results showed frictional losses and poor PCR were likely to play a major role in the reduced performance. Gas pressure to gas torque conversion may also have contributed to reduced power but without combustion pressure data this was not conclusive. The reduced volume behavior of the Wiseman piston may or may not increase combustion pressure enough to equal average gas torque output of the slider crank stock engine.

Future Work

The balance effort of the Wiseman engine in motion simulation proved very successfully and has merit as an effective method for balancing future Wiseman engines. Ideally the near perfect balance results of the simulation should be better validated in future efforts. The vibration testing equipment developed and used in this effort was not sufficient for high accuracy balancing and

measurement. The balance of the Wiseman engine could be improved by having it balanced on purpose built balancing equipment. Vibration data of a motored and running engine in a side by side comparison is also desirable once the Wiseman is professionally balanced. The weight of the Wiseman engine should be reduced or the stock engine weight increased so they are equal in mass when conducting future vibration tests.

There are many other variables that could contribute to the lower power output and operating speed of the Wiseman Engine. Port timing has a significant impact on peak power and peak power rpm. Because these engines are piston ported on the exhaust and intake, the port timing is identical in terms of piston position and volume. In other words looking only at piston position and volume versus port timing one would see no difference between the two engines. However piston velocity is not the same and so port opening time is different and this may play a role in the reduced performance of the Wiseman engine. Further analysis and testing is needed to better understand how port timing behavior and gas dynamics play a role in power output of the Wiseman engine. An experimental measurement that would help in understanding port timing and gas flow through the Wiseman engine is an intake airflow measurement. Knowing the amount of air flowing into the Wiseman and stock engine while producing maximum power would indicate if port timing is restricting performance. The end result of this type of testing would also provide volumetric efficiency for each engine at different operating speeds.

The effect of reduced expansion volume during combustion on cylinder pressure is still not well understood. Higher pressures may naturally occur in the Wiseman engine but are required in order to equal the same power and torque of

an equivalent slider crank engine. Without combustion pressure data it is difficult to conclude if and by how much the Wiseman engine combustion pressure is higher. Cycle to cycle variation and the large number of variables that affect combustion pressure may make this difficult to conclude empirically. A powerful 3 dimensional CFD combustion analysis would be ideal for predicting the effect of reduced piston speed (volume) on combustion pressure during the expansion stroke.

The later peak torque conversion (90º versus 75º ATDC) of the Wiseman hypocycloid mechanism indicates ideal ignition timing is an important variable worth further analysis. Typical ignition timing and advance curves for slider cranks may not be optimum for the Wiseman engine. Ignition timing was used extensively as a tuning variable to find peak power in the Wiseman engine in this research effort. However, the optimum ignition timing set for peak power in the Wiseman engine was not recorded or compared with the slider crank optimum.

The preliminary success of the connecting rod seal opens up many avenues of new research and development that ought to be explored. In two-cycle engines the amount of oil in the fuel-oil mix may be reduced or even eliminated by separating the crankcase with its own oil supply. In four stroke applications the seal provides a second working chamber available for compressing intake gasses without the need for an external turbo or super charger.

The balance results and conclusions from this research effort show there is great potential for the next generation Wiseman hypocycloid engine. A perfectly balanced half crank design has great potential in applications where minimum vibration is paramount. A single cylinder slider crank engine cannot equal the vibration performance of the balanced Wiseman engine. The next development

step for the Wiseman engine is to build a smaller and lighter version that incorporates the balancing technique developed here.

Although peak power and efficiency measured below equivalent slider crank engines in this research effort, the Wiseman engine, still early in development, shows great promise. With further optimization and sufficient engineering resources the Wiseman design has the potential to approach and possibly exceed the performance of its highly developed competition.

REFERENCES

Andriano, M. B. (1998). *Design, Construction and Testing of Hypocycloid Machines.* Detroit: SAE International.

Beachley, N. H., & Lenz, M. A. (1988). A Critical Evaluation of the Geared Hypocycloid Mechanism for Internal Combustion Engine Application". *Scociety of Auotmotive Engineers, Inc* .

Blair, G. P. (1996). *Design and Simulation of Two-Stroke Engines.* SAE International.

Heywood, J. B. (1988). *Internal Combustion Engine Fundamentals.* McGraw-Hill, Inc.

Hsu, M.-H. (2008). Planetary Hypocycloid (Epicycloid) Mechanism Design. *IAENG International Journal of Applied Mathematics , 38* (4), 197-204.

Ifield, R. *Unpublished engineering reports and drawings, covering the years from 1939 to 1981.*

Ishida, K., & Matsuda, T. (1975). Fundamental Researches on a Perfectly Balanced Rotation-Reciprocation Mechanism. *Bulletin of the JSME* , Vol 18, No. 116.

Ishida, K., & Yamada, T. (1986). Research on a Two-Stroke Cycle Single Cylinder Vibrationless Reciprocating Engine Chain Saw Utilizing an Internal Gear System. *Bulletin of the JSME* , Vol 29, No. 257.

ISO. (2004). *Forest Machinery - Vibration Test Code for portable hand-held machines with internal combustion engine - Vibration at the handles.* Switzerland: Internation Standard Organization.

Jeffrey, B. (2011, June 21). Raven Engineering. (T. Conner, Interviewer)

Karhula, J. (2008). *Cardan Gear Mechanism versus Slider Crank Mechanism in Pumps and Engines.* Lappeenranta: Lappeenranta University of Technology.

Lotus Cars Ltd. (2001). Getting Started Using Lotus Engine Simulation Ver 5.05.

Norton, R. L. (2005). *Design of Machinery* (Third ed.). Delhi, India: McGraw Hill.

Ortiz, A. (2011, December). MTD Engine Technician. (T. Conner, Interviewer)

Payne, J. (2011, October). Senior Engineer, MTD Soutwest Inc. (T. Conner, Interviewer)

Polly Model Engineering Limited. (2010, October). Retrieved from Stationary Engine Kits: http://www.pollymodelengineering.co.uk/sections/stationary-engines/anthony-mount-models/murrays-Hypocycloidal-Engine.asp

Ruch, D. M., Fronczak, F. J., & Beachley, N. H. (1991). 911810 - Design of a Modified Hypocycloid Engine. *SAE International* , 73-89.

SAE International. (2008). *Engine Power Test Code - Spark Ignition and Compression Ignition - As Installed Net Power Rating.* SAE International.

Wiseman Engine Group. (2010). *The engine of the future - today!* Business Plan.

Wiseman Technologies, Inc. (n.d.). Retrieved from UAV Design: http://www.wisemanengine.com/AUVSIWisemanPaPer.doc

Wiseman, R. (2001). *Patent No. 6,510,831.* United States of America.

Wolfram MathWorld. (2010, October). Retrieved from Hypocycloid: http://mathworld.wolfram.com/Hypocycloid.html

APPENDIX A: LES MODEL INPUT PARAMETERS

Fuel	
Fuel System	Carburettor
Fuel Type	Gasoline
Calorific Value (kJ/kg)	43000
Density (kg/liter)	.75
H/C Ratio Fuel (molar)	1.800
O/C Ratio Fuel (molar)	0.00
Molecular Mass (kg/k.mol)	114.23
Maldistribution Factor	1.000

Steady State Test Conditions	
Ambient Air Pressure (bar abs.)	1.01
Ambient Air Temperature (C)	20
Inlet Pressure (bar abs.)	1.01
Inlet Temperature (C)	20
Exit Pressure (bar abs.)	1.01
Equivlance Ratio	1.1
Specific Humidity	0.00

Intake	
Total length (mm)	10.00
No. of Diameters	2
Start diameter (mm)	6
End diameter (mm)	6
Pipe Volume (l)	.0003
Surface area (mm^2)	1.8850e+002
No. of meshes	2
Wall thickness (mm)	1.000
Cooling Type	Air Cooled
Temperature (C)	20
Ext. HTC ($W/m^2/K$)	20
Wall material	Aluminum

Intake disk valve	
Disk valve option	Standard
Valve Dia. (mm)	120
Port Dia. (mm)	10
Valve open (deg)	24
Valve Close (deg)	290
Max Area CD Coeff	0.99

Inlet Variable Volume Plenum	
Equiv. Bore (mm)	35.94
Equiv. Stroke (mm)	28.45
Equiv. Rod Length (mm)	56.00
Equiv Compression Ratio (PCR)	1.14, 1.42, & 2.17
TDC Angle (deg)	180
Wall Temperature (C)	100
Plenum HTC ($W/m^2/K$)	5.00
Speed Ratio	1.000

Piston Ported Intake Valve	
Valve Option	Standard
Port Width (mm)	40.00
Max. Port Height (mm)	2.00
Stroke (mm)	28.45
Rod Length (mm)	56.00
Valve Open (deg)	124.00
Max Area CD Coeff	0.900

Cylinder	
Bore (mm)	35.94
Stroke (mm)	28.45
Cyl Swept Volume (l)	.02886
Total Swept Volume (l)	.02866
Con-rod Length (mm)	56.00
Pin Off-Set (mm)	0
Compression Ratio	8
Clearance Volume (l)	.004123
Phase (ATDC)	0.00

Piston Ported Exhaust	
Port Width (mm)	20.82
Max. Port Height (mm)	7.41
Stroke (mm)	28.45
Rod Length (mm)	56.00
Valve Open (deg)	108.00
Max Area CD Coeff	0.900

Exhaust pipe	
Total Length (mm)	30.00
No. of diameters	2
Start diameter (mm)	11.00
End Diameter (mm)	11.00
Pipe Volume (l)	.0029
Surface Area (mm^2)	1.0367e+003
No. of Meshes	2
Wall Thickness (mm)	1.000
Cooling Type	Air Cooled
Temperature (C)	20.00
Ext. HTC ($W/m^2/K$)	20.00
Wall Material	Aluminum